Project funded by the European Commission under the 6th (EC) RTD Framework Programme (2002- 2006) within the framework of the specific research and technological development programme "Integrating and strengthening the European Research Area"

Project UpWind
Contract No.:
019945 (SES6)

"Integrated Wind Turbine Design"

Remote Sensing (UpWind WP6)
SODAR Comparison Methods for Compatible Wind Speed Estimation

AUTHOR:	Benjamin Piper
AFFILIATION:	University of Salford
ADDRESS:	G11 Acoustic Research Centre, Newton Building, University of Salford , M5 4WT, UK
TEL.:	+44 7538 277816
EMAIL:	b.j.piper@edu.salford.ac.uk
REVIEWER:	Dr E Mursch-Radlgruber, Dr M.R. Avis, Project Members

Document Information

DOCUMENT TYPE	PhD Thesis Draft
DOCUMENT NAME:	SODAR Comparison Methods for Compatible Wind Speed Estimation
REV.DATE:	7th February 2011
CLASSIFICATION:	R1: Restricted to project members
STATUS:	Subject to Final Corrections and Approval by the University of Salford

SODAR COMPARISON METHODS FOR COMPATIBLE WIND SPEED ESTIMATION

Benjamin PIPER

Acoustics Research Centre
School of Computing, Science and Engineering
University of Salford, Salford, UK

Submitted in Partial Fulfillment of the Requirements of the Degree of Doctor of Philosophy, 2010

Table of Contents

List of Tables and Figures

I dedicate this thesis to the memory of Kerry Standerwick, 1983-2008

A true inspiration to me and everyone she met.

Acknowledgements

I would like to thank my supervisor Sabine von Hünerbein for all her support, knowledge and guidance. Without her help and encouragement I would not have finished this thesis. I would also like to thank Stuart Bradley and Paul Behrens for their enthusiastic input and discussions from the other side of the world. I am grateful for the financial support and the feedback received at meetings of the UpWind project.

Thanks to Windtest Grevenbroich, in particular Qi Wang and Monika Krämer, for allowing and helping me to carry out transponder measurements in very snowy conditions at their wind turbine testing field in January 2010. Also I would like to thank Kenneth Underwood and Gunter Warmbier for their discussion of the outcomes of these measurements.

A big thank you to everyone in the acoustics department at Salford University. There have been many people who have lent me equipment, offered me their knowledge and given me crucial encouragement throughout. In particular I would like to thank David Waddington, Andy Moorhouse, Paul Kendrick, Matthew Taylor, Tomos Evans, Andy Elliot and Richard Hughes. Finally I am hugely thankful for all the encouragement and support of my parents and friends that have spurred me on and offered my entertainment throughout the last 4 years.

Abstract

This thesis includes the results of a PhD study about methods to compare sonic detection and ranging (SODAR) measurements to measurements from other instruments. The study focuses on theoretical analysis, the design of a transponder system for simulating winds and the measurement of the acoustic radiation patterns of SODARs. These methods are integrated to reduce uncertainty in SODAR measurements.

Through theoretical analysis it is shown that the effective measurement volume of a range gate is 15% of a cone section based on the SODAR's full width half maximum (FWHM). Models of the beam pattern are used to calculate the ratio of air passing a turbine to that measured by a SODAR over 10 minutes with values of 3-5% found at $10ms^{-1}$. The model is used to find angles where significant sound pressure levels (SPLs) occur close to a SODARs baffle giving the highest chance of fixed echoes. This is converted into an orientation guide for SODAR set-up.

The design of a transponder system is detailed that aims to provide a calibration test of the processing applied by a SODAR. Testing has shown that the transponder can determine the Doppler shift equation used by a SODAR although further work is needed to make the system applicable to all SODARs.

It is shown that anechoic measurements of single elements are useful for improving array models. Measurements of the FWHM and acoustic tilt angle can be achieved in the field using a tilt mechanism and a sound level meter (SLM) on a 10m mast. The same mechanism can be used to calculate an effective tilt angle using the Bradley technique.

It is proposed that these methods are integrated to calculate error slopes for the SODAR measurement with regards to a secondary location. It is shown that the slopes could be between 0 and 5% if the methods are fully realised and a computational fluid dynamics (CFD) model is incorporated.

1. Introduction

1. Introduction

1.1 Statement of The Problem

SODARs are useful tools for measuring aspects of the atmospheric boundary layer (ABL) such as wind speed and turbulence. In the early stages of their development they were employed to measure the height of the boundary layer by recording the strength of the return echo. By employing several beams in a complimentary arrangement it is possible to solve a set of simultaneous equations to give the wind speed and direction at many points within the measurement height range.

There are some uncertainties in SODAR measurements that need to be overcome. Uncertainties in SODAR measurements can be divided into uncertainties caused by the measurement target and uncertainties caused by the SODAR itself. Uncertainties caused by the measurement target cannot be directly dealt with but methods to minimise their effect can be developed. Uncertainties caused by the SODAR itself can be dealt with and methods to remove these altogether are needed. These uncertainties include incorrect beam tilt, flaws in peak detection, incorrect height estimation, fixed echoes, broadband and tonal noise errors and incorrect handling of strong atmospheric shears. There is a statistical mismatch between measurements from different SODARs because most SODARs use different geometries and processing methods to achieve a wind estimation. Whilst these methods are similar an understanding of how measurements using different SODARs correlate together is required.

The main motivation for improving the accuracy and understanding of SODAR measurements is their potential use in the wind energy market. With increasing demands for green energy the size and scale of wind farms are growing rapidly. For the task of wind turbine siteing and power curve measurements wind speed data is required with at least a 99% accuracy. To date measurement masts fitted with several

anemometers and wind vanes have been used to collect data for these purposes. A SODAR could be a useful alternative providing many measurements throughout the turbine height without the need to build expensive masts. In order for SODAR to be a '*bankable'* measurement instrument for wind energy a means of reducing and confirming the uncertainty in the measurements is required.

1.2 Introduction

In this Chapter previous SODAR comparison work will be explored along with a brief overview of the acoustic operation of SODARs. How SODAR measurements relate to wind energy will be explained with the required accuracy of the wind industry identified. The state of the art for SODAR measurements and comparison methods will then be stated with reference to previous work carried out to qualify the accuracy and meaning of SODAR measurements. The work in this thesis forms part of the UpWind project and follows on from the Wind Energy SODAR Evaluation (WISE) report which is reviewed in depth here. The research questions and the aims of this thesis are stated with an outline of the proposed approach.

1.3 Previous Studies in SODAR Operation, Comparison, and Accuracy Testing

1.3.1 Outline of the Development of SODAR Instruments

SODARs have been used as tools for meteorological research for over 60 years. The first SODARs consisted of a single antenna operating a vertical beam to measure reflectivity such as the one used in Gilman (1946). The principal use of these early SODARs was to provide information about atmospheric boundary layer (ABL) depth and structure where McCallister (1968), Little (1968), Kallistratova (1968) and Cronenwett (1972) demonstrate results of using SODARs for this purpose. In the 1970s Doppler SODARs were introduced in both bi-static and mono-static single axis configuration where the return signal is analysed to find the frequency shift caused by

the movement of turbulent reflectors. This frequency shift gives the wind speed along the direction of the SODAR measurement beam known as the radial wind speed. Bi-static types are described in Georges (1972), Beran (1973), Gaynor (1977) and Davey (1978) and they operate with an output antenna and several receiving antenna separated by a distance. The advantage of this set-up is a gain in the strength of the reflection due to the contribution of both velocity inhomogeneities and temperature inhomogeneities. The disadvantage is that they are difficult to set-up due to the large space separation between antennas. Single axis mono static SODARs are only capable of measuring along beam wind velocity but this is useful for air quality studies since the transport of gases in the ABL follows the vertical velocity. Examples of their use can be found in Caughey (1976) and Helmis (1985). The use of a mono-static SODAR or psuedo-mono-static SODAR featuring multiple antennas tilted in a complimentary arrangement allows for a set of simultaneous equations to be solved that gives an estimation of the horizontal wind speed and direction. Examples of this SODAR type can be found in Neff (1986), Elisei (1986) and Finkelstein (1986).

The SODARs discussed so far have tended to be large and heavy instruments that operate at lower frequencies with ranges of up to 1km. From the late 1970s smaller high frequency SODARs have been developed based on early work found in Mousley (1979) on the use of arrays of speakers . These SODARs are often referred to as mini-SODARs as they tend to be smaller than previous instruments allowing them to be easily transported and set up. Examples of these are described in Asimakopoulos (1987 and 1996) and Mursch-Radlgruber (1993a and b) . This capability of mini-SODARs makes them of interest to fields where wind speed and direction at a range of heights in the lower ABL, around 150-300m, are needed such as wind energy.

In the last ten years a new wave of SODAR developments have occurred to make mini-SODARs into useful tools for wind energy. These mini-SODAR are mono-static phased array types, except the AQ500, that have the ability to operate without a mains power supply and to transfer data to a remote computer. Increasingly the ability to operate autonomously is a feature included and autonomous configurations are

described in Underwood (2010) and Scott (2010). There are several different companies that produce SODARs with these features specifically aimed at the needs of wind energy. These SODARs represent the state of the art in commercially available SODAR instrumentation.

There are several experimental SODARs that are under development that aim to determine whether large changes in the method employed by a SODAR can give better quality results. The bi-static SODAR type that was initially used in the 1970s is redeveloped in Behrens (2008) making use of modern computer processing power to allow for the receivers to scan the SODAR beam though the use of a Fourier-domain shifting technique. The option of integrating this into a commercially available mono-static SODAR as an add on component is detailed in Bradley (2010a). The possibility of using coded frequency pulses to obtain more detailed information than can be achieved through single frequency pulses was discussed in Bradley (1999). Rao (2009) makes comparison between measurements made with a coded multi-frequency pulse and a single frequency pulse referenced to high resolution GPS sonde balloon measurements showing that the use of coded pulses improves the signal to noise ratio giving 30% more wind data and with a higher consistency observed. Von Hünerbein (2010) takes the coded pulse principle further presenting a SODAR design that also allows for complete control of all sound producing elements giving control of the beam steering. The aim of this experimental SODAR is to make use of intelligent data analysis methods to give significant gains in signal to noise ratio and data quality and an advanced atmospheric model has been created in Kendrick (2010) to test this idea.

The complexity and wind estimation ability of SODARs is improving at a steady pace but a 'black box' approach is required to confirm their uncertainty levels before they will be accepted by the wind energy industry. This approach would allow a user to ensure the quality of their data without requiring the manufacturer to publish proprietary details about the operation of the SODAR in question.

SODARs are used in other applications besides wind energy including

aeroplane wing wake vortex measurements as demonstrated in Bradley (2007), air quality studies shown in Gera (1990) and Emeis (2006) and meteorological research with a discussion made in Kallistratova (2004). Whilst these disciplines have less stringent demands than the wind energy industry they would also benefit from a reduction in measurement uncertainty.

1.3.2 Motivation for use in Wind Energy

Recent growth in the wind energy market makes SODAR an attractive alternative measurement technique to previous tools due to their relative cost and portability advantages. From the 1990s onwards the number of wind farms and the size of the turbines used in these farms has continued to grow. Initially measurements for carrying out wind farm site assessments and the measurement of wind turbine power curves was exclusively carried out with cup or sonic anemometers and wind vanes attached to a mast structure.

The standard for power curve measurements has been a calibrated cup anemometer at turbine hub height as described in IEC 61400-12 This type of measurement is adequate for turbines of small height and blade span but for the larger modern turbines the cost of erecting a mast becomes very large and there is a strong argument that a hub height measurement is not representative due to the wind shear that occurs over the span of the turbine blades. This has been shown in Antoniou (2009) and Wagner (2008, 2009 and 2010) with a new approach to power curve measurement that takes into account the measurements from several heights to create an equivalent wind speed for calculating annual energy production (AEP) and this is likely to be included in a revision to the IEC standard for power curve measurements. This method is used in Gomez (2010) where AEP calculated from an equivalent wind speed found from LIDAR measurements is compared to AEP calculated from hub height measurements. This method is also used in Walls (2010) with data recorded using a Triton SODAR where comparison of AEP predicted from SODAR data used as a replacement for 40m and 60m anemometers is made to AEP calculated from the

whole SODAR profile with the latter showing smaller errors and an uncertainty of between 1% and 2%.

The problem with using SODAR measurements is that the accuracy and meaning of the measurements in relation to the measurements of other instruments is not completely known or understood. The majority of previous work has been carried out comparing SODAR measurements to the measurements of other instruments whilst a small amount of work has also been carried out on measurement of the SODAR beam tilt angles as this is seen to be one of the largest contributing factors to measurement uncertainty. Wind speed measurements for wind energy purposes need to have no more than a 1% uncertainty since power generated by the turbine has a cubic relationship to input wind speed. A 1% uncertainty in the wind speed estimation results in a 3% uncertainty in the turbine annual power output estimation and therefore a 3% uncertainty in the investment available for a wind farm project based on these measurements.

1.3.3 SODAR Comparison Studies

A SODAR comparison study is one in which measurements made by the SODAR are compared to measurements made by another instrument or instruments. The majority of work that has been carried out on SODAR performance has consisted of comparing SODAR measurements to mast mounted instruments. The rationale for this method is that by comparing one measurement to the measurement of a verified instrument it should be possible to find an indication of the accuracy through calculating the correlation coefficient, or R^2, and a linear regression slope for the data sets.

Crescenti (1997) presents reviews of comparison studies that have occurred between 1977 and 1997 including Mastrantonio (1982), Kurzeja (1994), and Vogt (1994), and attempts to collate these into an overall estimation of the accuracy of SODAR measurements. The analysis relies on the assumption that all studies are

comparable, which is not necessarily the case as differences in set-up, location topography, data type, data rejection and data analysis in the various studies result in some studies being incomparable with others. Despite this it is valuable to examine the similarities betweens these studies as it highlights the possibilities of SODARs for accurate wind measurements. The mean R^2 for wind speed was found to be 0.91 with it rarely dropping below 0.8. It is also noted that shorter averaging times in some studies may have lead to higher uncertainties. Similar results were found for wind direction with a mean R^2 of 0.92. Far less data was available for this comparison. The standard deviation of the velocity, $\sigma_{w,}$ and direction, $\sigma_{\theta,}$ were also compared although with even less data points than wind direction. The result is poor values of R^2. The conclusion that SODARs tend to underestimate σ_w is made. It is noted that in the majority of studies it is assumed that the reference instrument is exact and therefore imply that all error is due to the SODAR. However it is unlikely that SODARs and in-situ measurements would consistently give the same results as they are essentially measuring different things; SODARs give a time average of a volume averaged measurement whilst in-situ sensors give a time average of a single point measurement. Ultimately this study highlights that SODARs have the potential to make accurate wind measurements but work is required in order to find reliable methods to verify SODAR data as well as guidelines to set up in various different topographical situations.

Since 1997 many more comparison studies have been carried out between SODARs and in-situ instruments in similar fashion to those reported previously and with similar agreements found between the instruments such as those reported in Hayashi (2003) and Short (2003). These measurements alone are not likely to improve the wind industry's trust in the SODAR measurements as they continue to imply that a SODAR measures winds between 0% and 15% slower than mast mounted anemometers for the same height. Some recent studies have featured increased complexity of instrumentation and measurement aims. For example in Helmis (1997) a SODAR is used as part of an integrated measurement system for assessing the wind

field over the entire Greater Thessalonki area. The need for using SODAR measurements in conjunction with measurements from other instruments is partly due to the perception that SODAR measurements, at the time of the campaign, were not accurate enough to be used alone. It does point to a viable approach for performing wind resource assessments over large potential wind farm sites. A further example of the use of SODAR in a more complex comparison experiment can be found in Ormel (2003) where a comparison is given between offshore and onshore measurements and employing different parameter sets. The results showed weak agreement with mast mounted instruments with large differences occurring between the correlation for different parameters sets. This highlights that it is crucial to employ the right parameters when making SODAR measurements and understanding of exactly how each alters the measurement is required.

Comparison studies in flat terrain have shown that SODAR measurements generally show good agreement with mast mounted anemometry although often less than the 1% agreement that is desired by the wind energy industry. Further studies in flat terrain can add little more to the results that have already been found without introducing more complex methods. SODAR comparison studies in complex terrain are more useful since many wind farms are sited in complex terrain. Complex terrain is primarily hilly or mountainous terrain but forest and urban landscapes also fall into this category since the surface roughness and variability is much higher than flat terrain. Reid (2003) gives a comparison of measurements at two hilltop sites in NZ. Details about the specific problems of using SODARs in hilly terrain are examined. It was found that data loss was quite high at high wind speed but profiles could be recorded up to 200m.

A measurement campaign in forested terrain is presented Tomkins (2007). Whilst this is a demonstration of a SODAR comparison in forested terrain the principle point of interest in terms of finding methods to reduce SODAR uncertainty is the use of site calibration performed using two meteorological masts. One mast was then replaced by an AQ500 SODAR and measurements between the remaining mast

and the SODAR were compared taking into account the speed up effect that had been recorded between the two masts in the initial phase of the experiment. The results showed that the SODAR was consistently measuring 3-5% lower wind speeds than expected. This study highlights that a useful calibration technique is to measure with a mast or a different instrument in the proposed site of the SODAR in reference to a second mast. Then the expected difference between the SODAR and the secondary mast can be found within certain errors bounds. This is not a perfect calibration though since any bias from the calibration instrument is then added to the overall measurement uncertainty.

The majority of SODAR comparison measurements have employed SODARs that operate three sound beams in complimentary orientations although it is possible to measure in more directions and measurements with 5 beams have been explored in some campaigns. Ito (1997) examines the errors which occur when using a five beam phased array SODAR with regards to a comparison campaign between SODAR measurements and tower mounted sonic anemometers. It was found that five beam measurements have the advantage over three beam measurements of extracting errors from the measured variables and using them to correct the observed results. Behrens (2010a) presents a 'Multi-SODAR' approach to wind profiling in which the facility of a METEK SODAR to use 4 titled beams, with a separation of 90º between each, and a vertical beam is used to create independent SODAR measurements using a single SODAR. These separate measurements can then be compared to each other to give a robust estimation of the wind speed profile. This method is particularly designed for use in complex terrain where the wind speed can change significantly between the different volumes measured by each of the SODAR's beams. The method was tested in simple terrain and it was found that each set of beams gave statistically identical measurements. Further testing was carried out in complex terrain with a mean wind speed difference of $0.14 ms^{-1}$ over the scanning area. This is thought to be a real difference and not instrumental error due to the agreement of the measurements in simple terrain. This method is the currently the state of the art for SODAR

measurements in complex terrain.

Comparison experiments have not only been carried out using mast mounted anemometry as a reference. Several campaigns, including Baumann (2001) and Piringer (2001), have included comparisons between SODARs and tethersonde. These comparisons have shown poor correlation and it is possible that SODAR averaging and data rejection methods can remove real meteorological occurrences. Further measurement campaigns using tethersonde as the comparison instrument for wind energy purposes are of little use since the the tethersonde moves around making it a less precise comparison instrument than a mast mounted anemometer and only measures one height at a time. The tethersonde does present a useful way of ascertaining the influence of a SODARs data processing when faced with unusual wind conditions and could therefore be useful as a reference for measurements made in valleys and similar terrain.

1.3.3.1 Comparison Studies Specifically Aimed at Wind Energy Requirements

In the last ten years increasing amounts of effort have been put into making SODAR measurements suitable for wind energy. Several studies have examined this with the Wind Energy SODAR Evaluation (WISE) in de Noord (2005), which contains several component parts of which Antoniou (2003) and Bradley (2005) are the most relevant to discussion of SODAR accuracy and calibration, being the largest contribution in this effort.

The WISE report is an extensive report on the ability of SODARs to be useful for the wind energy market. It is the main foundation on which the work carried out for the SODAR related parts of the UpWind project is based. Within it SODAR technique, wind energy calibration methods, operational characteristics, power performance measurements and the application of SODARs in difficult conditions are discussed. As part of this study the Profiler Inter-comparison Experiment (PIE) was performed where several SODARs were set up at the same test field at Høvsøre

(Denmark) and their measurements were compared both to mast mounted anemometry and to each other. SODAR theory is covered in detail giving rise to Table 1.3.1 which highlights the contributions of the operational parameters to measurement uncertainty.

Source	Parameter	Slope error $\frac{\hat{u}}{u}-1$	Parameter range	Error range
Temperature	ΔT [K]	$+\frac{\Delta T}{2T}$	±20 K	± 3 %
Out of level	$\Delta\varphi$ [radian]	$-\frac{1}{2}(\Delta\varphi)^2$	±15° (±0.3 rad)	-3.5 % to 0 %
Fixed echoes	Δx [m]		0 to 500 m	0 to -100%
Rain	R [mm/h]		0 to 50 mm/h	20 - 30 m s^{-1}
Beam spread	σ_φ [radian] φ [radian]	$+2\frac{\sigma_\varphi^2}{\sin^2\varphi}$	4°-8° (0.07-0.14 rad) 15°-24° (0.26-0.42 rad)	+6 % to +25 %
Beam drift	u/c	$\pm\sqrt{2}\frac{u}{c}$	0 to ±0.06	0 % to ±8.5 %
Beam separation	$\rho(\Delta x)$	-(1-ρ)	0.8? to 1	-20 % to 0 %
Vector averaging	z_0 [m] z [m]	$\frac{1}{2\left(\ln\frac{z}{z_0}\right)^2}$	0.01 to 2 m 10 to 1000 m	0 to 10 ?
Peak position	$\sigma_{\Delta f}$ [Hz] φ [radian] f_T [Hz]	$\pm\frac{c}{\sqrt{2}\sin\varphi}\frac{\sigma_{\Delta f}}{f_T}$	±0.5 Hz 15°-24° (0.26-0.42 rad) 1000 to 6000 Hz	0 to 10

Table 1.3.1 – Table of the error contribution from various aspects of a SODAR's measurement process. Bradley (2005).

From examination of the error contribution from the different parameters it can be seen that five of the aspects are related to the acoustic beam shape so reducing the uncertainty in this aspect is imperative if SODAR accuracy is to be improved. In WISE the theoretical analysis assumes that reflections are received from a conical volume with a half angle θ given by Equation 1.3.1 where z is the height above the SODAR, c is the speed of sound and τ is the time length of the pulse.

$$V = \pi z^2 \frac{c\tau}{2}$$ (Equation 1.3.1)

This gives an outline of the measurement volume but it does not take into account the weighting across the volume caused by the SODAR beam shape and the amplitude window applied when extracting a range gate from the backscatter signal. This will be addressed in this thesis. In WISE it was shown that SODARs will estimate wind speeds 0.5%-2% lower than measurements by cup anemometers. This is a largely a result of volume averaging and in WISE it is stated that this adds to the uncertainty of the measurement.

A part of this report that is of particular interest for this thesis is the proposed calibration methods including PIE. PIE was a measurement campaign where three SODARs were operated simultaneously at the same site with comparisons to mast mounted anemometry. The aim was to use a linear model to find calibration slopes for each of the SODARs. 10 minute averages were recorded at 5 heights with varying data availability found in the different SODARs. The analysis showed that most of the uncertainty in the measurement was a result of the volume separation between the SODARs and the mast instruments. The results are shown in Table 1.3.2.

System	Parameter	40m	60m	80m	100m	120m
AV4000	N	6580	6555	6281	5453	4676
	$\hat{m}$	1.082	1.085	1.083	1.079	1.080
	$\hat{m}/\hat{m}_{40}$	1	1.002	1.001	0.997	0.960
	$\sigma_{\hat{m}}$	0.0009	0.0009	0.0009	0.0012	0.0016
	r^2	0.983	0.984	0.982	0.972	0.960
Metek	N	9454	9429	9408	8232	8292
	$\hat{m}$	0.944	0.935	0.928	0.923	0.936
	$\hat{m}/\hat{m}_{40}$	1	0.991	0.983	0.978	0.991
	$\sigma_{\hat{m}}$	0.0012	0.0012	0.0012	0.0017	0.0014
	r^2	0.949	0.947	0.945	0.908	0.935
Scintec	N	6580	6555	6281	5453	4676
	$\hat{m}$	1.013	0.984	0.978	0.961	0.942
	$\hat{m}/\hat{m}_{40}$	1	0.971	0.966	0.949	0.930
	$\sigma_{\hat{m}}$	0.0008	0.0008	0.0009	0.0010	0.0013
	r^2	0.982	0.982	0.979	0.977	0.965

Table 1.3.2 – Regression Coefficients from the PIE Measurements. Bradley (2005).

The regression slopes found are all within 10% but only some are within 5%. The R^2 correlations are generally above 0.96. Figure 1.4.1 shows the slope errors measured in the experiment for the three SODARs with respect to range gate height.

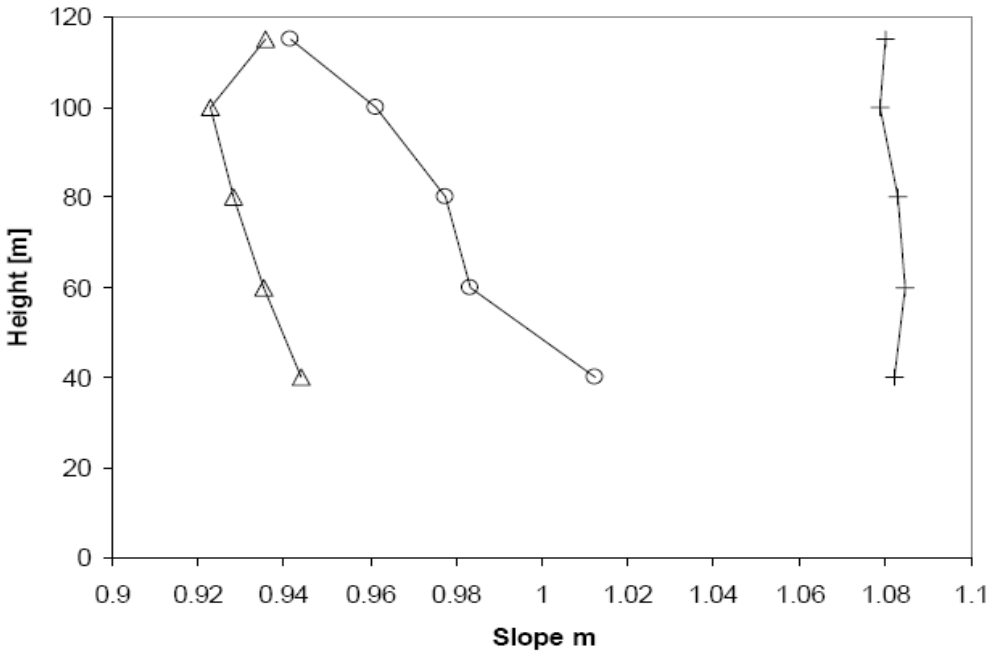

Figure 1.3.1 – Variation in regression slope with height for the measurements of a METEK (Δ), a AV4000(+) and a Scintec(O) SODAR made in the PIE from Bradley (2005).

These results show that the differences between the SODARs and the cups are between 0 and 10% and that the different SODARs give different results.

Using these results a calibration method is suggested where measurements are made with a cup at 40m to provide a base measurement and SODAR measurements are used for the rest of the height range and calibrated to the 40m cup measurement. Results of testing this calibration method showed 1% uncertainty in the wind speed estimation but this is unsurprising since the SODAR measurements are forced closer to a cup measurement. This method is a part calibration that is convenient since cup anemometers are the current standard method for wind energy. It is not an absolute calibration and it does not account for the differences between what is actually being measured by a SODAR and a cup.

A similar inter-comparison experiment to PIE is presented in Clive (2008) and performed at Myres Hill in Scotland with a comparison between a SODAR, a LIDAR (Light Detection and Ranging) and mast mounted anemometry. The principle problem

identified with the SODAR measurements is the inability to co-locate the SODAR with the mast due to the fixed echo effects SODARs are subject to. Despite a separation distance of 300m the data between the mast and the SODAR showed good agreement. The experiment continued and the final data was revisited in Bradley (2010b) where a LIDAR was co-located with the SODAR as well as the mast in order to give a better indication of the SODARs performance. It was identified that both the SODAR and the LIDAR tended to underestimate wind speeds in comparison to the mast. The reason for this is given as the differences in measurement technique combined with the influence of the moderately complex terrain. A simple two dimensional flow model was created to explore these differences and it was found once the output of this model was taken into account the agreement between the instruments was within 2%. This study shows the most advanced use of an integrated methodology for finding the uncertainty in the SODAR measurements with the use of flow modelling and collocation of a simultaneous measurement instrument. This is the state of the art measurement approach for SODAR comparison studies. The problem with this approach is that any uncertainties in the LIDAR and mast measurements are passed on to the SODAR measurements making the best SODAR case already less certain than the LIDAR measurements and this suggests that perhaps just the LIDAR measurements at the mast position should be used.

One of the principle aims of work into improving acceptance of SODAR measurements is so that they can be used for making power curve measurements. Within the WISE report SODAR data calibrated using the 40m mast method was used to make power curve measurements with the results showing that a SODAR could derive AEPs within 4% deviation of those measured with cups. The uncertainty in these measurements was 10-30% higher than those measured with the cups alone and therefore the SODAR measurements in this case are not reliable enough for calculating AEP. Warmbier (2007) presents a comparison of measurements made using a mini-SODAR and cup anemometers specifically discussing the implications with regards to wind turbine power curve estimation. Using the standard linear regression R^2 was

found to be 0.958. Power curves were calculated using both sets of measurements according to IEC 61400-12.

Whilst it is clear that a large volume of work has been carried out exploring the quality of SODAR data in comparison to other sensors, the results are varied and no complete calibration technique has been found using this approach. There is a risk in comparing SODARs to in-situ anemometers that an error is being introduced. Take a hypothetical case of a SODAR and a cup-anemometer measuring the exact same point in space and time, both instruments could measure exactly the same wind speed at this point however the SODAR may give a different result for the range gate containing this point due to the contribution from other parts of the volume measured. This would result in a higher error than if the SODAR result were assumed to be correct without comparison. The state of the art comparison technique consists of using CFD modelling techniques, including those demonstrated in Mann (2000), Stangroom (2004), Bingöl (2009) and Behrens (2010b) to explain the terrain effects and the use of collocated sensors in order to find the relationship between the SODAR measurement position and that of the comparison sensors. In Boquet (2010) it was found that for one particular measurement using a WindCube LIDAR the regression slope between the wind measured by the instrument and a cup anemometer in complex terrain could be reduced from 6% to 1% through the use of CFD. Currently the use of CFD to explain wind flow in complex terrain is not fully developed although results are promising. In simple terrain the accuracy of the models is thought to be good.

1.3.4 SODAR Comparisons with Transponder Based Simulated Echoes

One alternative to performing conventional comparison studies is to operate the SODAR in known conditions. This in principle could be achieved in a very large wind tunnel but it is not a very cost effective or physically simple solution. It should be possible to simulate known wind speeds in a computer and use these to generate an echo signal that represents these wind speeds. In Baxter (1994 a and b) an acoustic

pulse transponder (APT) system was created that contained several pre-programmed pulses to correspond to a reflection from specific heights as well as a continuous signal mode with frequency changes at known times. It has modes for both single frequency and multi frequency SODAR operation. The principle aim of this method is to ascertain whether a SODAR can correctly measure a frequency shift and how accurate its timing is. This method was used in Fujita (1998) as part of a full quality assurance programme for air quality measurements. Figure 1.3.2 shows the flow diagram of the APT's operation. The APT itself has two variables that need to be tested in order to ensure that it provides fair testing of SODARs. These are the ability to produce known frequencies and the timing of the pulse returns, which is both the length of the pulse and the time in which it takes it to respond to the SODAR. It is stated that the system has a frequency accuracy of 1 Hz but it does not operate in 1 Hz steps due to the clock base used by the computer. Therefore SODARs tested with this system need to be operated at a matching frequency or the difference needs to be taken into account in the analysis. The system was designed to run from a small notebook and batteries meaning that it is a highly portable system which is an important design feature considering that a lot of wind turbine sites are remote or offshore and external power is not always available. This transponder system is a diagnostic tool as it only allows the performance of a SODAR's peak detection to be tested.

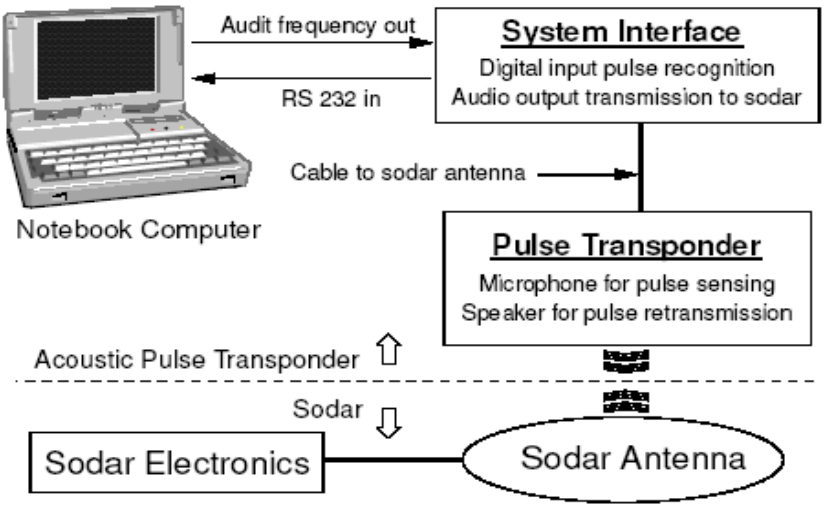

Figure 1.3.2 – Flow Diagram of the Acoustic Pulse Transponder designed for USEPA quality assurance and detailed in Baxter (1994 a & b)

The early stages of a transponder system that aims to be able to find more information about the SODAR's performance is presented in Piper (2008). This transponder system features the use of signals that represent the whole measurement height and due to the signal generation methods it could theoretically represent any wind profile. Further developments in this transponder system were presented in Piper (2010) and tested in an outdoor configuration with two SODARs although the results from one highlighted that the transponder system required two further improvements before it could be a useful part of a comparison method. Part of this thesis contains results presented in these papers and continues the work on this transponder system with the aim of finding out how much information can be obtained about the operation of a SODAR through the use of a transponder containing simulated wind profiles. It is unlikely that a transponder system of this type can explain all of the uncertainty in a SODAR measurement so further alternatives to conventional SODAR-mast anemometry comparisons are required.

1.3.5 Methods to Measure Contributing Aspects of a SODAR's Acoustic Beam Pattern

Two important aspects of SODAR measurements are defined by the SODAR's acoustic behaviour. These need to be known in order to make accurate wind speed estimations and they are influenced by the physical set-up of the SODAR including the changes caused by any baffles employed by the SODAR.

The width and shape of the measurement beam dictate the volume sampled by the SODAR and how this sampling is weighted. Measurements of the acoustic beam shape can be performed in anechoic chambers using the same approach applied to directivity measurements of Hi-Fi loudspeakers by measuring the sound pressure level at many angles in relation to the centre of the sound source. This could be performed by either measuring the whole SODAR array or measuring a single element and creating a model to find the complete directivity of the array. This is often done in SODAR design. Danilov (1992, 1994) presents a method for measuring SODAR calibration parameters in a normal sized anechoic chamber for a single horn and focussing dish SODAR measuring the sound producing element of the SODAR. This method is related to measurements of the temperature structure parameter, C_T^2, and not wind speed but it is of interest here since measurement of the SODAR directivity pattern is part of the procedure. Measurements of the output efficiency and input efficiency of the SODAR transducer are made and then the directivity of the horn is measured and compared to a model. The agreement between the model and measurements are good and therefore this type of directivity model is thought to be reliable for modelling SODAR behaviour. Acoustic measurements of the SODAR directivity only allow for measurement of beam tilt angles if the whole array is measured requiring a very large space.

The angle from the vertical of the tilted beams is used in the conversion from frequency shift to wind speed and any error in the angle used results in incorrect wind speed estimation. In Bradley (2008) it has been shown that an angle error of 1º leads to

5% errors in the wind speed estimation. A technique is presented in Bradley (2010) for measuring the effective beam tilt angle through a level perturbation. Measurements of the wind speed are made using a SODAR fixed to a tilting mechanism. If the effective tilt angle is assumed to be unknown the introduction of a physical tilt of the whole SODAR introduces a known angle. By performing wind speed measurements with the SODAR physically tilted at two or more significantly different physical angles analysis can be performed to to derive the effective beam tilt angle that the SODAR array is using. This method assumes a horizontally stratified flow and a constant wind speed between measurements and therefore several measurements at each tilt angle are required spread over the whole measurement period to find a reliable estimation of the tilt angle. Results from measurements made with an AeroVironment 4000 SODAR are presented and it was found that the the measured mean tilt angle was within 0.2º of the tilt angle calculated from the SODAR array geometry. This method makes no assumptions about the SODAR and only requires a tilt mechanism and a short measurement time. It does not give any information about the beam width of the SODAR. This method will be tested and compared to other methods of measuring beam tilt angles in Chapter 4 of this thesis.

Whilst it is possible to measure the acoustic qualities of individual sound sources from within a SODAR relatively easily knowledge of how baffles alter the behaviour of SODARs is needed to give a true picture of the directivity pattern and tilt angles of a SODAR. Werkhoven (1997) investigates the use of Kirchoff integral theorem to predict the diffraction of side lobe energy at SODAR baffle edges. It is identified that the the baffles need to provide at least 45dB of attenuation to prevent side lobe reflections from solid objects interfering with atmospheric reflections of the main beam. A near field method for finding the velocity potential for different baffle illuminations and shapes is demonstrated. The results of this work do not give a conclusive picture of the full influence of the baffles on the acoustic behaviour of the SODAR with only some design guidelines given.

1.3.6 Summary

Various methods for obtaining the acoustic qualities of a SODAR have been performed but without a complete approach that is suitable for wind energy SODAR measurements. One of the aims of this thesis is to examine the possible approaches for measuring the beam shape and tilt angle in order to find an approach that can be used to reduce the uncertainty of the SODAR measurements.

1.4 Overview of the Acoustic Operation of SODARs

Mono-static SODARs operate by emitting pulses of sound in to the atmosphere and measuring the backscattered signal. The pulse is sinusoidal and it can be written as in the form of Equation 1.4.1 where $A(t)$ is the amplitude envelope applied by the SODAR to form the pulse and $D(\theta)$ is the beam pattern of the SODAR transmitter, ω is the angular frequency of the pulse, t is time, k is the wave number and r is the distance the pulse has travelled.

$$y(t) = A(t)D(\theta)e^{-j(\omega t - kr)} \quad \text{(Equation 1.4.1)}$$

The beam pattern of the SODAR is either formed from an array of loudspeakers or a single loudspeaker and a focusing dish. Each SODAR type will have a different beam pattern but all are based on first order Bessel functions of the form shown in Equation 1.4.2 where a is the radius of the loudspeaker.

$$D(\theta) = \frac{2J_1(ka\sin\theta)}{ka\sin\theta} \quad \text{(Equation 1.4.2)}$$

Figure 1.4.1 shows the behaviour of this function. The result is that the beam pattern of all SODARs have a strong main lobe with some weaker side lobes.

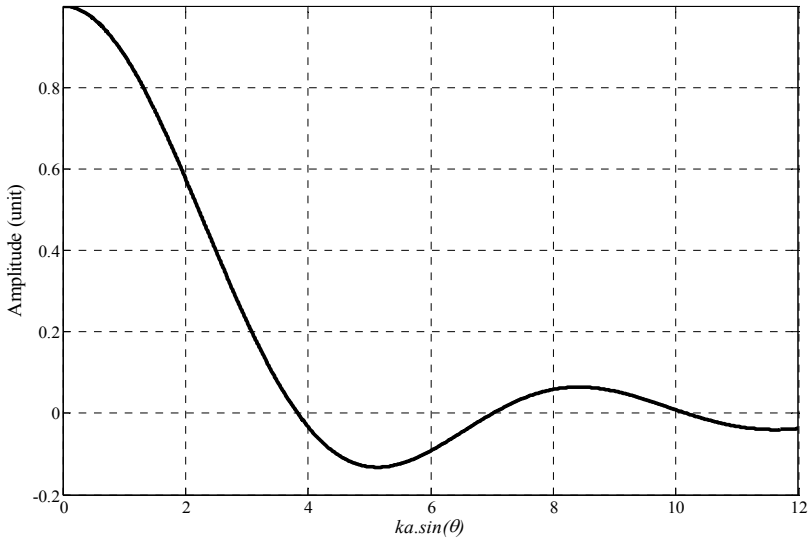

Figure 1.4.1 – Amplitude Vs Angle Function, *ka.sin(θ),* of a First Order Bessel Function

The pulses emitted by the SODAR travel spherically away from the SODAR array and continue to travel until all the energy is dissipated through absorption and scattering. Energy which is scattered at 180 degrees is received by the SODAR as backscatter. Therefore the atmosphere can be thought of as a space containing many partial reflectors which reflect some energy back towards the SODAR. Each of these reflections has spherical wave behaviour but as the SODAR only appears on a small portion of the arc, demonstrated in Figure 1.4.2, the behaviour of the sound recorded by the SODAR can be considered to be approximately plane.

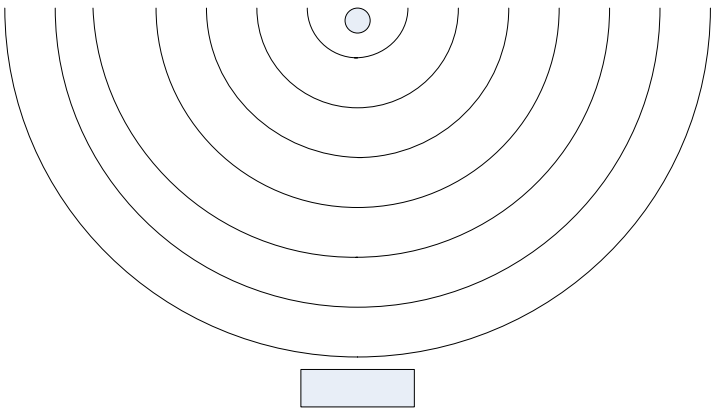

Figure 1.4.2 – Wave Front Shape of a SODAR Reflection

The energy received by the SODAR at a single point in time is a spatial average over a volume which has a weighting function formed from the beam pattern of the SODAR and the amplitude envelope applied in the range gate extraction part of the SODARs processing. The shape of the function means that most of the energy received by the SODAR is from within a cone with a width of between 10 and 15 degrees depending on the frequency used, the shape of the SODAR's beam pattern and the envelope of the range gate. Different SODARs employ different range gate envelopes and have differing beam patterns, although most are similar, resulting in the effective volume of the atmosphere measured by each SODAR not being the same . This will be explored further in Chapter 2 where the directivity of different shaped speaker arrays will be modelled and the effects on the SODAR measurement explained.

The sources of reflection for mono-static SODARs are temperature fluctuations that have a size comparable to half a wavelength. The fluctuations travel with a velocity that is the sum of the mean wind speed and local turbulence. Sound which is reflected by a moving medium is shifted in frequency according to the Doppler Effect. Therefore sound received by the SODAR will have a frequency content which is directly related to the wind speed at the point of reflection. As the sound received by the SODAR at a single point in time is a spatial average of many reflections, the recorded backscatter is a signal which has a frequency peak which corresponds to the mean wind speed in the volume but with spectral width determined by the level of variation over the measurement volume. The magnitude of the temperature fluctuations will also vary and therefore the strength of the return will change accordingly.

The amplitude of SODAR echoes decay in time due to the effects of spherical spreading and atmospheric absorption. The amount of decay is dependent on the atmospheric conditions at the time of the measurement. Temperature, humidity, and the frequency of the sound all affect the amount of absorption. The following equations from 1.4.3 – 1.4.9, that are used to find the amplitude envelope of a SODAR echo, are from Salomons (2001). Equation 1.4.3 describes the amplitude envelope of a

SODAR echo where σ_s is the scattering cross section, c is the speed of sound, τ is the pulse duration, α is the absorption of air and z is the height of the echo source. This envelope scales with the power transmitted by the SODAR.

$$E_t = \sigma_s \frac{c\tau}{2} \frac{e^{-2\alpha z}}{z^2} \quad \text{(Equation 1.4.3)}$$

The scattering cross section is described by Equation 1.4.4. where λ is the wavelength of the sound, C^2_T is the temperature structure function and T is the lapse rate corrected temperature based on the ground temperature, T_G. Typical values of C^2_T are close to 10^{-4}.

$$\sigma_s = 6 e^{-4} \pi^{-1/3} \frac{C_T^2}{T^2} \quad \text{(Equation 1.4.4)}$$

The absorption of sound in air is described in the empirical formula shown in Equation 1.4.5 where f is the frequency of the sound in Hz, t is the lapse rate (L) corrected temperature T divided by the ideal maximum temperature, 293.15 K, P is the atmospheric pressure given by Equation 1.4.6, f_n and f_o are relaxation frequencies for nitrogen and oxygen respectively and are calculated using Equations 1.4.7 and 1.4.8 respectively. g is the force due to gravity, which is approximately 9.81 ms^{-2}, and R is the specific gas constant, which is 287 $\mathrm{J\,kg^{-1}\,K^{-1}}$ for air. H is humidity and it is calculated using Equation 1.4.9 where RH is relative humidity in percent.

$$\alpha = 8.686 f^2 t^{1/2} \left(\frac{1.84 e^{-11}}{P} \left(\frac{0.1068 e^{-3352/T}}{f_n + f^2/f_n} + \frac{0.01275 e^{-2239.1/T}}{f_o + f^2/f_o} t^{-3} \right) \right) \quad \text{(Equation 1.4.5)}$$

$$P = \left(\frac{T}{T_G} \right)^{\frac{g}{L} R} \quad \text{(Equation 1.4.6)}$$

$$f_o = P \left(24 + 40400 H \frac{0.02 + H}{0.391 + H} \right) \quad \text{(Equation 1.4.7)}$$

$$f_n = \frac{P}{t^{1/2}} \left[9 \right] 280 \mathrm{He}^{-4.17 f^{-3} - 1} \left[\right] \quad \text{(Equation 1.4.8)}$$

$$H = \frac{RH}{P} 10^{4.615 - 6.8346 \frac{T_G}{T}^{1.261}} \quad \text{(Equation 1.4.9)}$$

From the above set of equations the expected time-amplitude envelope of a SODAR echo can be predicted for a given set of atmospheric variables. The effects of the different variables contained within the envelope equations are explored at length in Harris (1966), Evans (1972) and Bass (1972 and 1995).

A SODAR echo has a frequency shift according to the mean wind speed in the direction of the beam, a spectral broadening due to the velocity and reflection strength variation across the measurement volume, amplitude fluctuations which follow variation in the magnitude of temperature fluctuations and a time-amplitude envelope which decays in a partly exponential manner. The echo arrives at the SODAR from the direction in which the SODAR emitted the corresponding pulse and it has approximately plane wave behaviour. The SODAR itself contains a signal chain performing a combination of filtering, amplification and Fourier analysis in order to calculate a wind speed estimate. The aspects of this chain vary between different SODARs but are all aiming to find a reliable estimate of the wind speed. The different methods are discussed at length in various texts including the WISE report, detailed in the following section, and Bradley (2008) and some investigation of some aspects of this process that have an obvious and quantifiable effect on the wind speed estimation are discussed in Chapter 2.

1.5 Statement of the Aims of This Thesis

The primary objective of this work is to improve the accuracy and understanding of mono-static SODAR measurements by applying novel and independent measurement methods in combination with established ones to mono-static SODARs and exploring the statistical significance of SODAR measurements

with a focus on the measurements meaning to the wind incident or turbines. Conventionally the quality of SODAR measurements are determined by making comparisons with measurements made by mast mounted anemometers. This has some inherent problems due to the differences in the actual measurement which is being carried out and therefore such comparisons are limited to a coarse indication of measurement accuracy and highlighting strong mismatches rather than ensuring actual measurement accuracy. Many previous studies have been carried out using comparisons to mast mounted instruments with some studies suggesting rules for interpreting the differences between the two measurements. Some studies have suggested alternative methods to this approach although a comprehensive method has yet to be created. By review of this past work and through the development of a mast independent calibration techniques it is hoped that mono-static SODAR accuracy can be verified and quantified. This work should also increase understanding of the processes which affect mono-static SODAR measurements and improve acceptance of mono-static SODAR measurements in the wind energy field.

The principle research questions are as follows:

i) **Can the quality of SODAR measurements be improved and uncertainty reduced through theoretical analysis of the acoustic behaviour of SODARs?**

ii) **Can a transponder system be created that goes further than a simple diagnostic test to find information about the SODAR's operation and offer the possibility of direct comparison between the measurements of different SODARs with the ability to test in the field?**

iii) **What is the best method or methods for finding a SODAR's beam shape and tilt angle?**

iv) **Can these aspects be combined into a unified approach to**

improve SODAR measurement certainty and therefore increase the usefulness of SODAR measurements for the wind industry?

1.5.1 The UpWind Project

This thesis is written as part of the UpWind Project. The UpWind project is a European Government sponsored project which aims to increase the size of wind turbines for both on shore and off shore use by solving the design problems involved in up scaling turbine sizes to 8-10 MW. The work package it is part of is an examination of the use remote sensing techniques, focussed on LIDAR and SODAR, as potential replacements for mast mounted measurements. Specifically this thesis aims to form the SODAR part of Section 2 of the work package although there will be some overlap with Section 1. Section 2 is an investigation into traceable calibration techniques for remote sensing instruments and Section 1 is an in depth description of the measurement process. It is debatable whether a calibration is actually what is required for SODAR measurements to be useful for wind energy and it is thought that a verification is a more appropriate term for what can be applied although this is a semantic debate. The effect on the measurement made by a SODAR of a certain physical set-up and operational parameters is crucial to reducing uncertainty. The only part of the operation that offers the opportunity for a true calibration beyond individual component testing is the beam tilt angle and some effort is given to finding the best methods for quantifying this.

Within the UpWind work package investigation into several aspects of the use of remote sensing in wind energy has been and continues to be performed. This includes work on the measurement of turbine power curves in complex terrain detailed in Gómez (2010b), determination of the uncertainty in power curve measurements shown in Wagner (2010b)and measurement optimization for complex terrain shown in Foussekis (2010). This work is all carried out using LIDAR instruments and necessitates the work in Gómez (2010c) and Hill (2010a) on finding methods to correct or filter for cloud and fog. LIDARs are also required to have a traceable

calibration methods with work on this is detailed in Hill (2010b). How this is related to SODAR calibration will be discussed in Chapter 5.

1.6 Outline of Methods to Explore SODAR Measurement Uncertainty

The methods explored in this thesis are split into three parts following the first three research questions: theoretical analysis, transponder measurements and directivity measurements. Each adds a different aspect to improving the uncertainty and interpretation of SODAR measurements. The theoretical analysis uses acoustic theory to explore the behaviour of different common SODAR configurations focussing predominately on the effects of array geometry. The transponder measurements use a transponder system that has been developed for this thesis with some basis in the work carried out in Baxter (1994). Directivity measurements are carried out using several different methods with comparisons between these methods and recommendations of how to perform further measurements. These aspects of a SODAR's operation can lead to the largest uncertainties in the wind speed estimation and therefore it is of great importance to find a method that can measure these details to a high resolution. These separate aspects are then discussed and combined to answer the 4^{th} research question.

1.7 Summary

The problem that has motivated the work carried out for this thesis is how to reduce the uncertainty in SODAR measurements so that they can be used in the wind industry. Details of the initial development of SODARs and their potential use for the wind industry have been given. Then a review of past efforts to explain SODAR measurements, predominately through comparisons to mast mounted anemometry, has been carried out. The state of the art approach to SODAR comparison involves the use of other sensors as calibration reference points. This is suggested in the WISE report and carried out in the Myres Hill comparison experiment. These methods mean the best result achievable is that the SODAR has the uncertainty of the reference sensor.

Methods to reduce SODAR uncertainty without making comparisons to other sensors are required. A simple transponder system is one alternative although transponders have only previously been used as a diagnostic tool. Methods to accurately measure aspects of a SODAR's directivity form another approach that can be taken since volume averaging and beam tilt angles contribute significantly to the SODAR measurement uncertainty. Details of previous calibration work carried in the WISE report has been shown. This work directly precedes the work carried out for the UpWind project and therefore this thesis. The acoustic operation of SODARs has been examined to give an introduction to the concepts involved. The aims of the thesis have then been stated with theoretical analysis, development and testing of a transponder system, measurement of SODAR directivity and the integration of these aspects into one complete method being the principle aims.

2. Theoretical Comparison of Known Differences Between SODARs

2. Theoretical Comparison of Known Differences Between SODARs

2.1 Introduction

When comparing measurements from different SODARs the differences between how the SODARs operate need to be taken into account as well as differences in the locational set-up of the SODARs. If all aspects of the operation of the SODAR are known then this can be done theoretically. Taking the hypothetical case of two SODARs situated in exactly the same place at the same time it is possible to examine the effect of the various parameters on the measurements made since the physics of sound travelling through the atmosphere will be identical in each case. Both physical and processing parameters can be explored in this way.

The physical parameters of a SODAR are related to the directivity pattern, which can be modelled using a far field model of the radiation from two dimensional speaker arrays. The width of the central lobe alters the effective volume from which reflections are recorded. The directivity pattern in combination with the baffle shape alter the influence of fixed echoes on the SODAR measurement. The angles at which the SODAR beams are tilted affect the resolution, the volume separation of the beams and the susceptibility to errors caused by a non level set-up, which can either be a result of incorrect physical set-up or a consistent phase problem across a speaker array.

The processing parameters that can be tested are either inherent to the SODAR design or ones which are user selectable and therefore some optimisation is possible. The user selectable parameters include start height and step size and frequency. The parameters that are usually inherent to the SODAR design are averaging and peak detection methods, Doppler shift calculation method, pulse envelope shape and data rejection methods. To some degree beam tilt is a processing parameter but since the main source of error caused with this parameter happens when the effective physical beam tilt angle does not match the beam tilt angle that is used in the processing it is

preferable to consider this a physical parameter.

This chapter will examine each of these issues in turn and quantification of the effects of the possible options in each case will be given. Some of the topics described have been covered in depth in other works so are only outlined here with references for the sake of providing a full description.

2.2 Far-field Model of Sound Radiation from 2D Speaker Arrays

Analytical models for the behaviour of sound sources are well established in text books such as Kinsler (2000). The underlying principle is that any sound source can be modelled as an infinite number of point sources. A point source is a theoretical source which can be described as an infinitesimally small pulsating sphere radiating energy equally in all directions. An equation exists that describes the directional behaviour of a circular source such as a speaker as shown in Equation 2.2.1 where $H_s(\theta)$ is the angular dependent amplitude function for the source, J_1 is a Bessel function of the first kind, k is the wave number and a is the radius of the source.

$$H_s(\theta) = \frac{2J_1(ka\sin\theta)}{ka\sin\theta} \quad \text{(Equation 2.2.1)}$$

An example of this function is shown in Figure 2.2.1 for a ka value of 6.65 based on a frequency of 4500Hz and a source radius of 8cm. The assumption made in this equation is that the complete surface of the source vibrates in unison. This is a reasonable assumption when considering the impedance change at the end of a horn loudspeaker which causes a volume of air to move in unison as if it was a piston

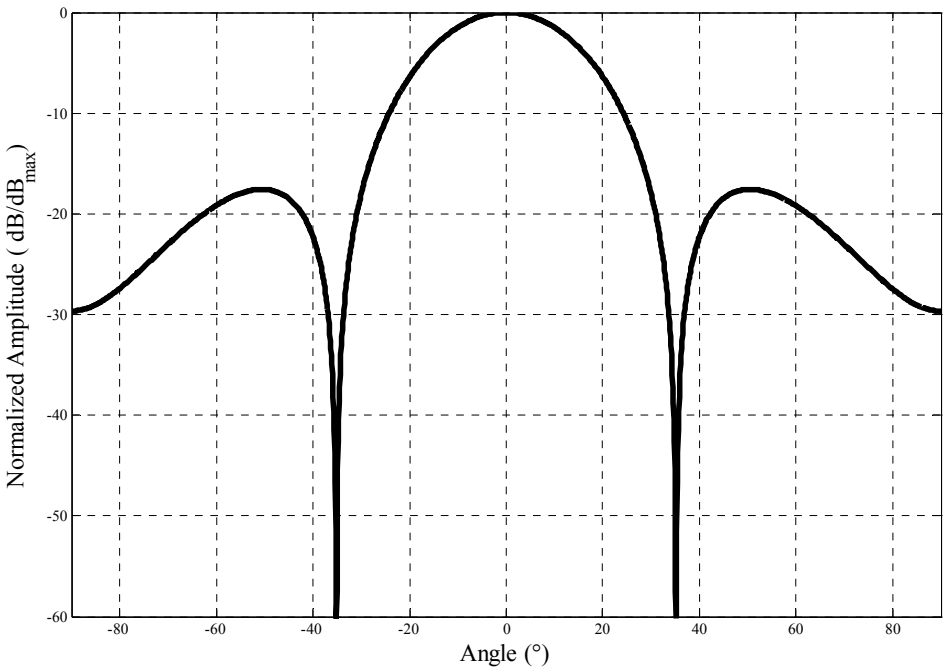

Figure 2.2.1 – Directivity pattern, $H_{s,}$ for a single circular source.

Expressions exist for the combination of a column of several separate monopole sources that emit either the same sound, Equation 2.2.2, or sounds with a known phase relationship, Equation 2.2.3, where $H_c(\theta)$ is the angular dependent amplitude function for the combination of point sources in a column, N is the number of sources in the column, d is the separation between the centre of each source and θ_O is the phase shift.

$$H_c(\theta) = \frac{1}{N}\frac{\sin\left[\frac{N}{2}kd\sin\theta\right]}{\sin\left[1/2\,kd\sin\theta\right]} \quad \text{(Equation 2.2.2)}$$

$$H_c(\theta) = \frac{1}{N}\frac{\sin\left[\frac{N}{2}kd\sin\theta - \sin\theta_0\right]}{\sin\left[1/2\,kd\sin\theta - \sin\theta_0\right]} \quad \text{(Equation 2.2.3)}$$

These equations give the directivity pattern generated by a column made up of monopole sources. Figure 2.2.2 shows examples of these functions.

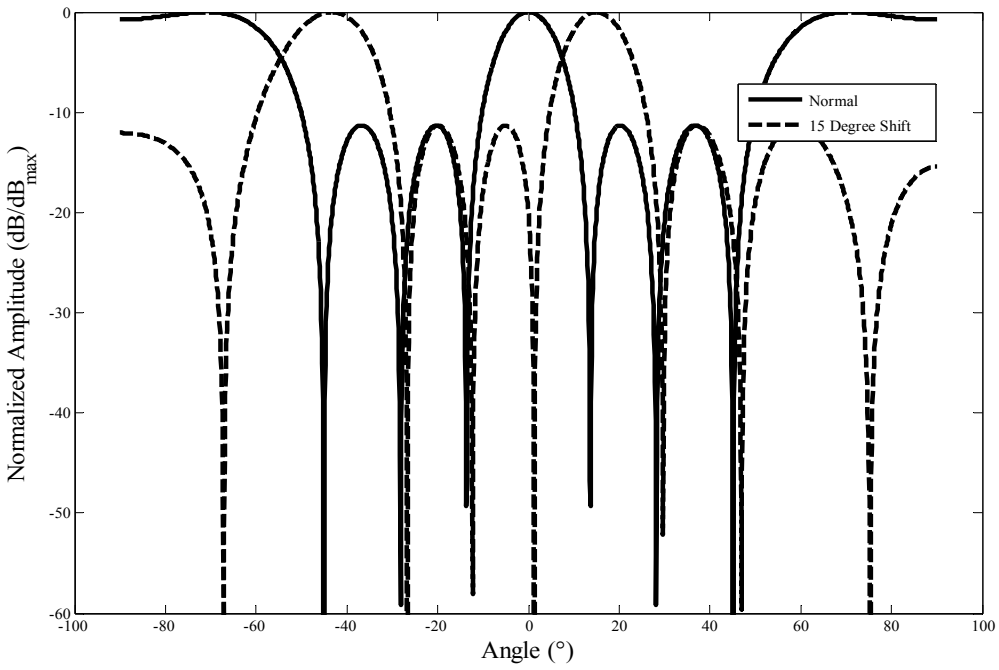

Figure 2.2.2 – Directivity function, H_c for a column of 4 point sources with a separation of 8cm at 4.5 kHz with no Beam shift applied (solid) and a 15° shift applied (dashed).

The addition of the sin θ term rotates the directivity pattern by the angle θ. In order to have a column of circular sources it is necessary to use the product theorem, which states that it is possible to multiply two directional factors to achieve a combined directivity. In order to expand from a single column of sources to a 2-dimensional array this theorem is also used. It is the equivalent of each column combining to create a single source that represents that column and then these being combined in the same way but as a row or being relative to the y axis instead of the x axis. This is shown in Figure 2.2.3.

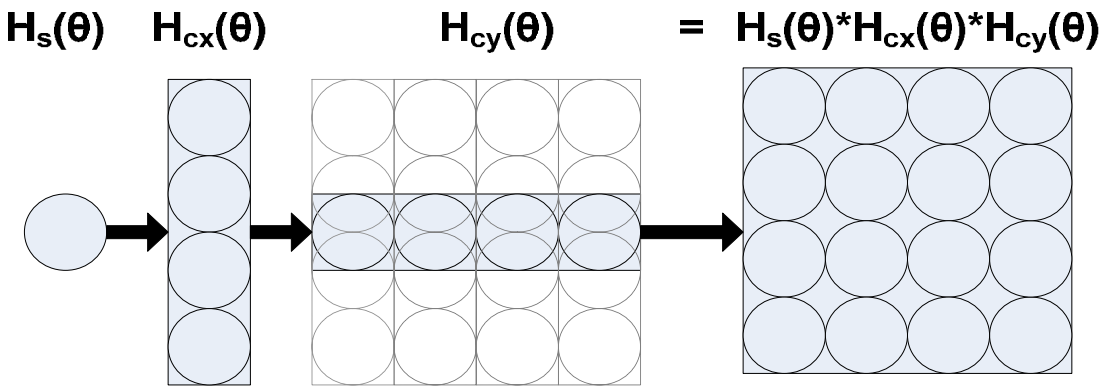

Figure 2.2.3 – Calculation of the directivity (H) of a 4*4 square array using the directivity of its layout (H_c) and source type (H_s).

In this way it is possible to create an array of a square or rectangle array containing any number of sources. In order to create more complicated array shapes the H_c terms need to be expanded to allow for the various layouts of sources that are possible. Equation 2.2.4 describes the directivity pattern from a square array of four loudspeakers expanded in full where x is given by Equation 2.2.5 with θ being the angle with respect to the x axis, and y by Equation 2.2.6 with ϕ being the angle with respect to the y axis.

$$H(\theta,\phi) = H_s(\theta,\phi)\left[\exp(-jx/2) + \exp(+jx/2)\right]\left[\exp(-jy/2) + \exp(+jx/2) + \exp(+jx/2) + \exp(+jy/2)\right]$$

(Equation 2.2.4)

$$x = kd\sin\theta\cos\phi/2 \quad \text{(Equation 2.2.5)}$$

$$y = kd\sin\theta\sin\phi/2 \quad \text{(Equation 2.2.6)}$$

Such an expression can be condensed into a more convenient form by describing each separate column using Equation 2.2.3 and and then substituting the resultant term for the exponential terms relating to x in Equation 2.2.4. Equation 2.2.7 shows this for the square array of four speakers example.

$$H(\theta,\phi) = H_s(\theta,\phi)H_{cx1}\left[\exp(-jy/2) + H_{cx2}\exp(+jy/2)\right] \quad \text{(Equation 2.2.7)}$$

Two examples of arrays that can be modelled in this way are a diamond shape and a staggered rectangle each consisting of 12 sources. The layouts for these arrays are shown in Figure 2.2.4.

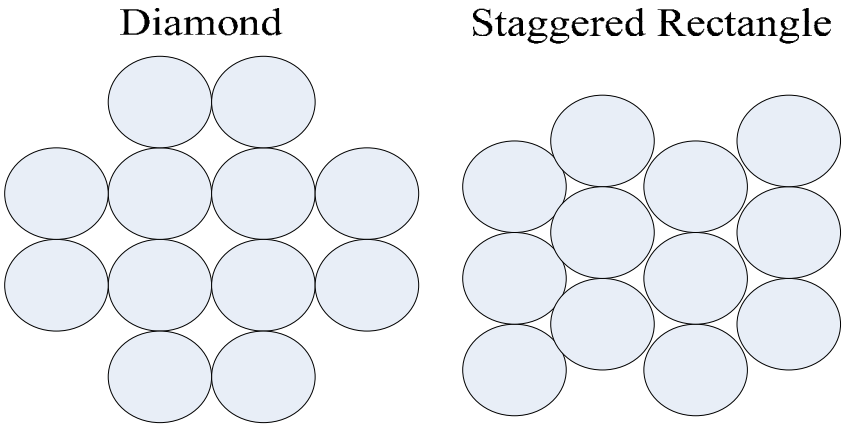

Figure 2.2.4 - Two examples of speaker array layouts.

For the diamond shaped array two H_{cx} terms can be used with 4 terms in *y (-3j,-j,j and 3j)* to create the model. For the staggered rectangle two H_{cx} terms are also required even though there are only 3 speakers in each column to account for the differences in position relative to the array centre of columns 1 and 3 compared to 2 and 4. The same 4 terms in *y* are used again. Figure 2.2.5 shows a comparison of the directivity patterns at 4.5 kHz for these two speaker arrays and the simple 4*4 square array shown in Figure 2.2.3 using circular sources with a diameter of 10cm.

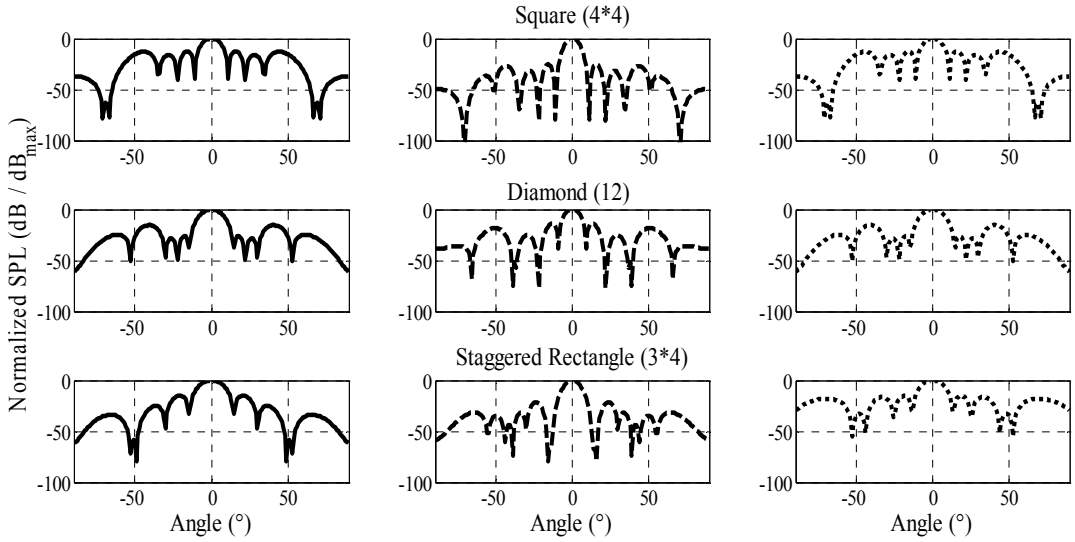

Figure 2.2.5 – Comparison of the 4.5 kHz directivity of three different array shapes using identical sources showing across the arrays' Y-Axis (solid), diagonal (dashed) and X-Axis (dotted).

Figure 2.2.5 shows that all three array shapes produce similar directivity patterns although there are some notable differences between them. The square array has a narrower central lobe, with a FWHM of 13.2º compared to close to 16º for the other two arrays, which is due to the increased number of speakers in this shape. The square and diamond shape arrays have the same layout only with the corner speakers removed in the diamond array. The directivity patterns of these two shapes shows the same number of nulls and peaks at similar angles but the strength of second and third lobes is weaker on the x and y axes for the diamond array and stronger across the diagonal axis. In both cases the pattern is identical across the x and y axes as the arrays are identical along these axes. The staggered array shows a different directivity pattern for each axis as the speaker distribution is different across each one. It is noticeable that all of the side lobes are significantly smaller than the central lobe across the y-axis and the diagonal. This is a result of the closer packing of the speakers and the odd number of speakers along the y axis. From this it is possible to conclude that larger numbers of speakers result in narrower central lobes but also stronger side lobes and that closer packing of sources and odd source layouts can reduce the side lobe energy produced by the speaker array. It should be noted that SODAR arrays commonly employ a larger number of speakers than those modelled here, with the exception of those which use a

focussing disc, and therefore the width of the SODAR beams are usually narrower than those shown in this section.

2.3 Measurement Volume Differences

One difference between the measurements made by two different SODARs is the volume from which reflections are received for each range gate. It is possible using some known and predictable quantities to calculate a comparative parameter that represents this volume. The measurement beam of a SODAR can be considered a cone shape where the edges of the cone are the points at which the sound level is significantly less than the the sound level at the centre such that the contribution to the reflection recorded by the SODAR is negligible. A 6 dB reduction represents a halving in the sound pressure level (SPL) and therefore this is assumed to be an appropriate point at which to limit the width of the SODARs measurement cone and the angular width between the -6dB on each side of the centre is known as the Full Width Half Maximum (FWHM). The distribution of sound energy across the cone is dependent on the shape of the SODAR beam along the x and y axes, since the directivity pattern of the SODAR at a certain height is a two dimensional amplitude function, and the range gate windowing function in the z or vertical direction. The range gate windowing function is an amplitude window applied to a section of the recorded backscatter signal that has the timing from within a certain distance range based on assumptions on the speed of sound. Typical windowing shapes include Hann, Hamming and Gaussian. The shape of the SODAR beam can be predicted using the model shown in Section 2.2. Table 2.3.1 shows the FWHM for each of the three arrays modelled in Section 2.2 along with the cross sectional area of the cone formed from these points at a height of 100m for SODAR pulse frequency of 4.5 kHz .

	X-axis FWHM (°)	Y-axis FWHM (°)	Area at 100m (m^2)
Square (4*4)	13.2	13.2	432.2
Diamond (12)	15.7	15.7	623.7

Staggered (12)	17.78	16.48	711.6

Table 2.3.1 – Angular width and cross sectional area at 100m for 3 SODAR array shapes for sound at 4.5 kHz.

Using this information the volume of a cone section can be calculated for each array. The height of the cone section is determined by the size of the range gates used by the SODAR and the effective reflection volume parameter (ERVP) can be determined by multiplying this volume by the amplitude distributions given by the beam and range gate windowing function. For the purpose of making a comparison of different arrays the ERVP is defined as a calculation over a 10m range gate from 95m to 105m. The volume of the cone section is calculated first based on the FWHM and then this is multiplied by the amplitude functions given by the beam and windowing shapes which are given as a value between 0 and 1. The frequency should be given in each case as different SODARs are designed with different optimum frequencies. The calculation of an ERVP is demonstrated in Figure 2.3.1.

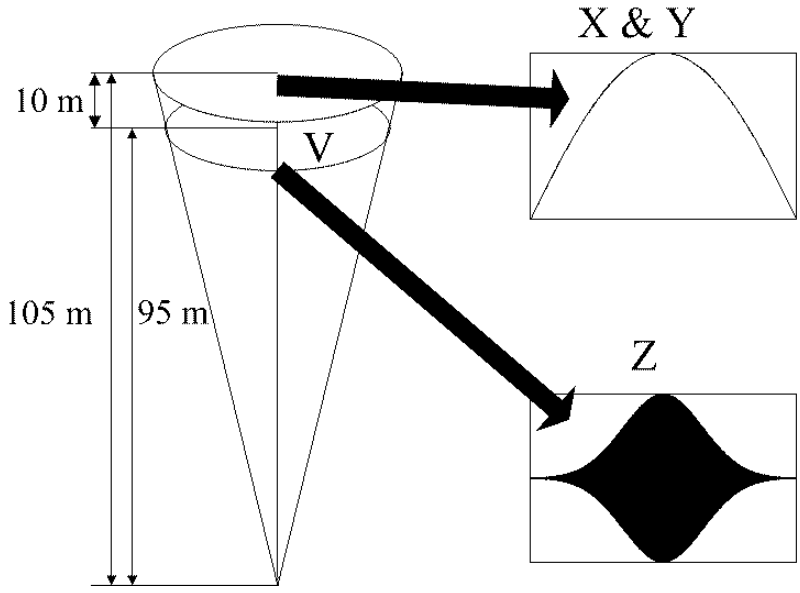

Figure 2.3.1 – Source of coefficients for calculating ERVP.

The formula for the ERVP is shown in Equation 2.3.1 where V is the volume of the cone section calculated using Equation 2.3.2 and X, Y and Z are coefficients found

from analysis of the directivity pattern and the window shape.

$$ERVP = V \cdot X \cdot Y \cdot Z \quad \text{(Equation 2.3.1)}$$

$$V = \left(\frac{1}{3} \cdot r_{x105} r_{y105} 105\right) + \left(\frac{1}{3} \cdot r_{x95} r_{y95} 95\right) \quad \text{(Equation 2.3.2)}$$

X and Y are derived from the directivity pattern and they give an estimate of the proportion of the maximum possible energy that beam shape gives. They are both found by normalizing the section of the central beam that occurs inside the FWHM limits to form a 1 by 1 square. This is achieved by finding the minimum sound level in the beam section and taking this away from all the values within the beam section and then dividing by the maximum value in the section. This can then be plotted against an axis of zero to one with divisions based on the original number of points between the FWHM limits. The result is a simple curve that a quadratic or a higher degree polynomial can be fitted to allowing for analysis of the area under the curve. Figure 2.3.2 shows an example taken along the x-axis of the square array with residuals shown. A definite integral can then be computed to find the area under the curve and therefore the coefficient. It has been found that the residuals for a quadratic are too high. Cubic and 4th degree polynomials have also been tried but it has been found that a 5^{th} degree polynomial has sufficiently small residuals to produce satisfactory estimate of the coefficients.

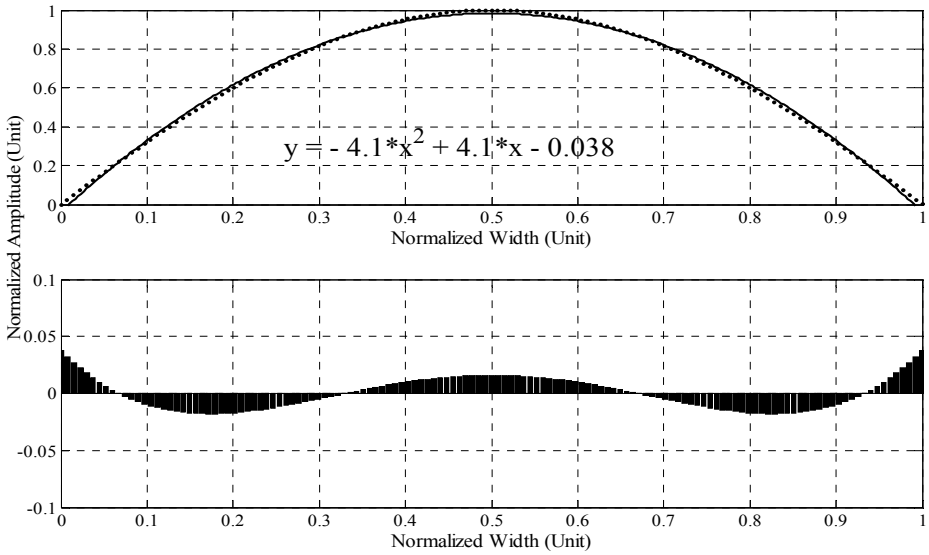

Figure 2.3.2 – Example of curve fitting to find X coefficient for the square shaped array.

As a Gaussian window of 60 ms is being used to calculate the ERVP for each array the Z coefficient is therefore the same for all array shapes. The shape of the Gaussian is defined using Equation 2.3.3 where *a* controls the peak height which is 1, *b* controls the centre position which is 0.5 and *c* controls the shape of the pulse and 0.15 is selected for this.

$$f(x) = a\,e^{\frac{-(x-b)^2}{2c^2}} \quad \text{(Equation 2.3.3)}$$

Figure 2.3.3 shows an example of this pulse shape. SODARs use a range of windows but most have similar characteristics to a Gaussian. Equation 2.3.3 can be integrated directly to give the area under its curve and therefore the Z coefficient of the ERVP. This result is shown in Equation 2.3.4.

$$F(x) = \int_{-\infty}^{\infty} a\,e^{\frac{-(x-b)^2}{2c^2}}\,dx = ac\sqrt{2\pi} \quad \text{(Equation 2.3.4)}$$

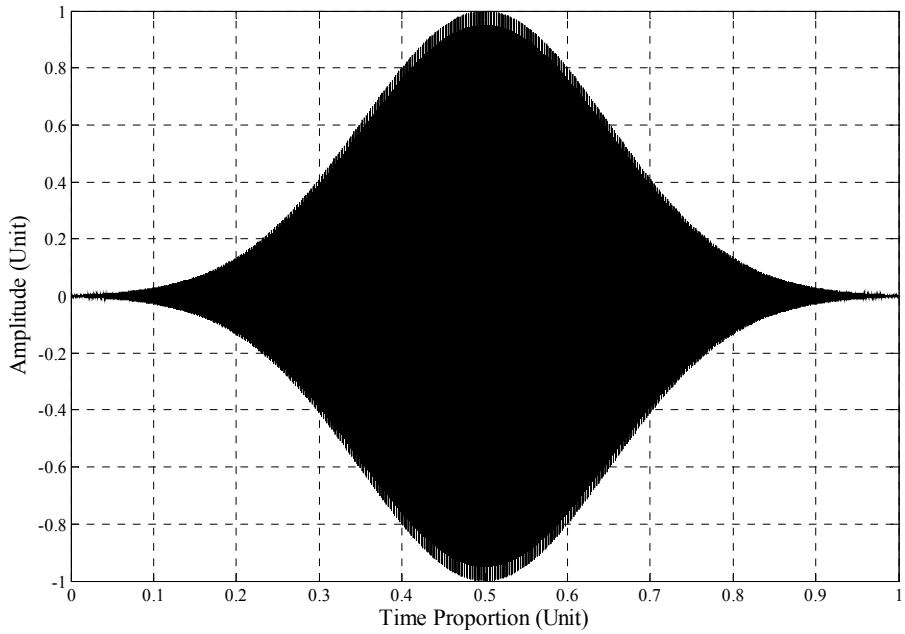

Figure 2.3.3 – Signal multiplied by the Gaussian window used to calculate ERVP.

For the Gaussian coefficients selected the Z coefficient is calculated to be 0.376. Table 2.3.2 shows the calculation of the ERVP for the three array shapes that have been modelled in this chapter already.

	Cone Section Volume – V (m^3)	X Coefficient (Unit)	Y Coefficient (Unit)	Z Coefficient (Unit)	ERVP (m^3)
Square (4*4)	4325.9	0.654	0.654	0.376	696
Diamond (12)	6241.9	0.643	0.643	0.376	971
Staggered (12)	7122.1	0.634	0.627	0.376	1065

Table 2.3.2 – The ERVP and the coefficients used to calculate it for the 3 SODAR array shapes.

The ERVPs calculated in table 2.3.2 show that there is significant difference in the reflection volume of different shaped SODAR arrays. A wind speed measurement made by a SODAR is the average wind speed over this volume. Therefore the

differences in ERVP will only cause small differences in the measurements made by two different SODAR arrays and the range of these differences are dependent on the strength of the turbulence found in the volume with differences in complex terrain being significantly higher than those found in simple terrain. The Square array shape is more subject to turbulent variations as it has a smaller ERVP than the other two shapes; it is also more comparable to measurements made by mast mounted anemometers. It is clear from Table 2.3.2 that the X, Y and Z coefficients are similar for all the array shapes modelled. The outcome is that the effective measurement volume measured by a SODAR is approximately 15% of the physical volume of a cone with a width based on the SODAR beams FWHM.

This information can be used to compare the volume of air that passes a wind turbine over a certain time and the probability that the measurement is representative of actual wind conditions can be calculated based on turbulence statistics. The ERVP, derived above, is used to find the volume measured in a 10 minute average and this can be compared to the volume of air incident on a turbine over the same period. Statistical parameters that describe turbulence can then be used to find how related the volumes are given that the volume measured by the SODAR is much smaller than the volume incident on the turbine and that the volumes are separated by a certain distance. This comparison is specific to each measurement as the size of the turbine, separation distance and terrain are different in each case.

A hypothetical example is given here where, initially, separation distance is neglected and the SODAR is placed in the same space as the turbine. The turbine has a rotor radius of 40m and a hub height of 90m. The SODAR uses the same Gaussian window used to calculate the ERVPs which results in range gates with a span of 10m. In order to calculate the volume of air passing the wind turbine over a ten minute period the velocity of the air needs to be known. A typical wind profile will increase in speed up to a certain height following a Ekman spiral but for ease of calculation a mean speed of 10ms across the whole turbine height is used. The volume passing the turbine can be calculated by multiplying the cross sectional area of the turbine by the

amount of air that passes or the distance that the first air has travelled over the 10 minute period, giving a cylinder of air as shown in Figure 2.3.4.

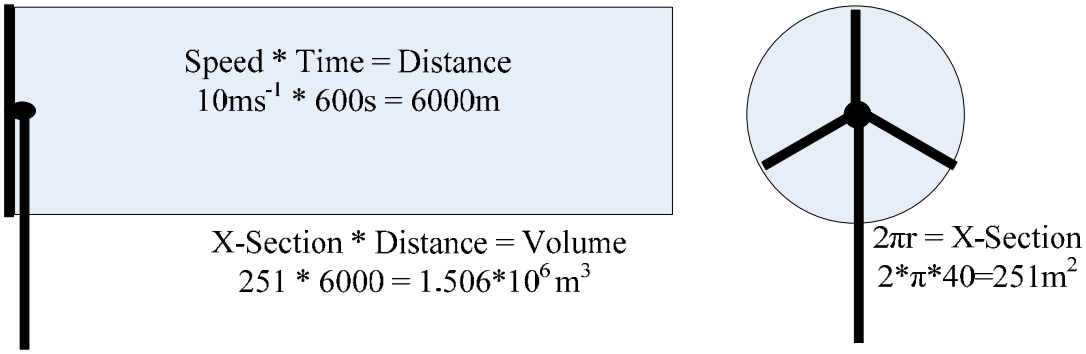

Figure 2.3.4 - Calculation of volume of air passing a turbine.

Using the parameters set for this comparison the volume of air passing the wind turbine of a ten minute period is $1.506*10^6$ m^3. In order to compare this to the volume measured by a SODAR this needs to be split into sections that match the range gate size employed by the SODAR in question. The ERVP is calculated for a 10 metre range gate centred at 100m so the resultant volume for comparison in this example is $3.253*10^5$ m^3. The SODAR measurements can be thought of as snap shots of the volume within each beam. If each set of three snapshots is assumed to take 6 seconds to record then the total number of measurements made in a ten minute period is 100 and the measured volume is therefore 100 times the ERVP. Each set of three beams is assumed to represent only one measurement volume since all three are needed to give one wind speed estimation and therefore can be thought of as measuring separate aspects of the same volume. There is some separation in both space and time between each beam but this is neglected here. Table 2.3.3 shows the volumes measured by each of the three SODAR array shapes modelled in this Chapter over ten minutes and as a ratio of the volume that passes the turbine example for the same period and corresponding height range.

	ERVP (m^3)	10 Minute Volume (m^3)	Ratio of SODAR Volume to Turbine Volume (m^3)
Square (4*4)	696	69600	0.014

Diamond (12)	971	97100	0.019
Staggered (12)	1065	106500	0.024

Table 2.3.3 – Ratio of volume measured by a SODAR to the volume passing a turbine over a 10 minute period for a 10m range gate centred at a height of 100m and with a wind velocity of $10ms^{-1}$.

The ratio changes with respect to the assumed wind as higher wind speeds result in larger amounts of air passing the turbine without increasing the volume measured by the SODAR. This is shown in Figure 2.3.5.

Figure 2.3.5 – Ratio of the volume measured by 3 SODAR array shapes to the volume passing

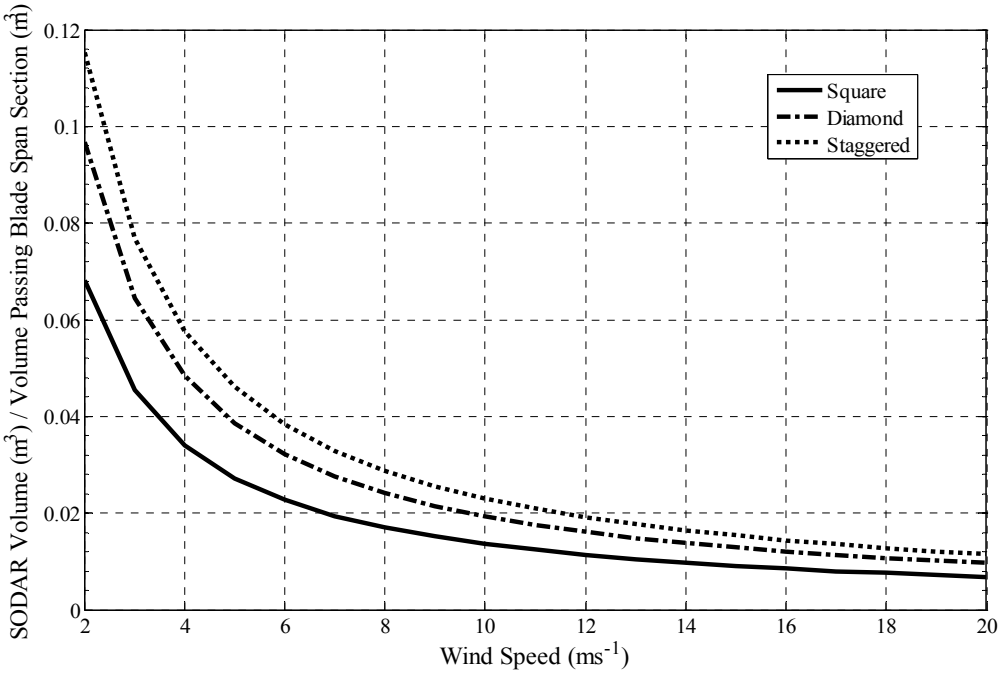

a turbine example for the 10m range gate centred at 100m.

At low wind speeds the size of the volume measured by the SODAR tends towards that which passes the turbine and it is possible at really low speeds that the SODAR is measuring parts of the same volume more than once. However commercial wind turbines do not operate at these speeds so that is not significant. This is the comparison for a single range gate. The SODAR measures several ranges gates that coincide with the turbine blade span that overlap in space with the centre of one range gate occurring at the limit of adjacent range gates. Therefore the effective measurement volume

sampled by the SODAR for the profile in the range of the turbine blade span is the sum of the volume measured in all the range gates coinciding with the turbine. Figure 2.3.6 shows the ratio of the effective volume for the whole profile to the total volume passing the turbine.

Figure 2.3.6 – Ratio of the whole profile volume measured by 3 SODAR array shapes to the

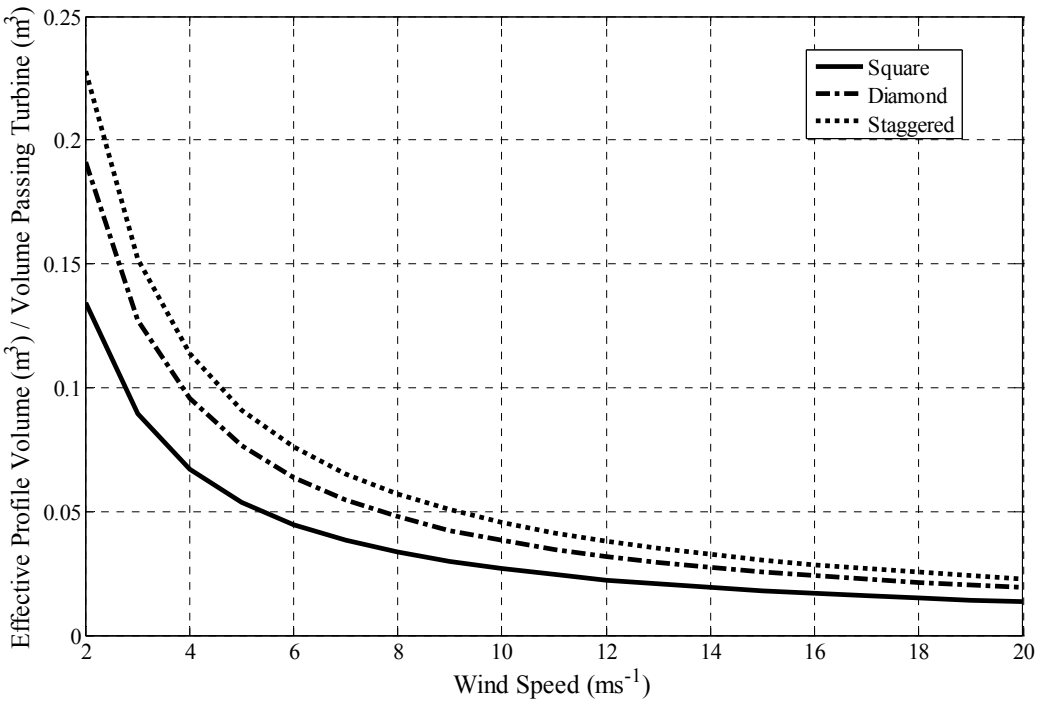

total volume passing a turbine example.

The ratio of the profile volume to the whole volume passing the turbine shows that the SODAR measures around 5% of the volume of the turbine for the most common wind speed range reducing to less than 3% at higher wind speeds. If the positions of the SODAR and wind turbine are now separated by a realistic distance a method for stating whether the volume measured by the SODAR is statistically representative of the volume incident on the turbine is required. In order to carry out this kind of comparison a model of the wind behaviour in the local area of the turbines and the SODAR based in fluid dynamics is required. In simple terrain this model should show that the relationship between the wind at the two locations is linear with increasing speed and therefore the statistical significance of each SODAR measurement will be

high. In complex terrain the relationship is less likely to be linear in relation to speed and the statistical significance of the SODAR measurements is reduced.

The calculation of the SODAR measurement volume and the effect this has on the statistical significance of the SODAR measurement with regards to a wind turbine is a complicated process and is individual to a particular measurement site and SODAR. Here it has been shown that due to the weighting within the measurement volume caused by the directivity and the windowing function applied by the SODAR the effective volume measured is approximately 15% of the volume of a cone with a width based on the FWHM of the SODAR beam. Using this information the volume passing a turbine can be correlated with the volume measured by the SODAR in question. This would be simple if the SODAR and the turbine were situated in the same location however due to the susceptibility of SODARs to fixed echo problems this is not possible. Instead a statistical relationship is needed to relate the wind flow at the position of the SODAR to the wind flow at the position of the turbine. This requires further work involving a complex fluid dynamics simulation for the individual site being modelled.

2.4 Effect of Sound Frequency on SODAR Measurements

The frequency of the pulse emitted by the SODAR has several implications on the way in which the SODAR performs. The beam pattern and therefore measurement volume, scattering cross-section, maximum range and susceptibility to background noise are all altered by the frequency selection. In this section each of these factors is examined.

2.4.1 Effect of Frequency on the FWHM of the SODAR Beam

In Section 2.2 a far-field model of the directivity pattern of a speaker array was shown. This is used to show how frequency affects the beam pattern of the SODAR and consequently the measurement volume of a SODAR. Figure 2.4.1 shows the

FWHM for each of the 3 array shapes modelled as a function of frequency.

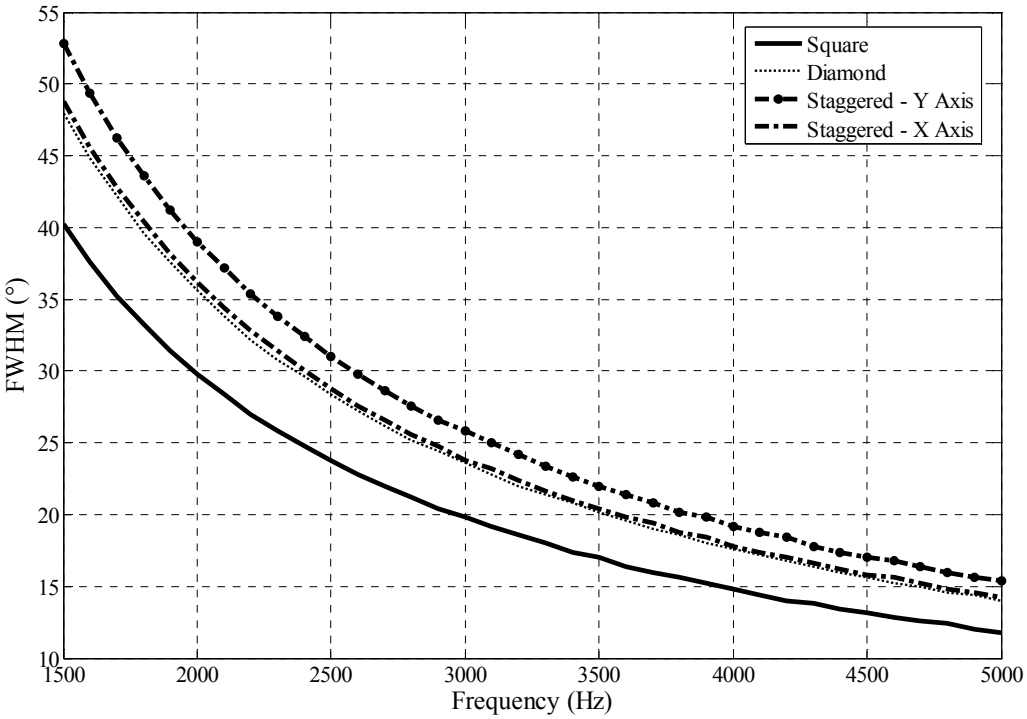

Figure 2.4.1 – FWHM as a function of frequency for three different array shapes.

The FWHM reduces in width as frequency is increased meaning that the measurement volume of a SODAR operating a higher frequency is smaller than the volume measured by a SODAR operating a lower frequency. The effect of measurement volume size has been discussed previously in this chapter and it is a trade off between the statistical meaning of the volume against the susceptibility to incorrect mean wind speed estimation due to turbulent effects.

2.4.2 Relationship Between Frequency and Scattering Cross-Section

The scattering cross section is defined by Equation 1.3.4 which contains a term relating to wavelength. The scattering cross section defines the size of the turbulent structure that causes the sound to be reflected back to the SODAR. Figure 2.4.2 shows the size of the scattering cross section as a function of frequency assuming a ground

temperature of 10ºC and C^2_T value of 10^{-4}.

Figure 2.4.2 – Scattering cross section as a function of frequency for a ground temperature of

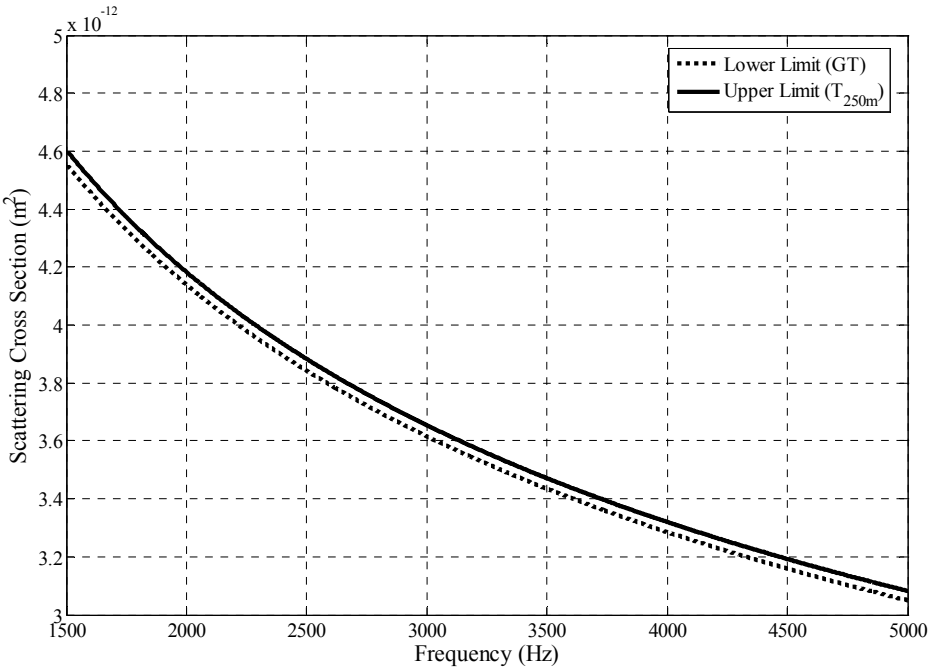

10ºc at the ground (solid) and at a height of 250m (dashed).

The size of the scattering cross section reduces as frequency is increased and therefore there are more reflecting structures as frequency is increased. An increased number of reflecting structures means that the wind speed estimation within the measurement is a higher quality as the sample size is bigger. This is contrary to the findings in the previous sub-section where increased frequency was shown to reduce the size of the total reflecting volume.

2.4.3 Effect of Frequency on the Maximum Height Range and Susceptibility to Background Noise of SODAR Measurements.

The maximum height range and susceptibility to noise are two related factors that are affected by the frequency of the SODAR pulse. The maximum height range is defined by the point at which the reflection from the SODAR pulse is too weak to be detected above the background noise level. Higher frequencies have higher absorption

rates and consequently smaller possible height ranges. Figure 2.4.3 shows the atmospheric sound absorption as a function of frequency for six humidities and a constant temperature of 10ºC and constant pressure of 101.3 kPa based on Equations 1.3.5 – 1.3.9.

Figure 2.4.3 – Absorption as a function of frequency for humidity values of 0% to 100% with

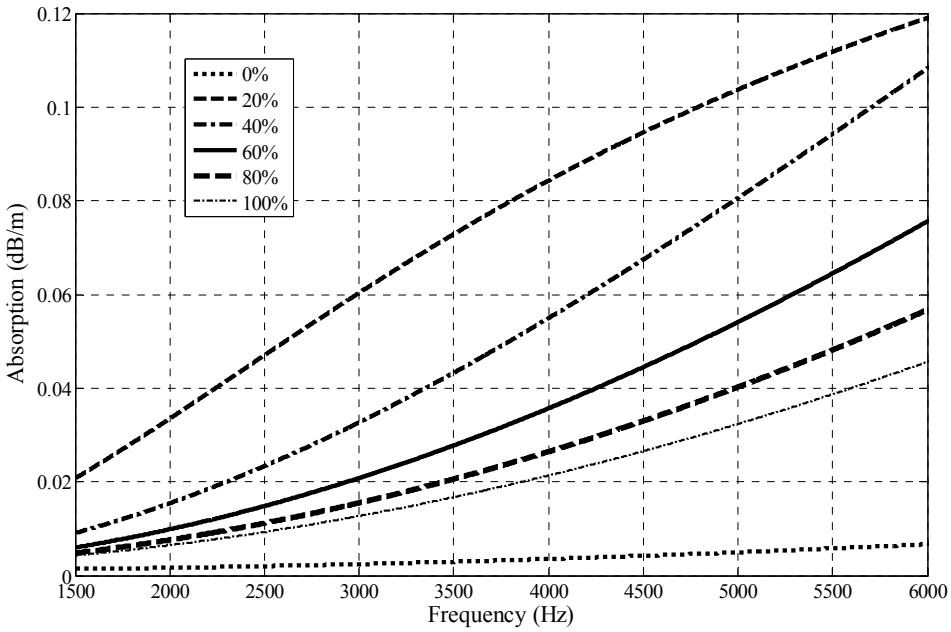

a constant temperature of 10ºC and pressure of 101.3 kPa.

The amount of absorption per metre increases with frequency for all humidities although the rate of increase is much higher for 20%-60% humidity. At 20% humidity more than twice as much energy is lost to absorption per meter at 5 kHz compared to 2.5 kHz. The maximum height that a SODAR echo exists above the level of background noise can be found from Equation 2.4.1 where H_{max} is the height at which the echo has decayed to the level of the background noise, SPL_{pulse} is the the SPL of the pulse emitted by the SODAR, $SPL_{background}$ is the SPL of the background noise in the frequency band of interest. The absorption coefficient, α, is multiplied by two because the sound has to travel to and from the reflection height.

$$H_{max} = \frac{SPL_{pulse} - SPL_{background}}{2\alpha} \quad \text{(Equation 2.4.1)}$$

Figure 2.4.4 shows the maximum height as a function of frequency using absorption curves for 20,40,60 and 80% humidity assuming that the difference between the pulse SPL and the background SPL is 50 dB.

Figure 2.4.4 – Height as a function of frequency at which a SODAR echo has an SPL

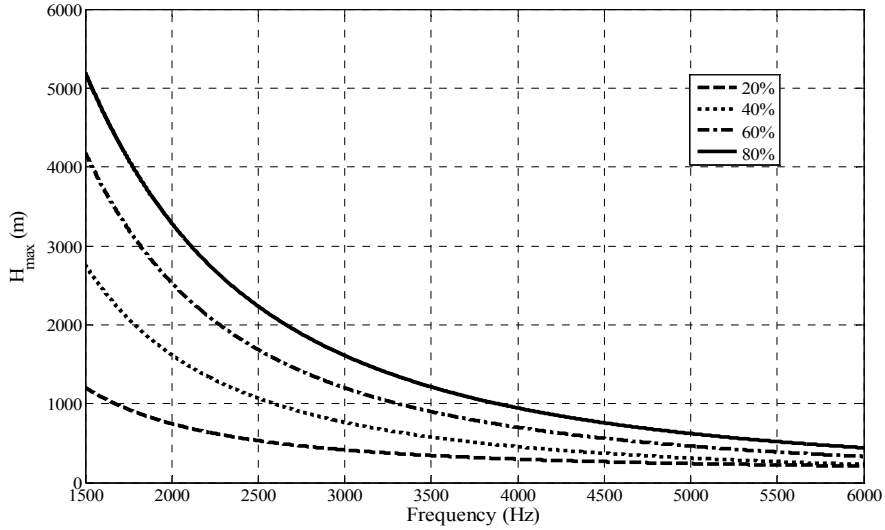

matching the background noise level for 4 humidity values and a difference between pulse SPL and background noise SPL of 50 dB.

This shows that for any humidity the maximum height for a reflection of a 4.5 kHz pulse is less than 1 km. This plot does not take into account the effects of spherical spreading of the scattering cross section. From the absorption curves shown above it is logical to assume that a lower frequency would allow for a larger height range. However, typical outdoor background noise has higher SPLs at lower frequencies and follows a 1/f relationship meaning that the power level reduces by 3dB per octave. This spectrum type is known as pink noise and most real background noise spectra are similar to this although they are likely to contain features related to the exact location such as bird song or traffic noise. Figure 2.4.5 shows the maximum reflection height when the background noise is pink noise with the difference between SODAR output and background noise level at 2 kHz being fixed as 50 dB. The maximum range is significantly reduced at the lower frequencies and increased at higher frequencies. At 20% humidity the maximum range is similar across all frequencies although there is a

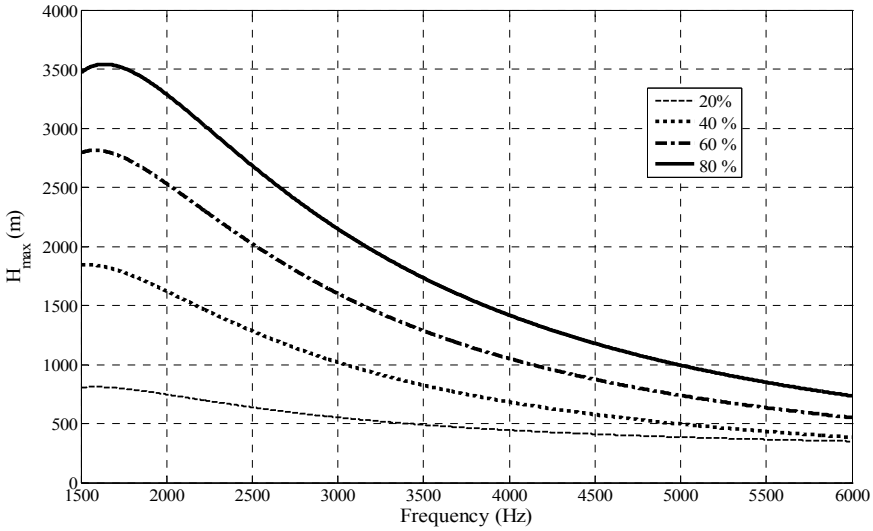

slow reduction as frequency is increased.

Figure 2.4.5 - Height as a function of frequency at which a SODAR echo has an SPL matching the background noise level for 4 humidity values for pink background noise with a difference between SODAR pulse and noise of 50 dB at 2 kHz.

The exact limit on the height range imposed by atmospheric absorption depends on the conditions as temperature, humidity and pressure all alter the absorption rate. At 4.5 kHz the maximum range can be thought to be around 500m for average conditions. Measurements for wind energy are required up to 250m so atmospheric absorption alone should not cause any significant data loss for SODAR measurements of this type.

2.5 Effect of Beam Tilt Angle

The beam tilt angle employed by a SODAR defines the wind speed resolution that is achievable in the SODAR measurement and impacts on the level of uncertainty in the measurement through altering the level of volume separation between the beams and changing the amount of beam spread that occurs. SODAR wind speed measurements are made by measuring the Doppler shift that occurs in a set of beams

orientated in different directions with a specific angular relationship . Common sets are to have a vertical beam and two tilted beams separated by 90º horizontally or three tilted beams separated by 120º horizontally.

2.5.1 Wind Speed Resolution in a Single Measurement

The estimation of Doppler shift frequency carried out by a SODAR requires an FFT to be taken of the return echo. FFTs have a finite resolution which depends on the number of points used in its calculation but for a SODAR a typical resolution would be 6 Hz. The bigger the tilt angle employed by the SODAR the larger the amount the horizontal wind speed, which is usually much larger than the vertical speed, contributes to the Doppler shift. If the vertical speed is assumed to be 0ms^{-1} then the Doppler shift can be calculated using Equation 2.5.1, for one tilted beam in a set of beams with two tilted and one vertical, where $\Delta\omega$ is the frequency shift, k is the wavenumber, V is the wind speed and θ is the beam tilt angle.

$$\Delta\omega = -2kV\sin\theta \qquad \text{Equation 2.5.1}$$

This can be rearranged to find the wind speed resolution if the Doppler shift is set to size of the frequency steps in the FFT, in this example 6 Hz. Figure 2.5.1 shows the wind speed resolution for different angles of beam tilt.

Figure 2.5.1 - Resolution of the horizontal wind speed estimation from one tilted beam as a

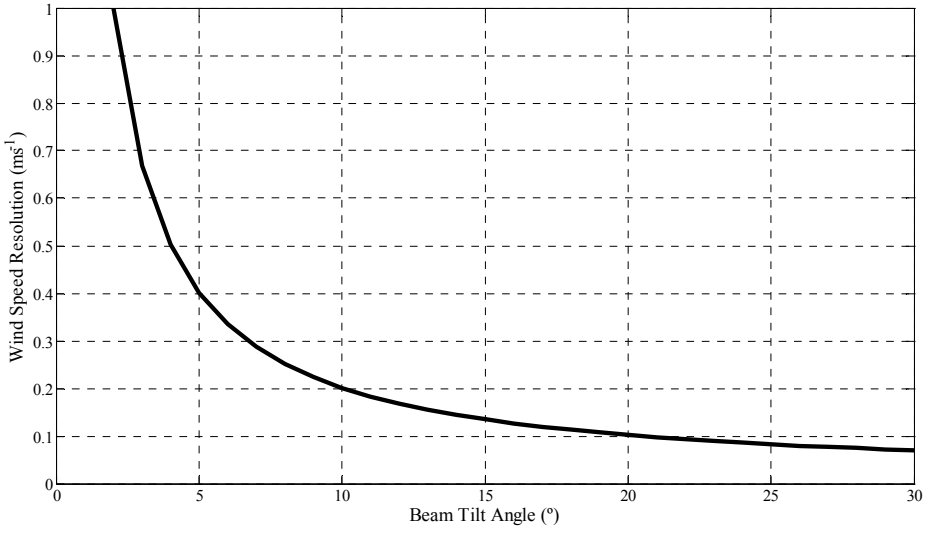

function of tilt angle for a single measurement.

It can be seen that at tilt angles of less than 10º the resolution becomes poor very quickly but above this there is only a small increase in the resolution as the beam tilt becomes larger. It is desirable not to have too large a tilt angle as the the volumes measured by each beam become too separated to give a statistically meaningful estimation of the wind speed and direction. This is a particular problem in complex terrain where large variations in wind speed occur over small distances. The majority of commercial SODARs operate with angles near to 15º. The resolution given here is the resolution for a one measurement along a single beam. The wind speed measured for a whole set of beams is therefore the square root of this resolution multiplied by two. Averaging over many measurements improves the resolution further by a factor of 1/N, where N is the number of estimates within the average. Therefore when using a tilt angle of 15º if 100 estimates are recorded in an averaging period then the horizontal wind speed resolution would be $0.015ms^{-1}$.

2.6 Potential Fixed Echo Influence Based on Side Lobe Pattern and Baffle Shape

One flaw in the SODAR measurement principle is that any echoes received from solid objects such as surrounding buildings, masts, trees and turbines result in the measured wind speed tending toward $0ms^{-1}$ or being rejected depending on how the SODAR's processing is set-up to deal with these problems. These type of echoes are named fixed echoes since they come from static sources although it is also possible that echoes could be received from moving objects such as birds and vehicles. Fixed echoes occur because the SODAR beam has a width and side lobes. Most SODAR manufacturers design baffles to surround their SODARs in order to eliminate or at least lessen the effects of fixed echoes. However, no baffle is perfect at eliminating side lobe energy and the introduction of a finite edge can cause diffraction of parts of the main beam or first side lobes when it is tilted. A SODAR should be set-up to measure in a way that minimizes the possible effects of fixed echoes so prior to

measurement an exploration of the angles and magnitudes of side lobes and baffle diffraction effects is needed.

2.6.1 Side Lobe Position and Magnitude

The far field directivity model described in Section 2.2 can be used to find the angles at which side lobe energy is large enough to cause fixed echo problems. A definition of how large this is is also needed. To find this the energy returning from the atmosphere should be compared to the level expected to return from a fixed object given the reduction in power contained within the side lobe and the expected attenuation of any baffles included.

The envelope of a SODAR echo is described by Equation 1.2.1 and explained in Section 2.4.3 and this equation is true for fixed echoes but the scattering cross section will be orders of magnitude higher than an atmospheric scatter. If absorption and spherical spreading is assumed to be identical for both the fixed echo and the atmospheric echo then the comparative amplitudes of the two echoes depends on the sound pressure output by the SODAR in the direction of the echo source and the value of the scattering cross section only. A comparative amplitude value can be found from these two values. If the assumption is made that for a fixed echo to influence the SODAR's measurement its comparative amplitude value must be no weaker then 6 dB less than the atmospheric echo then angles at which fixed echoes could be problematic due to the SODAR's sides lobes can be found. This level is influenced by the SODAR's processing methods and is therefore not the same for every SODAR. This analysis has been covered in Bradley (2008) with the acceptable value for side lobes being -50dB when compared to the main lobe.

The directivity pattern for an array shape can be plotted as a contour map with lines at -6dB to represent the main lobe and -50dB to represent where side lobe energy is not problematic. Figures 2.6.1, 2.6.2 and 2.6.3 show contour maps projected in a Cartesian projection for the square, diamond and staggered arrays modelled earlier in

this chapter with a white square outline at 30º to identify a typical baffle aperture space with a circular shape. White space represents SPLs within 6dB of the main lobe peak, light grey space represents SPLs within 20dB of the main lobe peak, grey space represents SPLs within 50dB of the main lobe peak and black space represents all

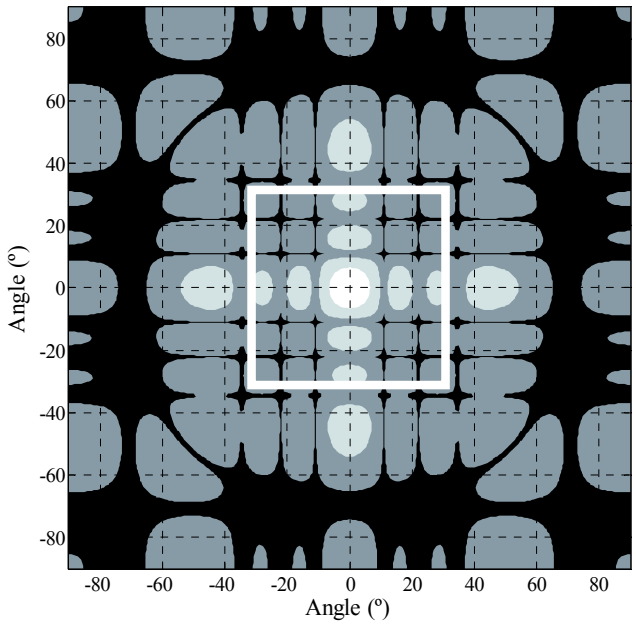

SPLs more than 50dB below the main lobe peak.

Figure 2.6.1 – Contour map in Cartesian projection of the directivity pattern of a 4*4 square array with above -6dB (white), above -20dB (light grey) above -50dB (grey) and below -50dB (black) contour areas shown and with A white square to represent a typical baffle aperture.

Figure 2.6.2 – Contour map in Cartesian projection of the directivity pattern of a 12 element

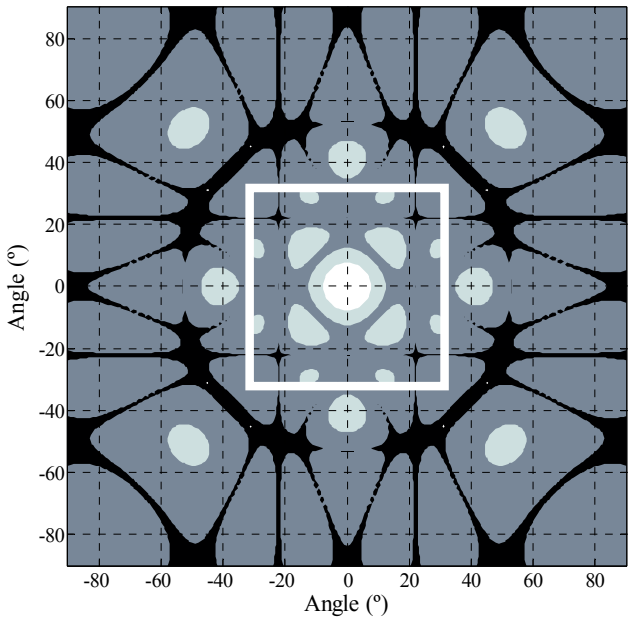

diamond array with above -6dB (white), above -20dB (light grey) above -50dB (grey) and below -50dB (black) contour areas shown and with a white square to represent a typical baffle aperture.

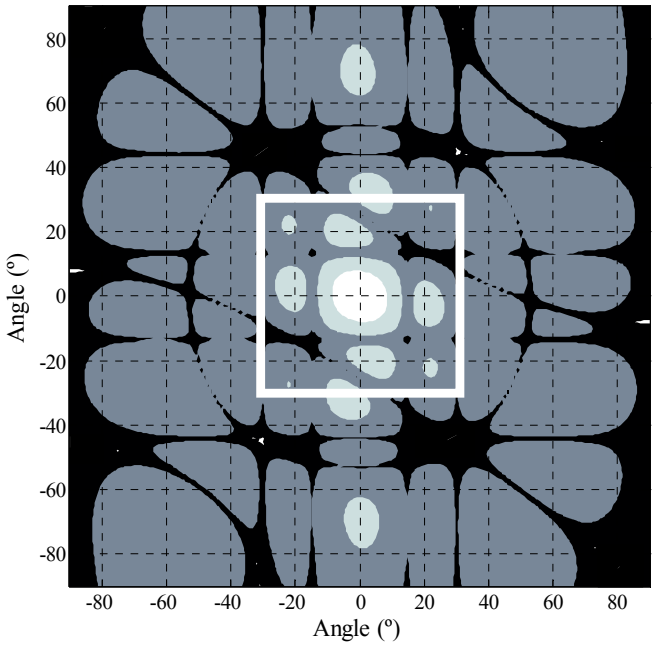

Figure 2.6.3 – Contour map in Cartesian projection of the directivity pattern of a 3*4 staggered rectangle array with above -6dB (white), above -20dB (light grey) above -50dB (grey) and below -50dB (black) contour areas shown and with a white square to represent a typical baffle aperture.

For all three array shapes some side lobes that are within 20 dB of the main lobe occur inside and outside the baffle aperture and inside the aperture almost all of the radiation is within 50 dB of the main lobe peak. The side lobes on the outside of the aperture should be reduced in amplitude by the baffles so that they no longer present a problem in terms of fixed echoes. The side lobes close to the main lobe add to the overall measurement volume but as they are more the 6dB weaker than the main lobe their contribution to the wind estimation is negligible. The side lobes that cause the significant problem are those that occur near the baffle edge as diffraction effects cause them to travel horizontally away from the SODAR resulting in echoes from solid objects in the surrounding area. This is described in the next sub-section. The SODAR should be carefully orientated when setting up to minimise these problems. The side lobe distribution of the tilted beams needs to be examined in the same way so that the best SODAR orientation can be found. Figure 2.6.4 shows the square array

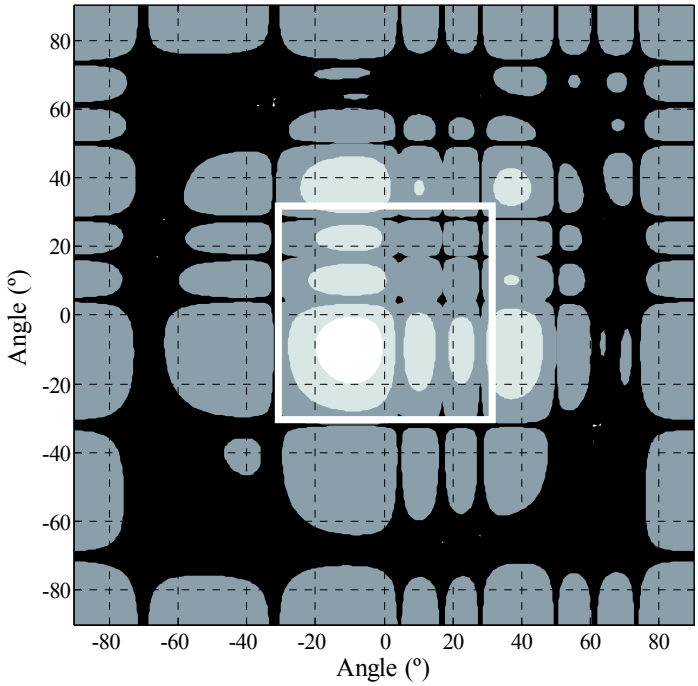

with a 15° tilt angle applied.

Figure 2.6.4 – Contour map in Cartesian projection of the directivity pattern of a 4*4 square

array with a 15º tilt applied. Above -6dB (white), above -20dB (light grey) above -50dB (grey) and below -50dB (black) contour areas shown and with a white square to represent a typical baffle aperture.

The baffle edge does not interfere with the main lobe and there is actually a null at the baffle edge on the sides near the main lobe. In this example side lobes occur in two places along the baffle edge at 15º on the opposing edges from the main lobe. These would be two directions which should not coincide with solid objects. The information from Figure 2.6.1 and 2.6.4 can be used to generate a guide circle for the array type showing the directions of the strongest side lobes that occur near the baffle edge. An example based on the square array and assuming one vertical beam and two titled beams with a 90º separation is shown in Figure 2.6.5.

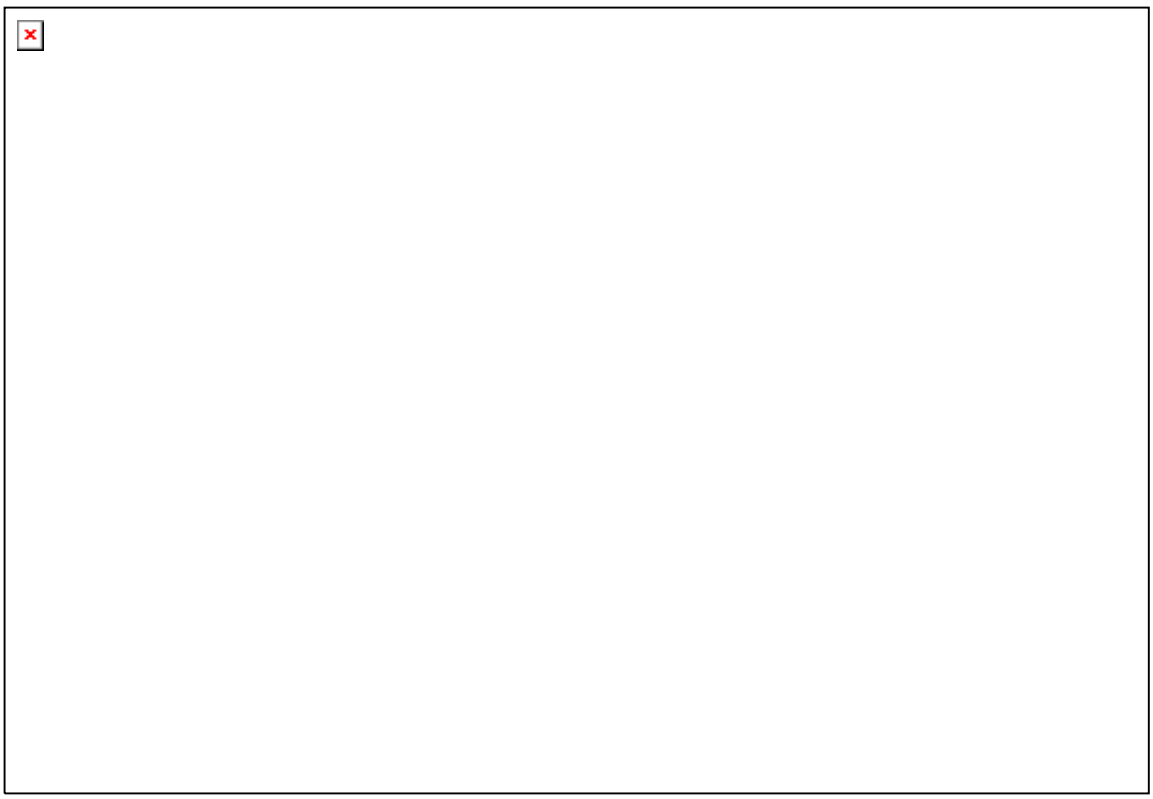

Figure 2.6.5 – Large side lobe direction guide generated from SPL maps of the sound radiation from a 4*4 square array.

This type of strong side lobe angle prediction can be carried out for any array type and baffle shape. The guide can be overlaid onto a topographical map of the proposed measurement site in order to identify the best orientation for the SODAR. Objects with

small dimensions within 20m of the SODAR position can be neglected since any reflections from them will be received by the SODAR before reflections from the first range gate are expected so long as there is no secondary reflection. In the past the SODAR orientation has been carried out using empirical methods applied by the manufacturer or user in the initial set-up to good effect. The approach suggested here is an way of increasing the traceability of a measurement so that it can be compared to other measurements within a known framework.

2.6.2 Diffraction of the SODAR Beam by Baffle Edges

Sound that is incident on the top edge of a SODAR baffle is diffracted away from the SODAR in a different direction to the direction it was originally travelling in depending on the angle it arrives at the edge from. Figure 2.6.6 shows this idea approximating the sound from different parts of the SODAR array as light rays.

Figure 2.6.6 – Diffraction behaviour at SODAR baffle edge with sound rays represented by

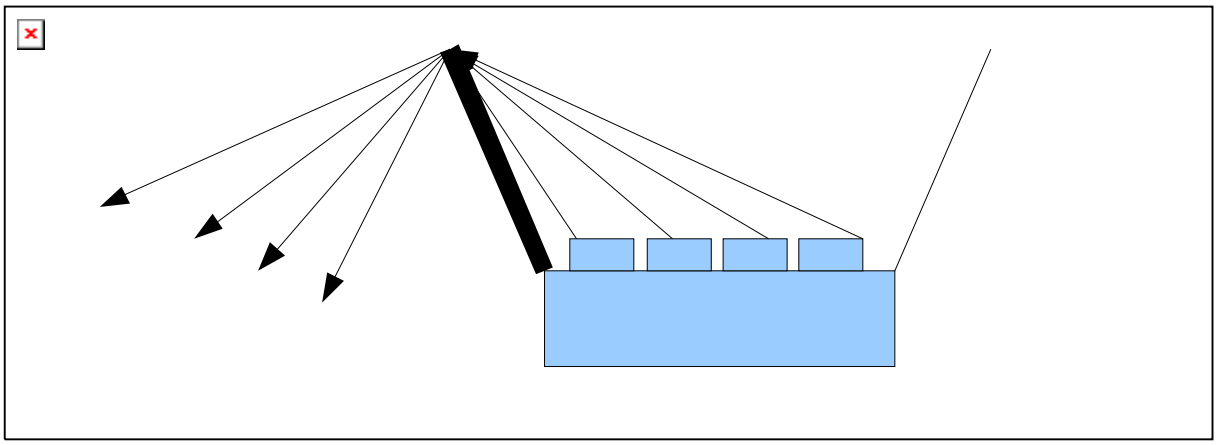

black arrows.

The sound is diffracted with spherical wave behaviour so each sound ray is spread from the diffraction point with the centre following the arrow direction. Werkhoven (1997), which was reviewed in Chapter 1, explains the process of sound diffraction at a baffle edge using Kirchoff's integral theorem to predict the behaviour of the diffracted sound. This is also covered in Chapter 4 of Bradley (2008). The principal conclusion is that the the point of diffraction modulates the sound radiation following

a Bessel function shape similar to that of the piston source approximation used to model the array loudspeakers. The axis of this Bessel is not the same the original array axis though. It is modified by the angle at which the sound meets the baffle. This occurs at every point along the edge so that the sound combines to create a line source. Whilst modelling this process is complex it can be assumed that the width of the side lobes that are diffracted is effectively widened by this process whilst the amplitude of the sound is reduce by the amount of spreading that occurs. Finite difference time domain (FDTD) or boundary element modelling (BEM) methods could be used to gain a clearer insight into the diffraction behaviour of the baffle edges. Reduction of the SPL and the amount of diffraction at the baffle edge is achieved through the use of 'thnadners'. These are small triangular structures that present a changing edge height around the baffle rim and have been shown in Werkhoven (1997) to give more than a 6dB reduction in the power of the diffracted wave. The combination of the spreading effects caused by the edge diffraction and the gradient reduction caused by the 'thnadners' means that the energy that was within 50 dB of the main lobe peak in the directivity maps shown in the previous section is not problematic so long as they are properly designed for the operating frequency of the SODAR. The side lobes that were 20dB less than the peak could still be problematic but with correct SODAR orientation their influence can be minimised.

2.7 Influence of Peak Detection and Averaging Processes

Two operations that all SODARs perform in order to estimate wind speeds are peak detection and averaging. Peak detection is an operation that identifies the peak within the FFT of the return echo that is representative of the mean radial wind speed along the measurement beam. The radial wind speed is calculated from the frequency change between the echo and the original signal. Averaging is carried out to reduce the variability and increase the resolution of the wind speed estimation. The order in which the peak detection and averaging is carried out depends on the SODAR type being used. In this section a simulation is presented that tests how the order of these

two processes affects the resulting wind speed estimation. It is performed with the peak detection and the averaging in very simple forms. It should be noted that commercial SODARs operate with more sophisticated versions of these approaches.

A single SODAR echo has a frequency content that is a combination of the output signal, the mean radial wind speed, turbulent variation and background noise. A set of signals is generated with a single frequency representing the the output signal plus the frequency shift that occurs due to a single mean radial speed with a random variation to this speed added for the turbulence. The random variation follows a normal distribution centred on the mean radial wind speed with a variance of $2ms^{-1}$. Once this signal is generated a random noise element can be added with an amplitude that matches the wind speed part of the signal. Equation 2.7.1 shows the creation of this signal where ω_{output} is the frequency of the SODAR pulse, $\Delta\omega_{shift}$ is the frequency shift due to the mean radial speed, $\Delta\omega_{turb}$ is the random variation due to turbulence and $N(t)$ is the random noise component.

$$x(t) = \sin(\omega_{output} + \Delta\omega_{shift} + \Delta\omega_{turb}(t) + N(t)) \quad \text{(Equation 2.7.1)}$$

Over a 10 minute averaging period a SODAR records between 50 and 300 returns for each beam direction depending on the pulse length and height range of the measurement. Therefore 50 signals are generated for each iteration of the simulation as this represents the lowest number of points in the estimation. The first approach to deriving the mean frequency shift over the averaging period is to find the mean of all the spectra and then to identify the frequency with the peak power. The spectra are found by applying a 22050 point FFT to each of the return signals and then filtering above the Nyquist limit at 11025Hz. The mean spectra is then found and the peak frequency identified. The second approach is to identify the peak frequency in each individual spectra and then find the average of these. Figure 2.7.1 shows a comparison of these two approaches finding the average in 50 return signals of a signal centred on 2305 Hz for 100 iterations.

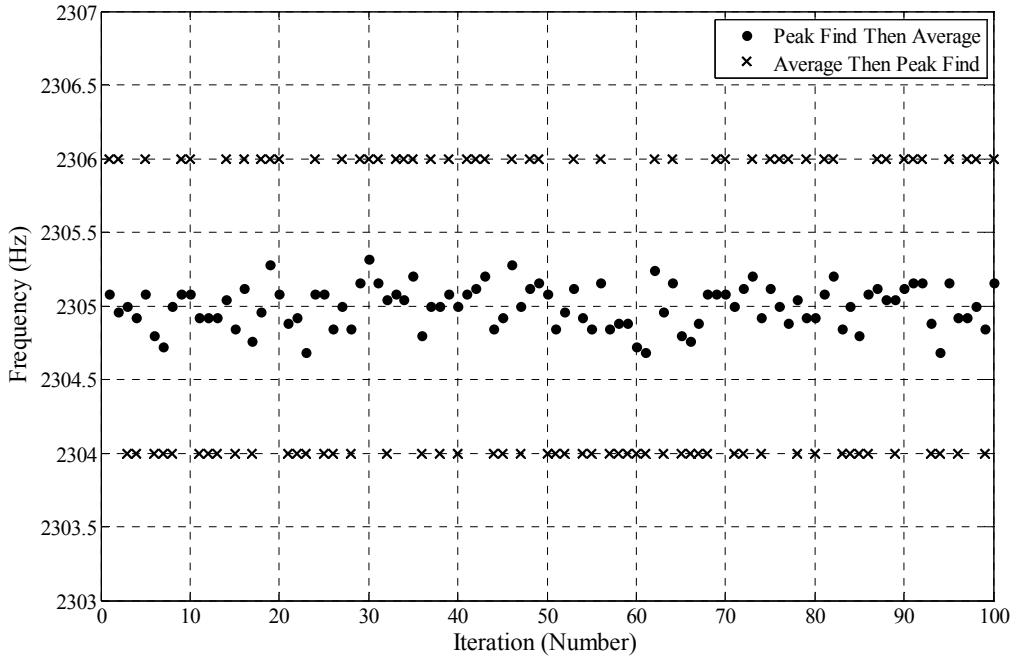

Figure 2.7.1 – Comparison between the peak frequency estimation for 100 iterations of averaging 50 signals using peak find then average (dots) and average then peak find (crosses) for signals centred at 2305 Hz.

Averaging the spectra before finding the peak results in the signal either being 1 Hz above or 1 Hz below the intended frequency. This shows that this approach is reliant on the frequency resolution representing the true frequency, in this case it does not as the resolution is 2 Hz. The variability is low in this approach as the frequency is only one of two frequencies. The variability in the second approach is much higher but the frequency estimations are a lot closer to the intended frequency. The variability is due to the mean of several estimation falling in between the possible frequency estimations for a single case. For example an estimation of 2305 Hz here could be the result of 25 peaks occurring at 2306 Hz and 25 peaks occurring at 2304 Hz as the frequency resolution of the 22050 point FFT is 2Hz. This is an over simplified simulation but it shows that averaging before finding the peak can reduce variability whilst restricting the frequency estimation to the resolution of the FFT. This can be overcome by using a more complex peak detection method such as fitting a curve to the averaged spectrum.

2.8 Doppler Shift Equations

In order to estimate the wind velocity from the SODAR reflections the frequency change found in the averaged signal needs to be converted. There are two common approaches to this process. Equation 2.8.1 and 2.8.2 show expressions for these two approaches.

$$Vr = \frac{\Delta f \, c}{2 f_t} \quad \text{(Equation 2.8.1)}$$

$$Vr = \frac{\Delta f \, c}{f_t \Delta f_r} \quad \text{(Equation 2.8.2)}$$

They only differ in the denominator but this can have a significant effect on the wind speed data output by a SODAR. Equation 2.8.1 is a common approximation where the travelling sound is considered to be a single ray with the change in frequency occurring as it is recorded at the SODAR. Equation 2.8.2, taken from Ostashev(1997) , treats the travelling sound as two rays with the first travelling from the SODAR to the point of reflection and the second returning from the point of reflection to the SODAR. In this case the frequency change occurs at the point of reflection, which is a more realistic analysis. In both cases it is assumed that scatterers move with the mean velocity of the medium and that the medium is homogeneous and therefore only a single frequency is present in the return echo. This is not the case in a real atmosphere as turbulence creates many inhomogeneities and as a result the return echo has a broad frequency spectrum. When a SODAR calculates a wind speed the return echoes have been averaged and a peak fitting algorithm applied to find the mean frequency shift and therefore these equations are appropriate for calculating the wind speed. Figure 2.8.1 shows the differences between radial velocity estimations calculated using these two equations.

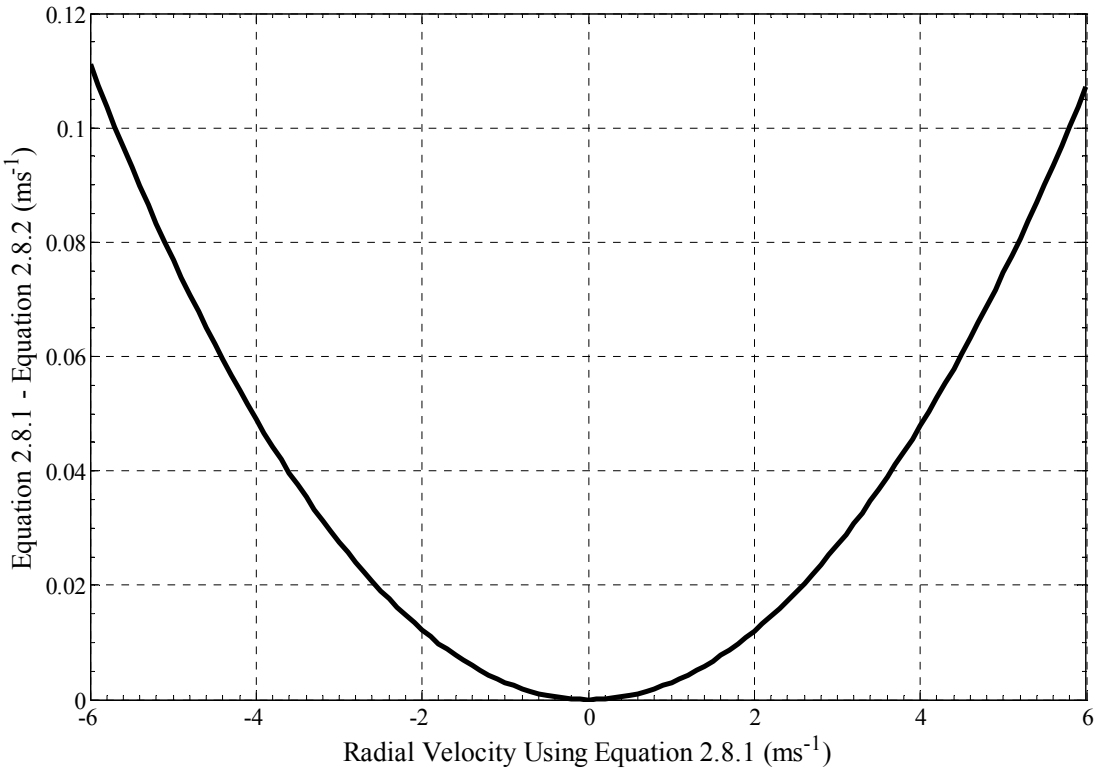

Figure 2.8.1 – Difference between the radial velocities calculated from equation 2.8.1 and 2.8.2.

The difference in radial velocity is small and there are slightly larger differences for the negative velocities, approximately 0.0025 ms-1. The magnitude of the differences increases when the radial velocities are converted into horizontal velocities. If 0ms^{-1} vertical velocity is assumed then the differences in the horizontal velocity can be found using Equation 2.8.3 which is found from simple trigonometry where V_H is the horizontal velocity θ_{tilt} is the tilt angle of the SODAR beam and V_R is the radial velocity.

$$V_H = \frac{V_R}{\sin \theta_{tilt}} \quad \text{Equation 2.8.3}$$

From Equation 2.8.3 it can be seen that the differences in terms of horizontal velocity are the differences in radial velocities divided by the sin of the tilt angle. For example if the tilt angle was 16º then if -20ms^{-1} was calculated using Equation 2.8.1 the same

measured frequency shift using Equation 2.8.2 would give a horizontal velocity of -20.34ms^{-1}. The differences for all horizontal speeds are shown in Figure 2.8.2.

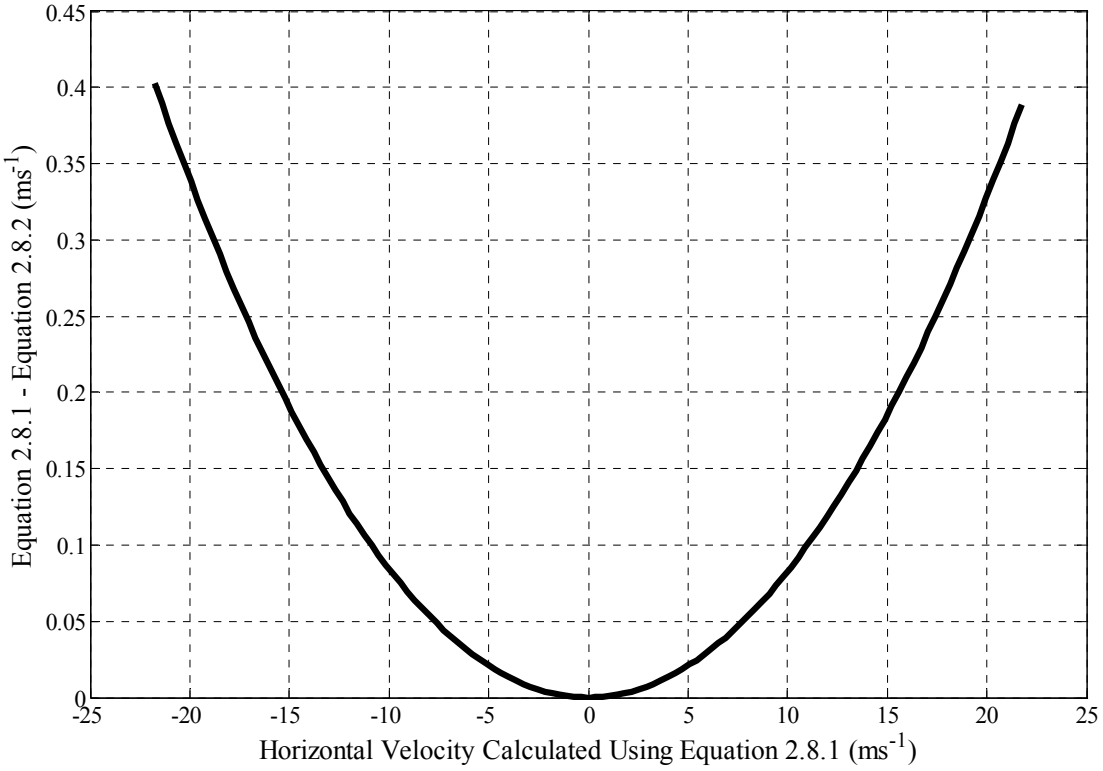

Figure 2.8.2 – Difference between the horizontal velocities calculated from Equation 2.8.1 and 2.8.2 assuming 0ms^{-1} vertical velocity.

The use of different Doppler equations has a significant effect on the wind speed estimations given by a SODAR instrument. Measurements made with a SODAR that employs Equation 2.8.1 should be converted so that they match measurements from Equation 2.8.2 since this equation gives a more realistic interpretation of the Doppler shift mechanism that occurs. However, in order to find out which equation is the most correct an experiment should be carried out on existing data. By collating a large amount of SODAR-mast inter-comparison data from SODARs where the use of Doppler equation is known it will be possible to ascertain which of the two equations gives the most realistic analysis. The transponder system presented in the following chapter is a tool that allows the Doppler equation used by a SODAR to be found.

2.9 Measurement Rejection Algorithms

SODARs often apply some amount of data rejection based on whether the measurement conforms to a set of expectations with regards to power levels, noise levels and spectral width. The consequence of this is that the statistical significance of each individual measurement is increased but the sample size in each average is reduced. Details of this are largely covered in the WISE report and in Bradley (2008). The amount of data that gets rejected reduces the sample size in relation to the wind field the measurement is representing. In Figure 2.3.5 it was shown that the ratio of volume measured by the SODAR to the volume passing a wind turbine decreases as wind speed is increased and therefore data rejection at low speeds is not likely to reduce the significance of the measurement detrimentally whilst at high speeds care must be taken about the number of data points rejected as removing too many points could make the wind estimation unrepresentative of the wind at the turbine site.

2.10 Discussion

In this chapter many aspects of the acoustic behaviour have been explored or discussed mainly based on models of the directivity patterns of arbitrary array shapes. Some aspects covered here have been covered in more depth in other sources but they are shown to provide a full description. The aim is to be able to examine different SODARs and explore how the measurements of each compare since the measurements made with one SODAR type are as different to the measurements of another SODAR type as a SODAR measurement is to a particular LIDAR measurement. Before using a SODAR for a measurement at a wind turbine site the model type presented here should be created and analysis of the statistical significance of the SODAR measurement to the turbine location or other location of reference should be made. In order to do this an approximate distribution of wind speeds and a flow model that relates the SODAR position and the turbine position are required. The significance of the SODAR measurements based on expected data levels and volume comparison can be found.

Acoustic models of the SODAR behaviour are useful for finding the correct set up for a SODAR at a measurement location. Analysis of the side lobe positions relative to the main SODAR beams allows a guide to be created that allows the SODAR to be orientated to avoid any fixed echo effects. The points on this guide should be considered to have some width due to diffraction effects and spherical wave behaviour. Further work to quantify the exact effect of baffle diffraction is needed so that this can be combined into the prediction of problematic directions. Some work is carried out in Chapter 4 of this thesis to measure the influence of a square baffle shape with 'thnadners' attached.

The existence of two equations for Doppler shift that show a small difference in result is important since the use of the wrong one adds a systematic bias to any measurements made. Equation 2.8.2 is more likely to be correct but since both exist in literature there is the possibility that a SODAR may use either. The transponder detailed in the following Chapter has been shown to highlight which Equation is being used by the SODAR being tested. An examination of data from a number of SODAR-mast comparison studies where SODARs operating the two different equations are included will allow for the confirmation of which equation is the most correct since cup and sonic anemometer measurements are absolute.

2.11 Summary

In this chapter the details of a model that predicts the directional acoustic behaviour of a SODAR array is detailed based on standard Bessel approximations of circular sound sources. This model is used to compare the measurement volume of different speaker arrays with it being shown that the effective measurement volume of a SODAR array is approximately 15% of a physical cone section with a width based on the arrays FWHM. The effect of frequency selection on the beam width, atmospheric absorption and cross sectional area is explored. The directivity model is used to find the angle of problematic side lobes for a given array shape providing a orientation set up guide for a modelled array that can allow minimisation of fixed echo

effects. A simple comparison is made of the order that peak detection and averaging is performed with further detailed exploration needed. The influence of the choice of Doppler shift equation on the wind speed estimation is shown with the possibility of errors of 1% - 2% being caused by the use of the different equations. A study is suggested to find which is the most accurate. A note is also made on the how data availability changes the statistical significance of a SODAR measurement.

3. A Transponder System As A Method For Comparing SODARs

3. A Transponder System As A Method For Comparing SODARs

3.1 Introduction

A Transponder system is developed to act as virtual wind in order to make comparisons between SODARs where some or all of the SODAR's operational parameters are unknown to the user. The details of the physical and processing design of the transponder are described. Then tests using the transponder system in both laboratory conditions and in the field are explained. Conclusions about the suitability of the system are made with further requirements highlighted.

3.1.1 Principle of Transponder Measurements

A SODAR probes the atmosphere by recording the reflection of a pulse of sound that it has emitted. The exact details of the atmosphere that reflect this pulse are unknown and therefore the accuracy is uncertain. If the wind field can be simulated with known conditions it is possible to ascertain if the SODAR processing has any influence on the wind speed measurements. A transponder system consisting of several speakers and microphones attached to a computer is used to achieve this. The physical set-up of the transponder system mimics the acoustic behaviour that the SODAR is subject to by a real echo and the computer contains programming that simulates the changes to a signal that would occur for a known set of atmospheric variables including wind profile, absorption and scattering characteristics.

3.2 Physical Design of Transponder System

The transponder system needs to incorporate an input stage to capture and respond to the output of the SODAR, a processing stage to create a return signal and an output stage to play the echo signal back to the SODAR. The input and output stages consist of microphones and speakers that have suitable characteristics. The processing is carried out in software on a laptop computer equipped with a

multichannel sound card allowing for a number of different speakers and microphones to be employed within the transponder system.

3.2.1 Transponder Sound Sources

Sound that is reflected in the atmosphere travels spherically from the point of reflection. The distance from the point of reflection to the SODAR determines the radius of the sphere of that reflection. As a result all reflections, which are useful for the SODAR measurement (from 20m upwards), arrive at the SODAR with close to plane wave behaviour due this spherical spreading effect and at the angle from which the SODAR beam was emitted. The output of the transponder therefore must try to emulate this. Placing a speaker less than 3 meters away makes this goal impossible to realise meaning the best achievable case is an omnidirectional source. Therefore a source is needed that has omnidirectional behaviour for the typical frequency range of SODAR operation (1.5-6kHz). Three options are available; a horn, a traditional loudspeaker or a distributed mode loudspeaker (DML). Figure 3.2.1 shows the anechoically measured directivity pattern of an RCF horn loudspeaker, which has been used in some METEK SODARs.

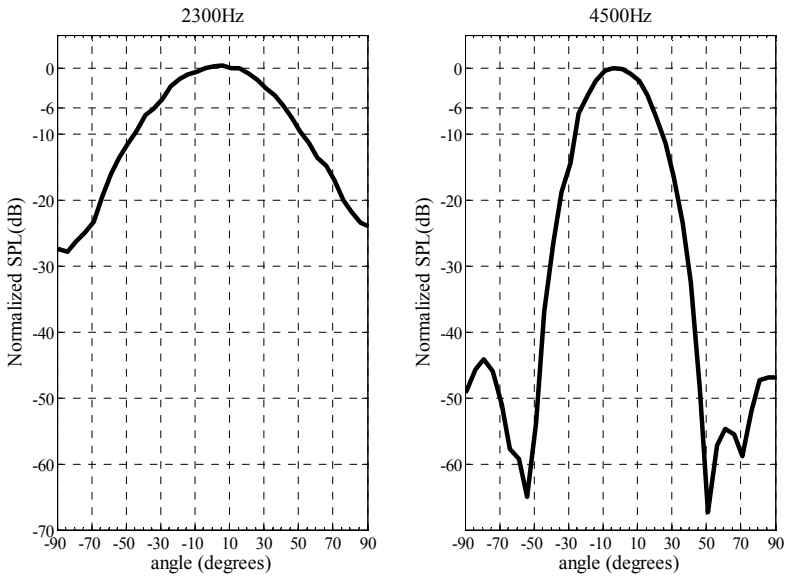

Figure 3.2.1 – Measured directivity patterns of a RCF horn loudspeaker at 2300 Hz (Left) and 4500 Hz (Right).

It is clear that the directional behaviour of the horn is quite strong making it unsuitable as a source for the transponder with -6dB points occurring at +/-45º for 2300 Hz and at +/-25º for 4500 Hz. However it will have a similar frequency response to a SODAR in which this type of horn is used. This means that amplitude fluctuations within the SODAR's frequency response are matched by the transponder. Instead a speaker with a more omni-directional directivity pattern could be used with amplitude fluctuations within the SODAR's frequency response neglected. This approach allows for a consistent set-up for testing with different SODARs.

DMLs have directivity characteristics that are not dependent only on the frequency of the sound input. Figure 3.2.2 shows the directivity pattern of DML panel in a small enclosure from Azima (1999).

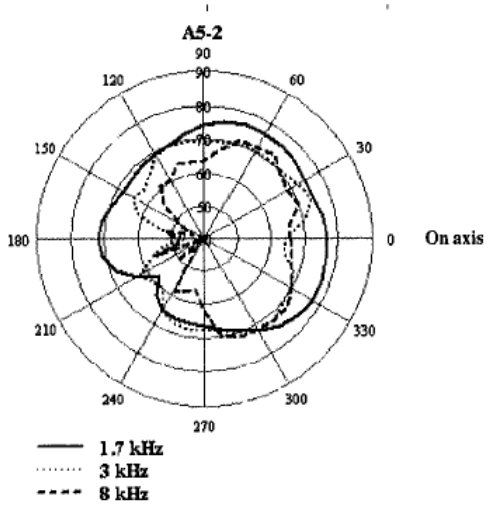

Figure 3.2.2 – Polar response of the A5-2 panel in 28mm enclosure, Azima (1999).

Figure 3.2.2 shows that DML panels can have a more even directivity than the horn loudspeakers. It is not omnidirectional but the +/-6dB points occur at similarly large angles for all three frequencies that are plotted. This suggests that a DML panel would be an ideal source for the transponder set-up however the sensitivity of the DML is insufficient to produce the very low amplitudes required in the later parts of each SODAR echo. DML panels take up a larger space than a tweeter loudspeaker which means that they would need to be placed further away from the SODAR in

order to give the same echo source size.

As the frequency range required is between 1.5 and 6 kHz a small tweeter type loudspeaker is an appropriate source. Figure 3.2.3 shows the measured directivity of a VISITON SC 4 ND Tweeter at 2300 Hz and 4500 Hz . The measured directivity patterns show that the sound emitted by the tweeter speaker has a broad main beam with less than 6 dB drop off at +/-50º. while this is not omnidirectional it is more suitable than the horn directivity patterns shown in Figure 3.2.1 and similar to the DML directivity patterns shown in Figure 3.2.2.

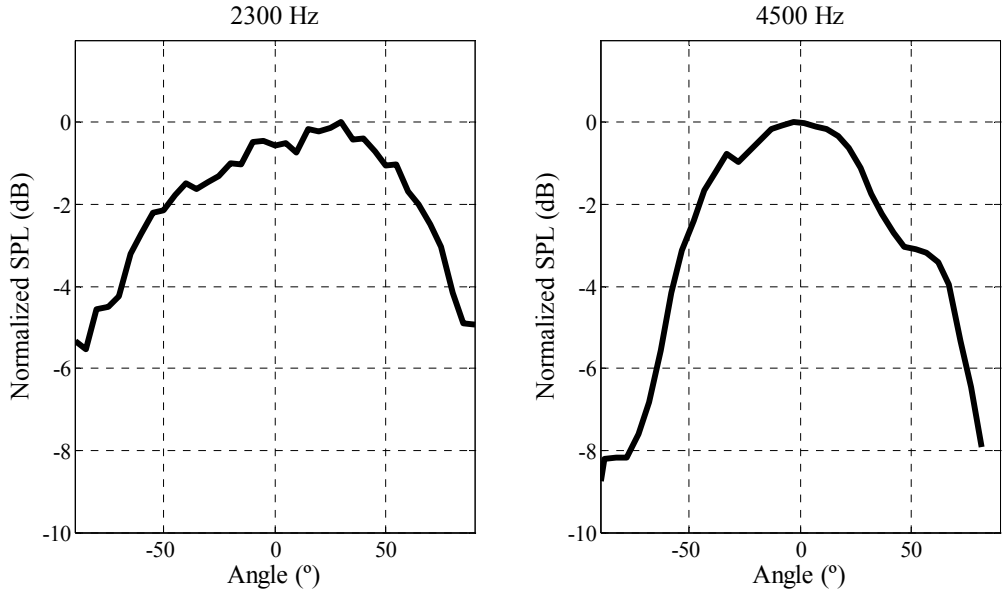

Figure 3.2.3 – Measured directivity of VISITON SC 4 ND tweeter loudspeaker.

This speaker was chosen for measurement as the manufacturer's published frequency response shows a flat response in the desired range. Figure 3.2.4 shows the measured auto spectrum of the tweeter speaker.

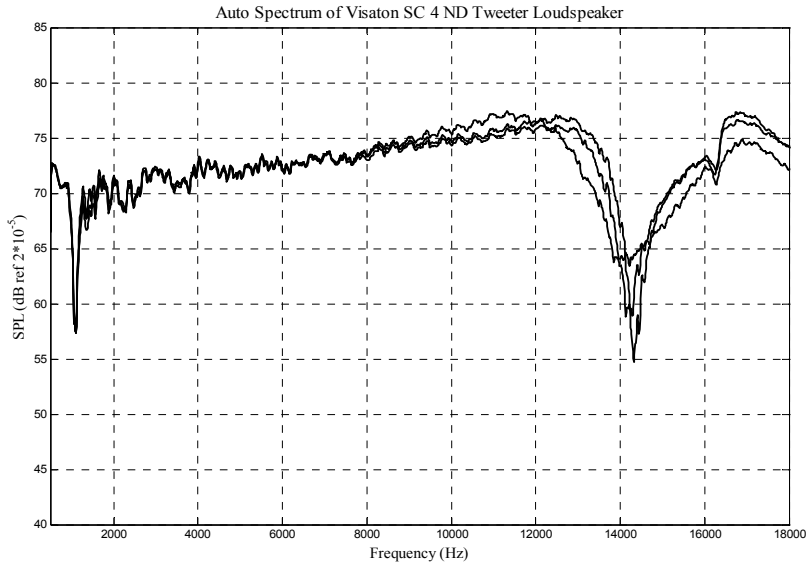

Figure 3.2.4 - Measured auto spectra of 3 VISITON SC 4 ND tweeter loudspeaker.

The auto spectra show that the speakers, taking into account experimental error and room effects, have an even response between 2 and 8 kHz for all three speakers tested. The measurements shown in Figure 3.2.3 and Figure 3.2.4 suggest that the SC 4 ND may be a suitable source for the transponder system. It will therefore be used for all transponder measurements explored in this thesis.

An individual speaker is employed for each SODAR beam in order to emulate the angle at which the return signal is incident on the SODAR transducers. Figure 3.2.5 shows this for an untilted beam and a tilted beam.

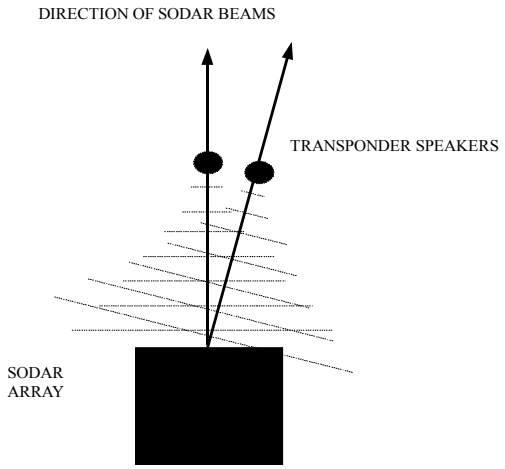

Figure 3.2.5 – Geometry of sound incident on SODAR ARRAY.

3.2.2 Transponder Input Microphone

In order to record an input signal from the SODAR a microphone is required. As in the output stage, a reversible horn transducer that is employed in the SODAR array could be used to cancel out any amplitude variations in the frequency response. This requires the transducer to be placed very close to the SODAR array in order to collect adequate power for the transponder processing unless amplification is applied. It raises an issue of consistency between measurements made with different SODARs since different transducers and different geometries are used in different SODARs. The alternative is to use one or more microphones placed in a SODAR's acoustic far field. Placing a microphone in the acoustic near field means that the recorded signal would be subjected to unpredictable amplitude variations caused by the proximity of the SODAR's loudspeakers. The extent of the acoustic near field, R_{limit}, can be calculated using Equation 3.2.1, from Kinsler (2000), where A is the sound producing area of the SODAR array and λ is the wavelength based on the speed of sound being 330 ms^{-1} .

$$R_{limit} = \frac{A}{\square} \quad \text{(Equation 3.2.1)}$$

Figure 3.2.6 shows the theoretical limit of the acoustic near field for several

commercial SODARs with the suggested operating frequency or frequency range for each SODAR marked using star symbols.. There are many other commercially available SODARs. These four are used as details of the array geometry are easily obtainable.

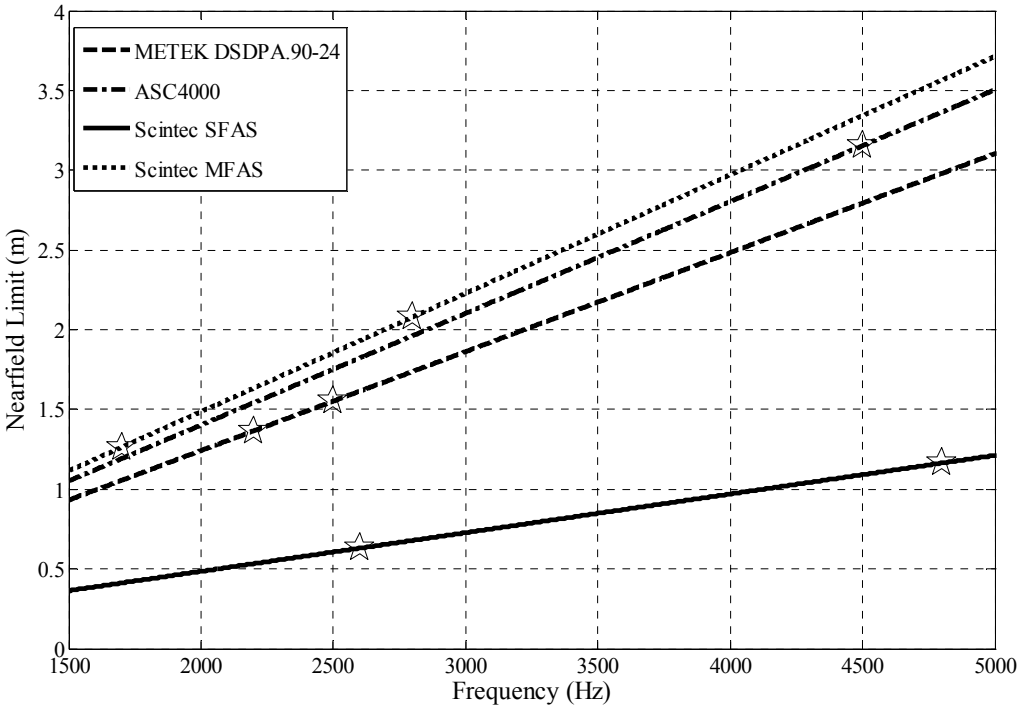

Figure 3.2.6 – Nearfield limit vs frequency for 4 commercially available SODARs with manufacturers suggested operation frequency or frequency range marked with star symbols.

The SODAR with the largest near field for its suggested operating frequency is the ASC4000 with a size of approximately 3.2 meters. This is therefore the closest distance to the SODAR array that the transponder microphone should be positioned.

The microphones need to have a flat frequency response and the capability to handle high sound pressure levels (SPLs). An appropriate microphone is a free field measurement microphone such as those manufactured by Bruel and Kjear or GRAS that has an upper SPL limit of 140-150 dB. A microphone of this kind can be attached to a computer sound card via a power supply with an amplitude control to prevent saturation of the sound card.

The microphone needs to be positioned in the centre of one of the SODAR's beams if the output pulse in each beam is assumed to be the same as this results in the best quality recording without overcomplicating the transponder set-up. If the SODAR employs different pulses for different beams then a microphone is needed for each beam so that the qualities of each pulse can be used in the creation of the return echo signal. In laboratory conditions background noise is not an issue so no additional equipment is needed to record a clean input signal. In a field situation some methods are needed to protect the microphone from wind noise and to reduce background noise levels in comparison to the SODAR signal. These are explored in Section 3.7.2.

3.2.3 Transponder Laptop

For the transponder system a laptop is required with a low latency multi-channel sound card. A standard modern laptop is fast enough to handle the processing demands required so a Samsung P200 is used. The ESI Maya 44 is a multichannel USB sound card with a low latency and four channels for both inputs and outputs allowing for some flexibility in the transponder set-up.

3.2.4 Transponder Set-up

Figure 3.2.7 shows how the transponder is set-up for measurements in a semi-anechoic chamber with a METEK DSDPA.90-24 SODAR.

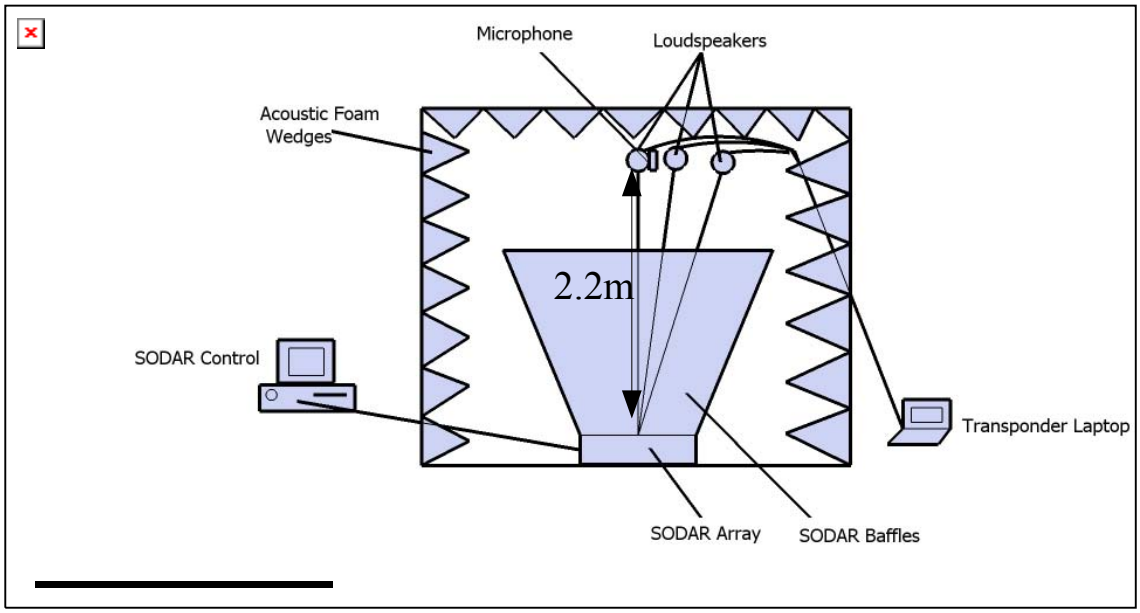

Figure 3.2.7 - Transponder set-up for measurements with a METEK DSDPA.90-24.

The positioning of the loudspeakers and microphone are checked using guide wires attached to the centre of the SODAR array. The chamber is big enough to hold the SODAR with its full set of baffles. A semi-anechoic chamber rather than a full anechoic chamber is used because solid ground approximates the conditions encountered by the SODAR in the field and the size and weight of the SODAR makes measurements in a full anechoic logistically difficult.

3.3 Transponder Processing

3.3.1 The Input Stage

The transponder processing needs to respond to an input from the SODAR for the creation of a return echo. The signal from the microphone is converted into a digital signal by AD converters in the sound card. The acquisition part of the transponder is set-up to record automatically when the input sound level rises above a predefined level. In order to capture the whole of the SODAR signal a pre trigger time is set. This is achieved by allowing for constant recording from the point at which the program is started. Only the amount specified by the pre trigger is stored at any time

and once the trigger level is reached the last pre-recorded data is added onto the front of the data that is recorded after the trigger. This prevents having a sharp cut-in envelope which would create distortion effects when the signal is analysed and used to create the return signal. The signal is recorded several times so that the consistency of the SODAR signal can be checked. It is unlikely that any serious inconsistency will be found as the technology used in SODARs to create a pulse is well established and highly repeatable. If inconsistency is found then it highlights a problem with the SODAR which needs to be solved before any further tests can be carried out.

3.3.2 Analysis of the SODAR Signal

The analysis of the signal consists of identifying the exact frequency of the signal and estimating its length so that these can be compared for consistency to the SODAR data. To identify the frequency of the pulse a high resolution Fast Fourier Transform (FFT) is performed on the signal and the peak frequency identified as the characteristic frequency of the SODAR pulse. This is a straight forward procedure that has been performed many times in different applications with a standard reliable method well established. Equation 3.3.1 describes the FFT as implemented in the standard MatLab toolbox where N is the length of vector ω_N is an Nth root of unity and is described by Equation 3.3.2.

$$X(k) = \sum_{j=1}^{N} x(j)\, w_N^{(j-1)(k-1)} \quad \text{(Equation 3.3.1)}$$

$$\omega_N = e^{-2\pi i/N} \quad \text{(Equation 3.3.2)}$$

Estimating the length of the pulse is a more complex procedure that requires extracting the amplitude envelope of the signal and identifying the number of samples that the signal is above the noise floor, which is defined as the level at which no obvious

SODAR signal is visible. The noise floor in semi-anechoic conditions using a measurement grade microphone is dependent on the background noise of the chamber, for the measurements in this thesis the level was 6.4 dBa, and outdoors it is dependent on the level of wind noise but is small compared to the amplitude produced by the SODAR. This operation can be achieved by calculating the discrete-time analytic signal using a Hilbert transform. The Hilbert transform implements a 90 degrees phase shift on the input data. This property makes it possible to analyse the amplitude envelope of an input signal using Equation 3.3.3 where *x* is the original signal, *H(x)* is the computed Hilbert transform and *E(x)* is the resultant envelope shape.

$$E(x) = \sqrt{x^2 + H(x)^2} \quad \text{(Equation 3.3.3)}$$

This process is demonstrated in Figure 3.3.1 shown below.

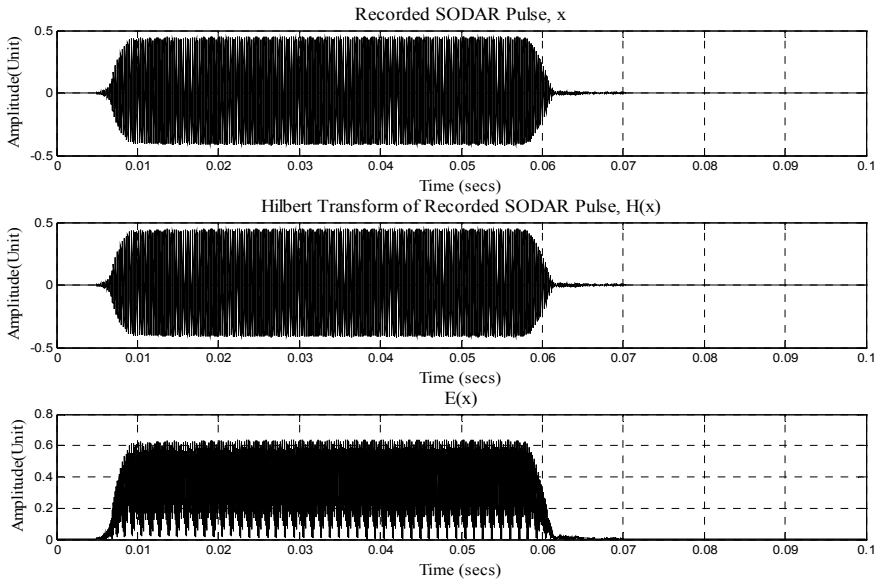

Figure 3.3.1 – Extraction of the signal envelope using a Hilbert function.

The calculated envelope is not a smooth outline of the signal and contains many dips. However for the length of the signal it remains above the noise floor for the majority of the time and therefore by counting the number of samples that have an amplitude

above this level it is possible to give a reasonable estimate of the length of the pulse although this will always be a slight underestimation.

3.3.3 Constructing the Return Signal

The return signal is a signal that is shifted in frequency, in relation to the signal output by the SODAR, by the amount required to represent the wind speed that the transponder is using to measure. Two approaches can be taken to create the return signal with a frequency shift. These are synthesis and modulation and the effectiveness was explored in Piper (2008). A full explanation is given here.

3.3.3.1 Synthesis

A return echo can be synthesised if the maximum measurement height is known and the frequency of the SODAR's pulse can accurately be identified. The maximum height is set within the user controllable parameters of most SODARs and therefore is easily known. The maximum height is converted into the length of the signal in time using the relationship that time equals distance divided by speed where the speed is the approximate speed of sound in the atmosphere. The accurate identification of the pulse frequency using an FFT was explained in Section 3.3.2. Using this information a signal can be synthesised using Equation 3.3.4 where *f* is an array of frequencies matching the required frequency after Doppler shift has been taken into account for each sample point and *t* is an array of time points corresponding to each sample.

$$x(t) = \sin(2\pi f t) \quad \text{(Equation 3.3.4)}$$

The problem with this approach is that the resultant signal has a very narrow spectral width which can lead to problems in the SODAR's peak detection. SODAR peak detection algorithms expect a signal with a spectral width within certain boundaries. If the spectral width is too narrow then some SODARs will reject the measurement while others will allow it but with an error message. This approach also ignores all phase information from the SODAR's signal.

3.3.3.2 Modulation

The original signal from the SODAR can be shifted in frequency to match a desired Doppler shift. Modulation involves multiplying the signal by a cosine that has a frequency matching the desired shift as shown in Equation 3.3.5 where t is time, y is the new signal, x is the original signal and $\Delta\omega$ is the shift in frequency.

$$y(t) = x(t)\cos(\Delta\omega t) \quad \text{(Equation 3.3.5)}$$

Modulation using this simple technique produces two signals; the first is the desired frequency and the second is a reflection about the original signal. As the frequency shifts required for creating SODAR return signals are small a method is needed to remove the reflection. This can be achieved by using a single side band (SSB) modulation technique based on a Hilbert transform. Equation 3.3.6, from Oppenheim (1999), describes this modulation method where jH_x is the imaginary part of the Hilbert transform of x.

$$y(t) = x(t)\cos(\Delta\omega t) + jH_x(t)\sin(\Delta\omega t) \quad \text{(Equation 3.3.6)}$$

This method results in the unwanted reflection being reflected twice so that it has the same frequency as the desired signal and therefore all the energy in the signal is shifted to the intended frequency.

The advantage of using the modulation approach over the synthesis approach is that the return signals created contain a slightly larger spectral width and, as long as it is constructed correctly, contains the phase information of the pulse emitted by the SODAR. Signals created in this way are not reliant on the accuracy of the analysis as only an estimate of frequency and time is needed to create the envelope.

3.3.3.3 Wind Speed Profiles

The wind speed profile that is used in the transponder processing defines the

amount that the signal is shifted in frequency. The most simple profile is a constant speed across an entire height range. This is the staring point for all measurements made using the transponder system. Theoretically any shape wind speed profile can be measured so long as it is possible to show that the transponder processing is accurately able to produce the correct frequency shifts to represent it. This has been carried out for constant speed profiles, profiles with linearly increasing speeds, profiles with a 180º change in direction and profiles following an Ekman model shape. The Ekman model is a simple model of the behaviour of wind in the atmospheric boundary layer featuring a gradual 45º change in direction that is based on the friction effects of the Earth's surface and the geostrophic wind speed. The shape of the profiles is shown in

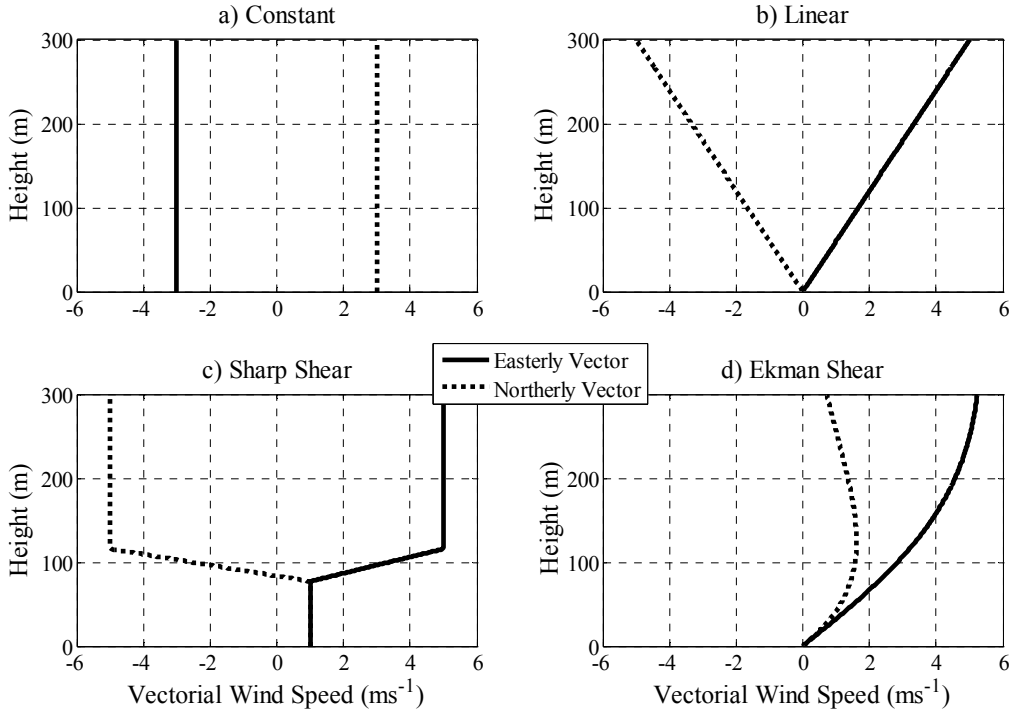

Figure 3.3.2.

Figure 3.3.2 – Wind speed profiles used in transponder processing to generate return echo signals.

3.3.4 Amplitude Envelope

The amplitude of real SODAR echoes decay in time due to the effects of spherical spreading and atmospheric absorption. The amount of decay is dependent on the atmospheric conditions at the time of the measurement. Temperature, humidity, and the frequency of the sound all affect the amount of absorption. Equations 1.3.3 – 1.3.9 can be used to calculate the amplitude envelope of a SODAR echo signal. There are two approaches that can be taken when applying the envelope to the Transponder systems return echo. The envelope can either be made to approximate the conditions in which the measurements are being made or to fit to a prescribed set of conditions. This can be achieved by making measurements of the ground temperature, humidity and pressure and entering these into the the transponder programming. This is a useful approach if the SODAR also measures these variables and uses it with its analysis to look for an expected decay shape. The second approach is to find a set of variables that are average conditions or fit a prescribed measurement aim and applying these regardless of the actual conditions. This approach allows for a more direct comparison between measurements as the only factor affecting the envelope in this case is the frequency of the SODAR pulse. This approach must be adopted for laboratory conditions to create a realistic return in any case. A set of values that is employed in all the transponder experiments within this thesis is shown in Table 3.3.1.

Variable	**Value**
Relative Humidity (%)	20
Ground Temperature (C)	10

Table 3.3.1 – Atmospheric values used in the transponder system.

Figure 3.3.3 shows the envelope based on these values for SODAR echoes at 4 different frequencies covering the normal SODAR operating range.

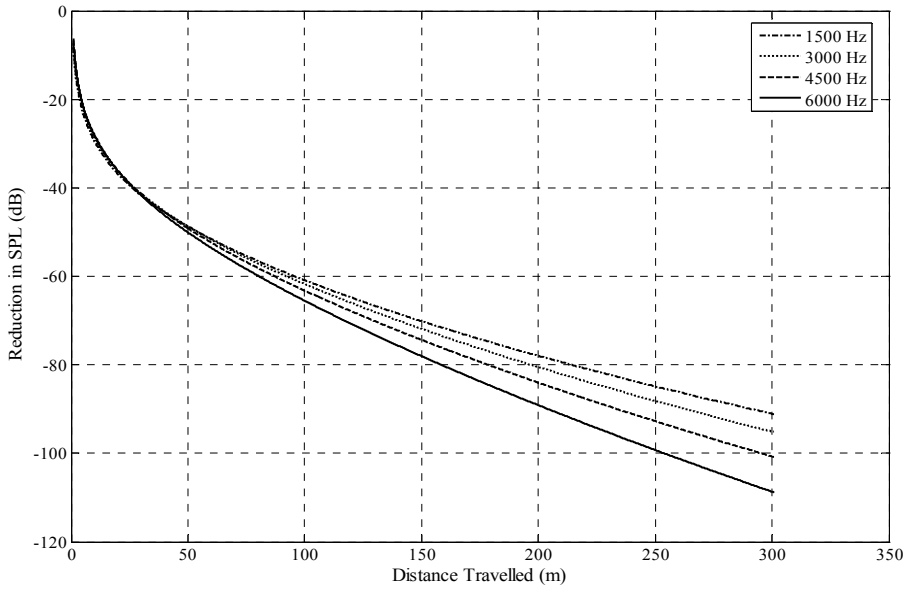

Figure 3.3.3 – Envelope used in the transponder processing for 1500 Hz (dot-dash), 3000 Hz (dot), 4500 Hz (dashed) and 6000 Hz (solid) input signals.

The reduction in SPL is large for all frequencies but it follows the equations for atmospheric absorption, scattering and spherical spreading. The output of a SODAR is normally more than 100 dB so this must be used as a reference for setting the initial amplitude of the return echo, taking into account that the echo should start from 20m and not 0m. Care must be taken to ensure that the amplitude of the return is not loud enough to damage the components within the SODAR.

3.3.5 The Output Stage

The output stage responds to every pulse emitted by the SODAR by playing back the corresponding echo signal. It is triggered in the same way as the input stage without the use of a pre-trigger. It is essential to set up the triggering so that it only responds to the SODAR's output and not to the transponders own output or to background noise so that the cycle of echo signals played by the transponder remains synchronised to the SODAR. To achieve this the trigger-on level is set higher than in the input stage. The required level should not be too high either as this could lead to

the SODAR failing to trigger the transponder. As the SODAR level is usually in excess of 90dB there is a large range of amplitudes that the trigger-on level can be set to. The output stage can be set to play a number of cycles for a given wind speed profile and a number of different profiles automatically through the use of software loops. This allows for large amounts of data to be generated without to much user interaction providing that the trigger mechanism is tested to prove that it stays synchronised. The amplitude of the transponder's echo signals is altered in the output stage so that a good level of signal to noise ratio is achieved in the SODAR measurement without distortion of the signal. This approach results in signals that are slightly louder than would be expected from an average atmospheric echo but within the range that would normally occur.

3.4 Initial Transponder Testing

Testing of the transponder system has been carried out to allow identification of any problems within the transponder system throughout its development. The first stages consisted of using a sine wave generator and a speaker to play continuous signals back to the SODAR. Figure 3.4.1 shows an example of the results recorded using this method where 100s averages of the vectorial wind speed in the east direction are recorded by the SODAR for one range gate centred 130m. The results follow the changes in frequency made in the signal generator but there is a large amount of variability in each frequency step. This is an expected result since the amplitude of the input signal is constant and a lot louder than a typical SODAR echo and the measurements were made in a room with normal levels of reverberation and background noise.

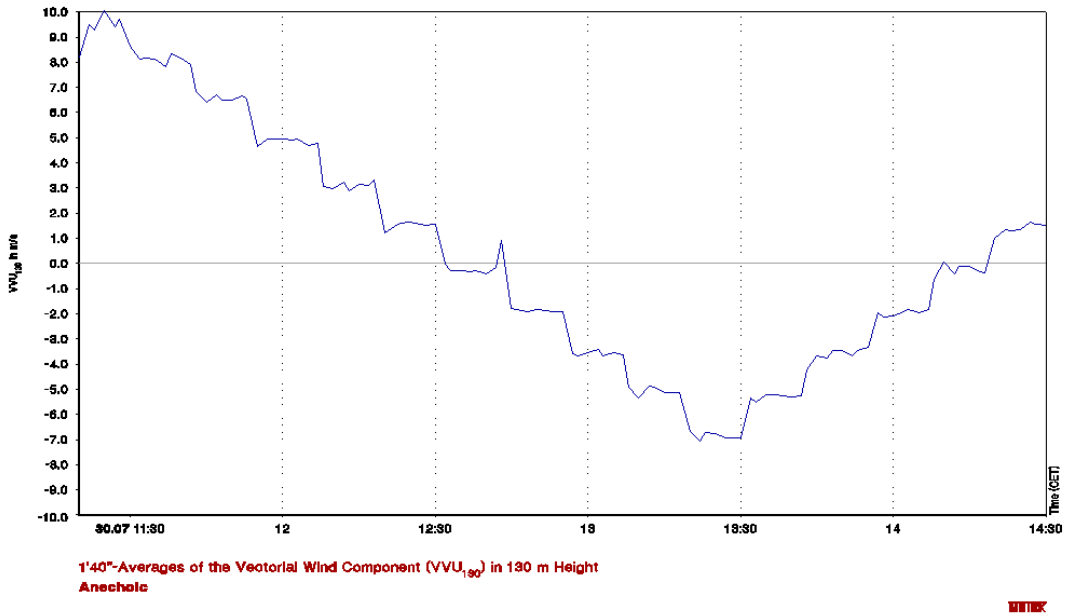

Figure 3.4.1 – Example of results recorded when using an early version of the transponder system with a METEK DSDPA.90-24 SODAR. Data shown is in METEK Grafik software format with time in 30 minute divisions along the X axis and horizontal U vector wind speed in 1 ms^{-1} divisions along Y axis.

As the complexity of the transponder increased to include microphones and the use of signals with realistic SODAR echo amplitudes the need to work in an environment where reverberation and noise were not problematic was identified. All laboratory testing is carried out in semi-anechoic conditions where the only reflecting surface is the floor and the background noise level is rated at 3.8 dBA. The advantage of using a semi-anechoic rather than a full anechoic is that SODARs are placed on hard floors in their normal operational set-up so any reflections from the floor form part of the way a SODAR would behave acoustically and removing these by using a full anechoic could lead to false conclusions. One of the first sets of measurements, after simple programming problems had been eradicated, is presented in Piper (2008) where a simplified system consisting of a single speaker and microphone was used to explore the differences between measurements made using synthesised signals and modulated signals. Figure 3.4.2 and 3.4.3 shows these results as averaged over all heights.

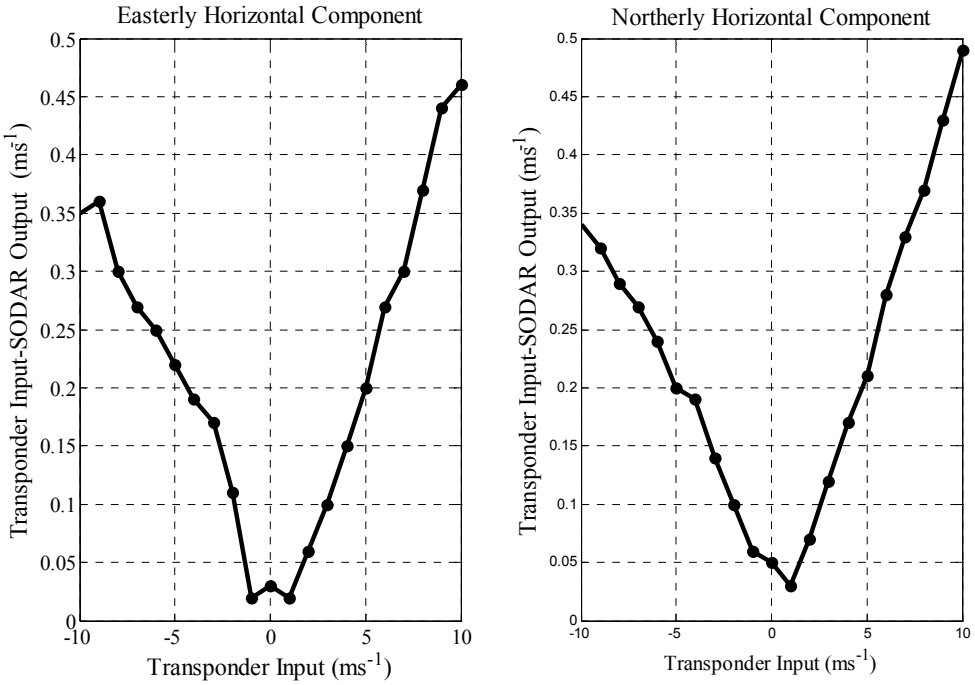

Figure 3.4.2 – Difference between transponder horizontal input speed and the all height mean of SODAR measured horizontal speed in easterly direction (left) and northerly direction (right) when using synthesis to generate transponder return signals.

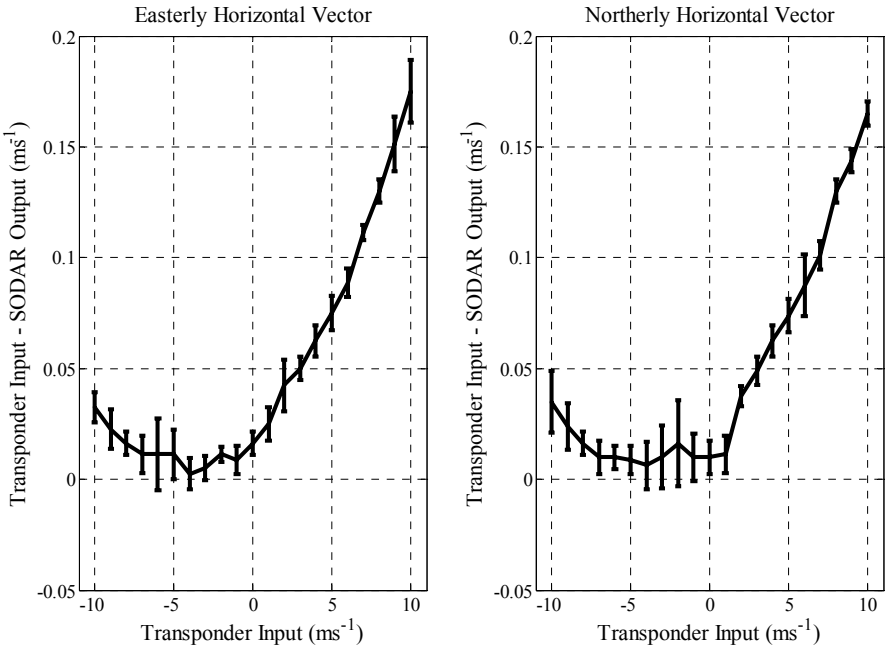

Figure 3.4.3 – Difference between transponder horizontal input speed and the all height mean of SODAR measured horizontal speed in easterly direction (left) and northerly direction (right) when using SSB modulation to generate transponder return signals.

The results show that the modulated signal produced better results and the reason for this was explained in Section 3.3.3 of this thesis. It was evident in these tests that the transponder system presented a bias on the SODAR measurements that was not explained at that point. Speakers were then added to the transponder system so that each SODAR beam had a speaker positioned in the centre of its beam. This resulted in the variance of the results being reduced. Testing carried out after this change have used the same set-up with only some efficiency improvements made to the transponder programming.

3.5 Expected Outcomes of Transponder Measurements

The transponder system is designed to test how different SODARs respond to a known input. Testing a SODAR with the transponder system can tell us if the SODAR's peak detection algorithm can respond to a known signal, how the averaging processes affect the measurement, if there is a systematic bias, if there is any range gate height dependent bias and what equations are being used to calculate the wind speed from the Doppler shift. Testing the peak detection is a diagnostic process as it is unlikely that a SODAR would produce serious errors unless something was wrong with the internal processing of the SODAR. In a field situation the transponder is able to highlight the presence of fixed echoes and it may be possible to quantify the magnitude of these.

3.6 Laboratory Testing of Transponder System

The version of the transponder system described in Sections 3.2 and 3.3 was employed in a semi-anechoic chamber and measurements were carried out using a METEK DSDPA.90-24 SODAR. The aim of these measurements was to explore the complete functionality of the transponder system in a controlled environment and to explore what information could be gained about how the SODAR operates. Further measurements were attempted using an AQ500 SODAR to see how transferable the system was for use with different SODARS.

3.6.1 Methodology

The transponder is set-up as shown in Figure 3.2.7 with the microphone and speakers positioned 2.2m above the SODAR array. 2.2m is the maximum separation distance possible in a semi-anechoic chamber that is available at the University of Salford. The separation distance between the transponder components and the SODAR needs to be large enough so that the microphone is not in the acoustic near-field thus ensuring a reliable recording of the SODAR output. Referring to Figure 3.2.6 this is a large enough distance for all small commercial SODARs except the ASC4000 where the edge of the near-field at its operating frequency is 3.2m. In order to make the measurements the SODAR is set to record 2 minute averages as this reduces the time required to collect the results and as there is no variability in the conditions or signal averaging for long periods is considered unnecessary. The transponder is set-up to run four different tests on the SODAR where in each case signals are created using the laptop and played back according to the triggers from the SODAR.

The first is a test on the vertical beam alone as a diagnostic test to ensure the transponder is able to test accuracy of the SODAR's basic peak detection algorithm. Returns are made for 5 different vertical velocities (-0.5, -0.2, 0, 0.2 and 0.5). These speeds are selected as they are all within the normal range of vertical velocities found in the atmosphere and any negative or positive bias will be highlighted by testing above and below zero. The aim of this test is to give a baseline confidence interval for any measurement made by a SODAR.

The second test is an extended set of measurements using constant wind speed profiles with all three of the SODAR's beams. At least two 2 minute averages are recorded by the SODAR for each horizontal wind speed input from the transponder at intervals between -30 ms^{-1} and 30 ms^{-1} with smaller intervals between -15 ms^{-1} and 15 ms^{-1} as this is the region of highest interest. The principle aim of this measurement is to see if the transponder can check the peak detection works at a simple level, to detect which Doppler shift equation the SODAR uses to calculate wind speeds and to see if

any range gate height dependent effects occur due to the envelope employed by the transponder. In Chapter 2 different equations for calculating wind speed from Doppler shift were shown and it is important that it is known which of these is being used by a SODAR as the difference is between 1 and 2 %. This is the total certainty required for the whole measurement by the wind energy market and therefore this knowledge is vital.

For the third test the transponder was set to use the wind profiles that had changing wind speeds shown in Figure 3.3.2. This test was carried out to examine whether the transponder system could be used to test wind profiles and atmospheric models of increased complexity.

In the fourth test the transponder used several constant speed wind profiles with white noise added to the signal at different levels. This test was carried out to test if the transponder can find a ratio between the signal and noise levels where the SODAR can no longer function correctly. The test is carried out with one wind speed set in the transponder. White noise is added in levels from 1% to 100% in relation to the peak amplitude of the transponder echo. It is expected that the errors will increase in the highest range gates first as the signal levels are lower with increased degradation as the noise level is increased. This test could also be carried out using specific types of sound interference such as birdsong or aeroplane passover sounds so that a prediction of the amount of SODAR data drop-out in the presence of such sounds could be predicted. These sounds are intermittent but they could reduce the number of points within an average by a significant percentage. For the purpose of testing a SODAR for use in a specific measurement site recordings of the background noise at measurement site could be used for this test to give an expectation about how the data will be affected.

3.6.2 Results from Testing with METEK DSDPA.90-24

The set of results in this section are from using the transponder with a METEK DSDPA.90-24 that the development of the transponder was carried out with. The results are split into the four tests that are described in the previous sub-section. The SODAR used a range gate size of 15 metres and a signal frequency of 2100Hz for all the tests except test two where 2300 Hz and 1900 Hz were additionally tested. These frequencies were tested as they are all within the manufacturer's suggested operating range and testing 3 different frequencies allows insight into any frequency dependent effects. The METEK uses spectral and cluster averaging methods providing two sets of data for analysis. These two averaging methods are related to the two simplified methods explored in Chapter 2 and their differing results are compared here.

3.6.2.1 Test One - Vertical Speed Estimation

The results are recorded for five 2 minute averages across the whole height range. Table 3.6.1 shows the mean difference and standard deviation recorded for each of the 5 speeds for all the data at that speed.

Input Speed (ms^{-1})	Mean Difference (ms^{-1})	Standard Deviation (ms^{-1})
-0.5	-0.018	0.027
-0.2	0.012	0.010
0	0.007	0.026
0.2	0.007	0.006
0.5	0.013	0.012

Table 3.6.1 – Mean difference and standard deviation of 5 tested vertical velocities over the complete data set recorded.

The trend is an overestimation close to 0.01ms^{-1} with no obvious positive or negative bias. To investigate these results further the height specific mean and standard deviation are calculated for each input speed. Figure 3.6.1 shows this data.

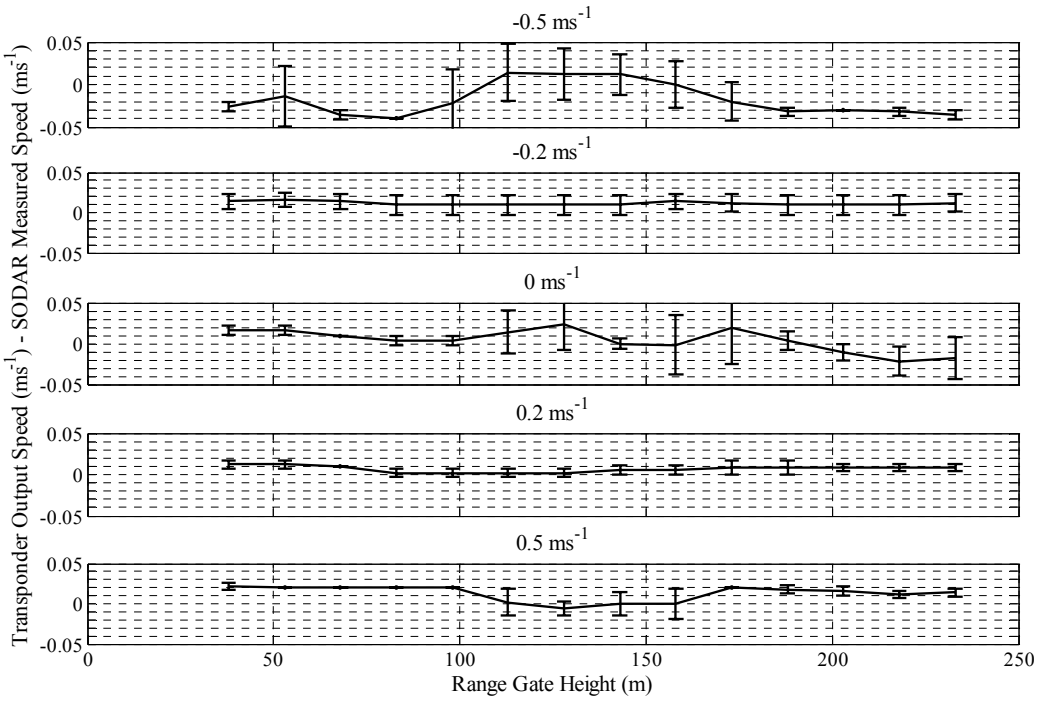

Figure 3.6.1 – Mean and standard deviation of the difference between the transponder input speed and the SODAR measured speed for each range gate height and input speed.

The results shown above highlight that there is high consistency across all the heights for positive and negative 0.2 ms^{-1} but for the other input speeds there is some variability across the different heights. The trend is not clear although there is some evidence that the higher heights have slightly less consistency and this is due to the lower signal to noise ratio recorded at these heights which is an expected result. The consistency at positive and negative 0.2 ms^{-1} may be due to some expectation within the SODAR processing since these vertical speeds are more likely to occur in nature than the other speeds. However +/-0.5 ms^{-1} is within the normal range and only 0 ms^{-1} is unrealistic.

3.6.2.2. Test Two– Constant Wind Speed Profiles

The SODAR was operated with three different frequencies for this test. The data for 2100 Hz is shown first and then comparisons to the data recorded for 1900 Hz and 2300 Hz are given. Figure 3.6.2 shows the differences between transponder input and SODAR measured horizontal velocity for the U and V vectors of the wind speed for both averaging methods.

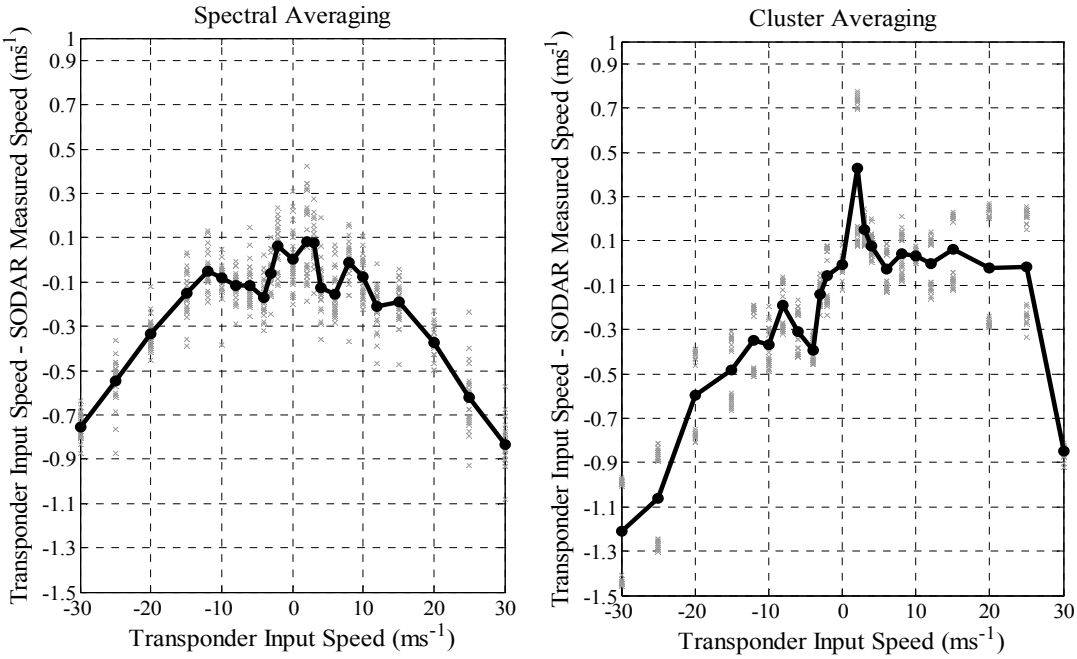

Figure 3.6.2 – Difference between transponder input speed and SODAR measured speed in vector components U and V for spectral and cluster averaging methods.

These results show a curve that is approximately a 3% difference for all speeds between the transponder and the SODAR. This occurs because the Doppler shift equation used by the transponder is different from the equation used by the METEK SODAR. In Chapter 2 two different equations for calculating velocity from Doppler shift are compared. The transponder system uses Equation 2.8.1 and the SODAR uses Equation 2.8.2. Figure 3.6.3 show the differences once the change in the Doppler shift calculations has been taken into account.

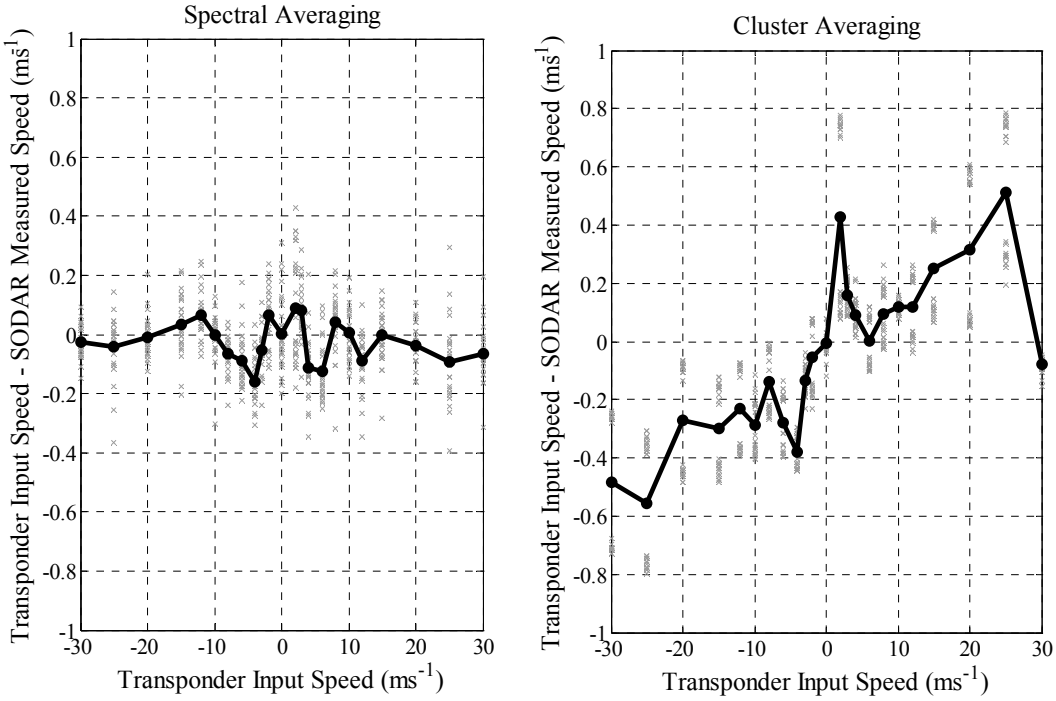

Figure 3.6.3 - Difference between transponder input speed and SODAR measured speed in vector components U and V for spectral and cluster averaging methods after difference in Doppler equation is accounted for.

From Figure 3.6.3 it can be seen that the spectral averaging method gives differences that are mainly close to 0 ms^{-1} but with some variation at lower input speeds. There is some data spread around the mean for each speed. To explore this the difference at each height for each speed is plotted to highlight any range gate specific differences. Figure 3.6.4 shows the average U component differences recorded for each height at each input speed.

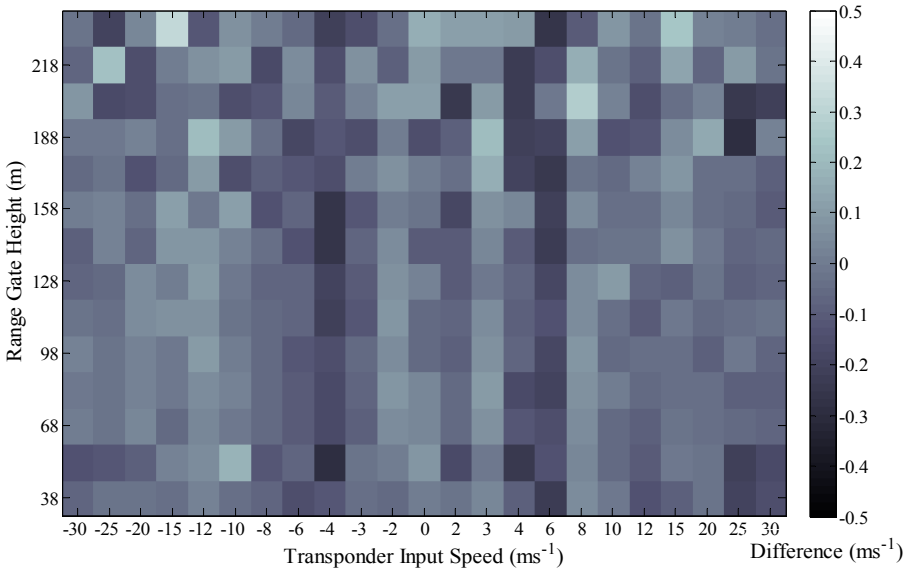

Figure 3.6.4 – Differences in U component at individual heights for each transponder input speed using spectral averaging.

while there is no strong height dependency in the results shown in Figure 3.6.4 the measured wind speed deviates from the transponder input speed more often at higher heights so it can be seen that the low amplitude of the transponder signal due to the amplitude envelope applied results in higher uncertainty. The frequency peak is closer to the noise floor and is therefore harder for the SODAR's peak detection algorithm to detect precisely. This result is expected and occurs in all normal SODAR measurements. In Figure 3.6.3 the results using the cluster averaging show a persistent underestimation of the transponder input speed by approximately 1.6%. The differences in the cluster averaging results are plotted for individual range gates to explore if there is any range gate dependent effects occurring. This is shown in Figure 3.6peak detection the average.5.

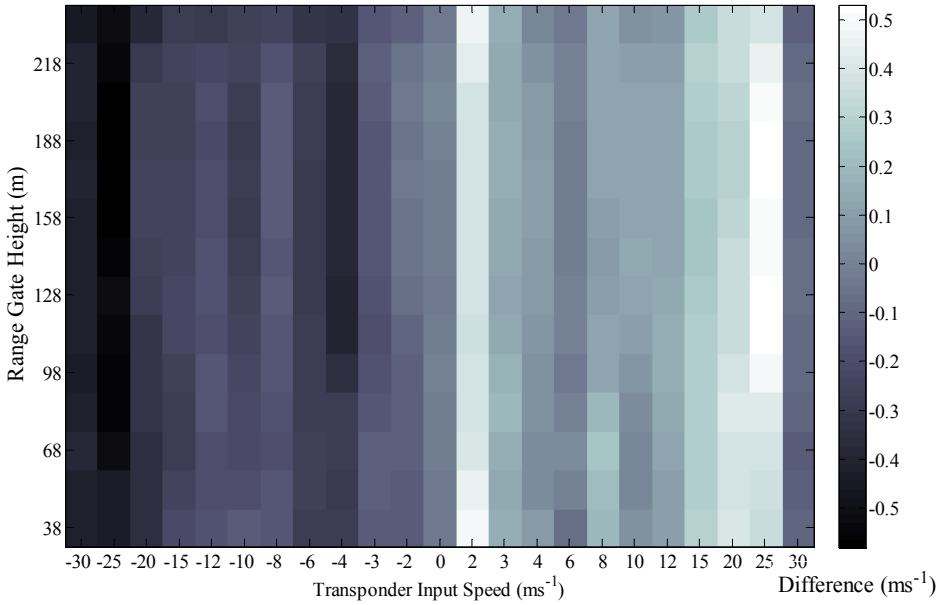

Figure 3.6.5 - Average difference in U component at individual heights for each transponder input speed using cluster averaging.

The profiles recorded using the cluster averaging method are very consistent across all heights. In Figure 3.6.2 the data for the cluster method appears in two distinct groups for each input speed. Two averages were measured for each speed and these are separated and shown in the Figure 3.6.6.

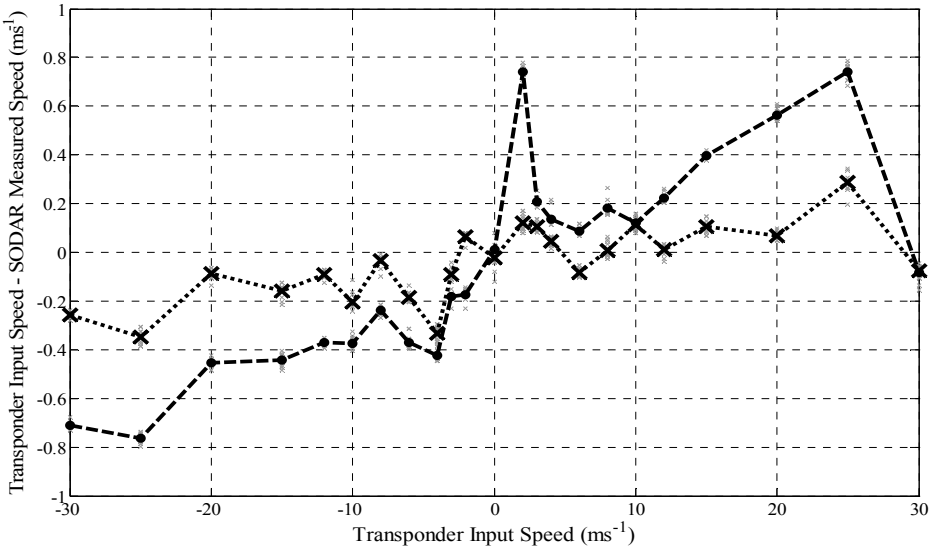

Figure 3.6.6 - Difference between transponder input speed and SODAR measured speed for

horizontal vector component U for two separate averages using the cluster averaging method (First average-dashed, second average-dotted).

It is clear that the second average has smaller differences than the first . The cluster method is a statistical analysis approach that is based on finding the most likely radial speed in an averaging period from all the radial components measured during that period. It is a complex version of an algorithm where the peak is identified for individual returns and then an average of all these peak positions is taken. As a consequence the consistency across all heights is expected. The difference between the two averages may be due to a residual expectation in the first average from the previous measurement speed causing a negative bias or it is a result of the first radial speeds recorded being estimated with the increased difference level and this difference then being carried through the average due to the expectation of the algorithm. It should be noted that the software used in the METEK SODAR that was used for these tests is an early version and newer versions will feature a more sophisticated cluster algorithm so if this difference is caused by the carry through of an initial error in this case it is unlikely to occur to the same degree in a newer METEK SODAR.

The same test was repeated with the frequency of the pulse emitted by the SODAR set to 1900 Hz and 2300 Hz. Figure 3.6.7 shows the mean error in the U and V horizontal speed components for all three frequencies tested for spectral average data.

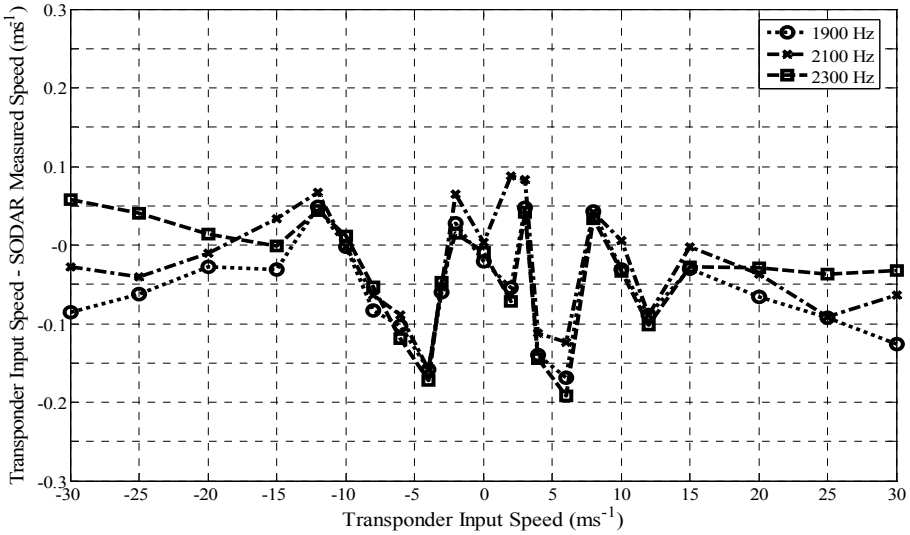

Figure 3.6.7 – Difference between the transponder input speed and the SODAR measured speed using spectral averaging for the U component of the horizontal wind speed at three different frequencies (1900 Hz – dotted/circle, 2100 Hz – dashed/cross, 2300 Hz – dot-dash/square).

The differences between the transponder input and the SODAR data for the three different frequencies are very similar and the presence of the same peaks at positive and negative 4 ms^{-1} suggest that there is a systematic artefact being introduced at these speeds that is likely to be a result of the DSP used in the transponder to create the return signal.

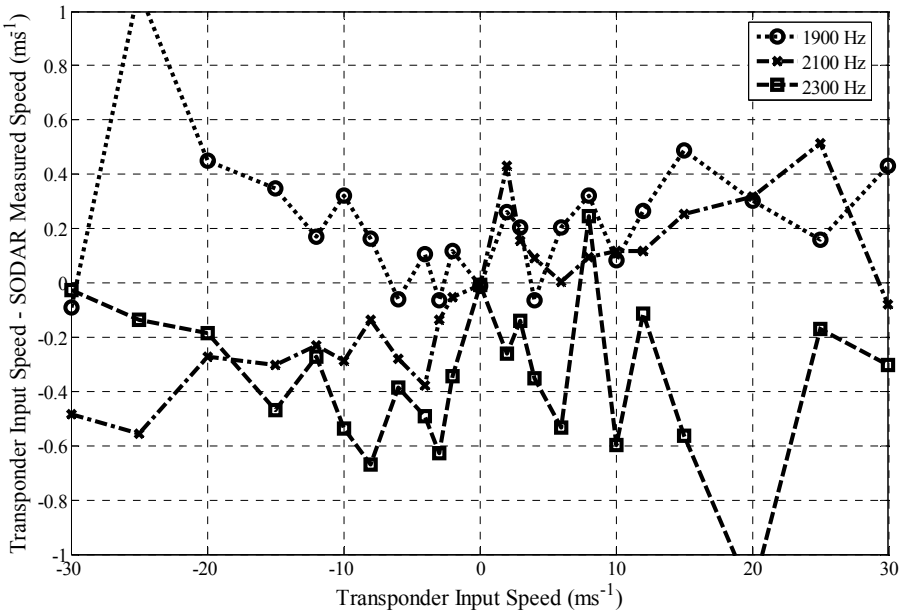

Figure 3.6.8 – Difference between the transponder input speed and the SODAR measured speed using cluster averaging for the U component of the horizontal wind speed at three different frequencies (1900 Hz – dotted/circle, 2100 Hz – dashed/cross, 2300 Hz – dot-dash/square).

The results using the cluster method show a large difference between the three frequencies tested. This occurs for the same reason that a consistent difference was found between the two individual averages made that are shown in Figure 3.6.6. It is thought that it is an artefact of an expectation within the peak detection algorithm that results from initial errors in the measurement. Tests with the newest METEK software may see results that are more consistent with the spectral averaging approach.

The results of this test show that the results measured by the SODAR compare well with the input speed from the transponder when using the spectral averaging method and that there is no height dependence except the slight increase in uncertainty due to the lower amplitude of the signal representing the higher range gates. The results show clearly that the METEK SODAR uses Equation 2.8.2 to calculate wind speeds from frequency shifts and therefore it can be concluded that use of the transponder allows the Doppler shift equation employed by a SODAR to be found. The results recorded using the cluster averaging method show a persistent

misinterpretation of the input wind speed which is consistent across all heights but not between separate averages. It is thought that is a result of expectation within the cluster averaging algorithm.

3.6.2.3. Test Three – Changing Wind Speed Profiles

The SODAR was operated at 2100Hz for this test where changing wind speed profiles were used to create the return echoes. The results are corrected for the difference in Doppler shift calculation. Figures 3.6.9 and 3.6.10 show the mean measured data for linear profiles and the difference between the transponder input and the SODAR measurement for the U and V components of the horizontal wind speed.

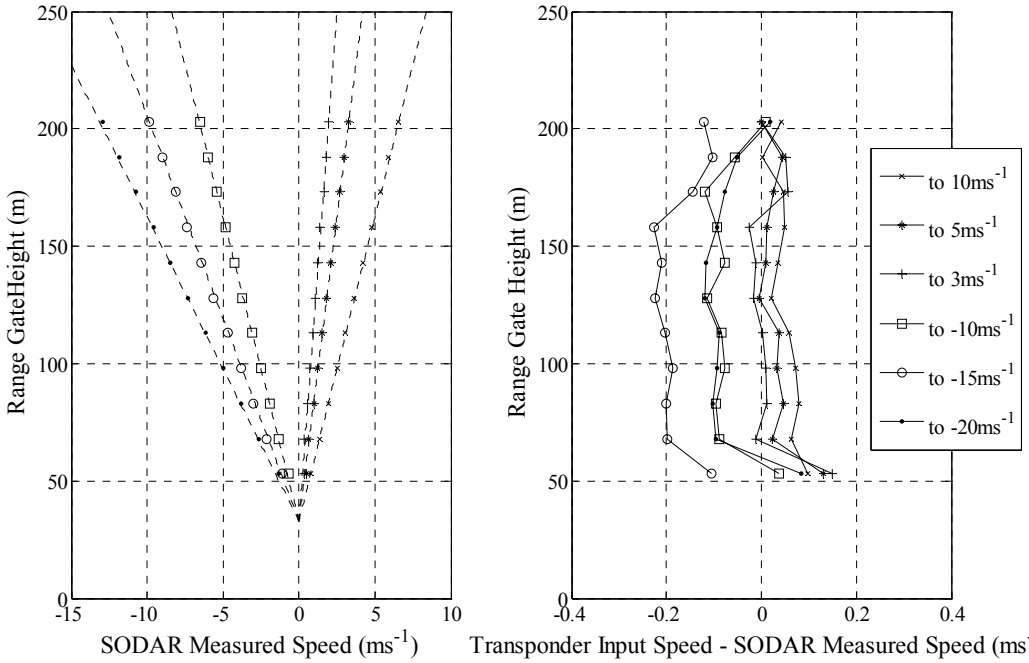

Figure 3.6.9 – Mean measured wind profiles and the difference between the transponder input speed and the SODAR measured speed for the U component of the horizontal wind speed.

Figure 3.6.10 – Mean measured wind profiles and the difference between the transponder

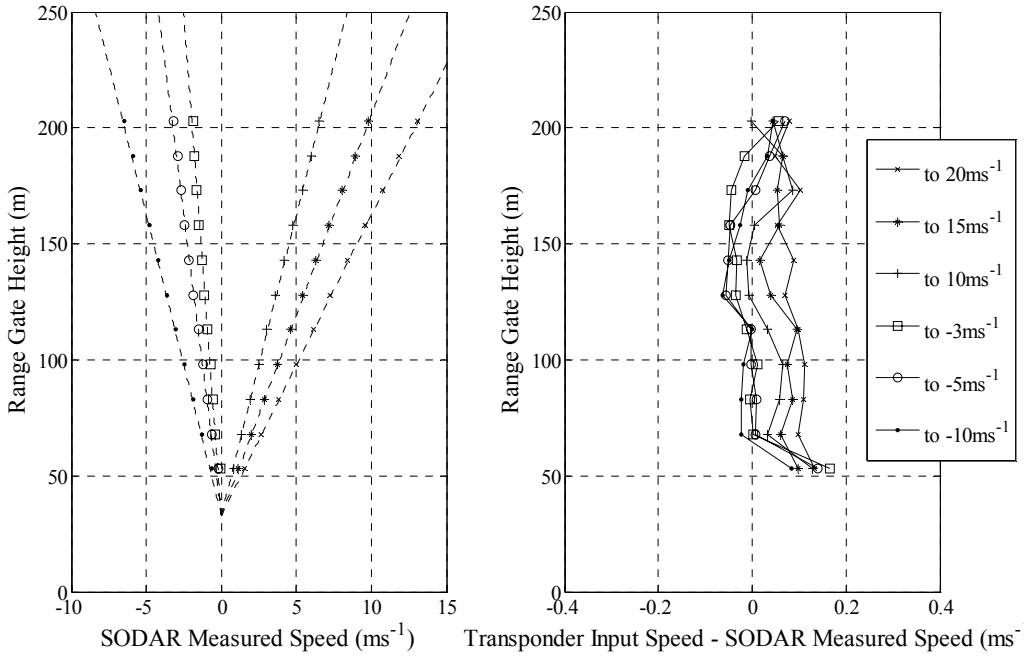

input speed and the SODAR measured speed for the V component of the horizontal wind speed.

The results are similar to those found with constant speed profiles although the differences tend to be marginally larger especially for large negative velocities. Figure 3.6.11 shows the measured results of a sharp 180º direction change.

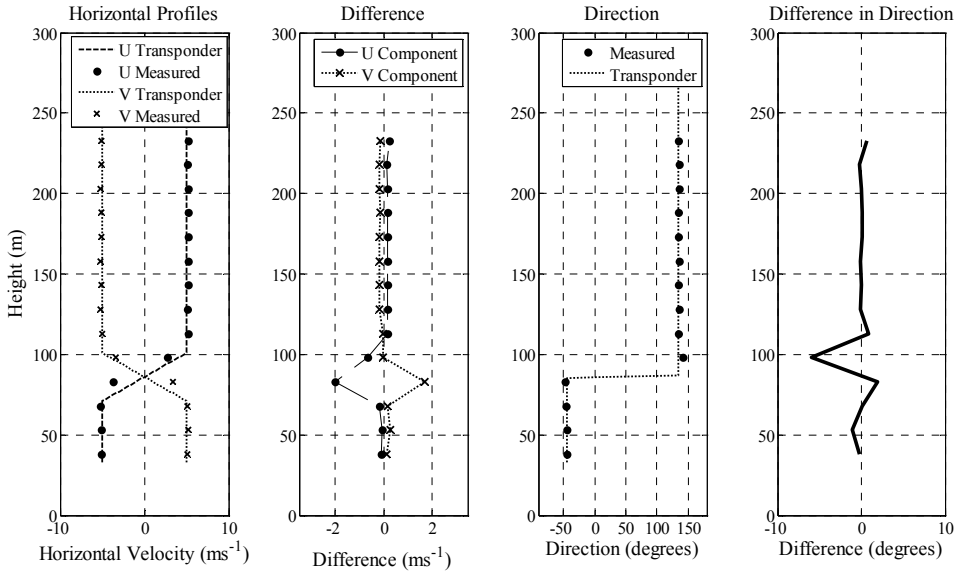

Figure 3.6.11 – Measured wind profiles that contain a 180º change in direction with differences between the transponder input and the SODAR measurement for U and V horizontal components and wind direction.

For both the U and V components above and below the direction change the velocity is measured consistently. At the change the measurement lags the profile by half a range gate. This is due to the way the SODAR averages in range gates and to a large spectral broadening of the transponder signal at the points were the change starts and finishes. This spectral broadening is an artefact of the Digital Signal Processing (DSP) used in the transponder and is unavoidable. The difference in the direction peaks at 5° where the change stops and then returns to near zero at the next range gate.

Figures 3.6.12 and 3.6.13 show the mean data for the Ekman model profiles and the differences between the transponder input and the SODAR measurement.

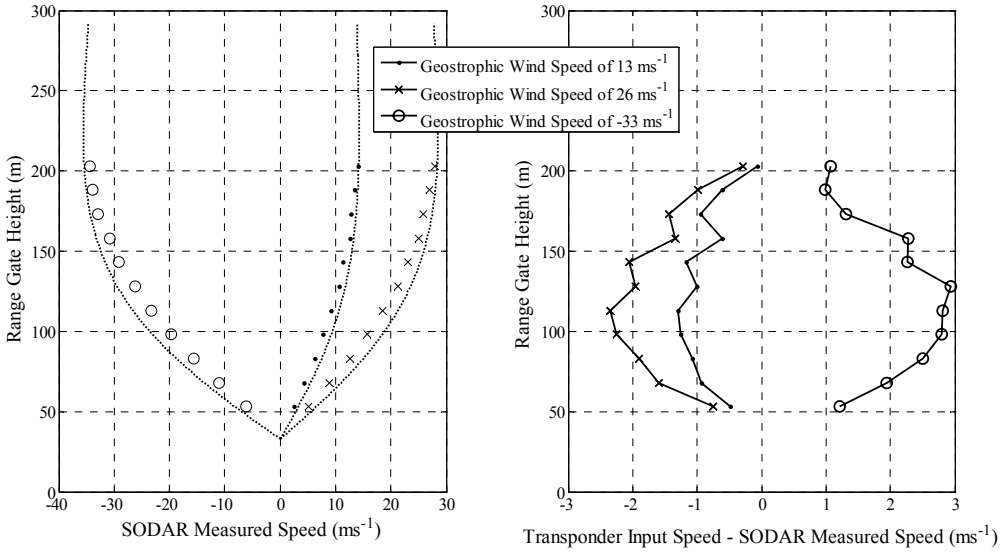

Figure 3.6.12 - Measured profiles and difference between transponder input speed and SODAR measured speed of the U component of the horizontal wind speed for profiles based on an Ekman spiral model.

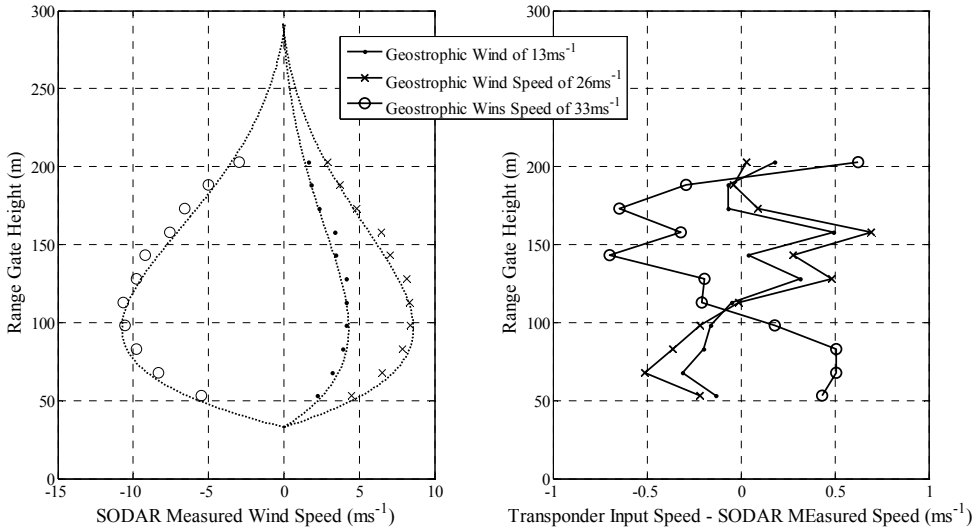

Figure 3.6.13 - Measured profiles and difference between transponder input speed and SODAR measured speed of the V component of the horizontal wind speed for profiles based on an Ekman spiral model.

As with the shear case there is a lag in the measurement compared to the transponder profile. In this case this is caused by the range gate averaging process used by the SODAR as gradual changes do not cause the spectral broadening problems

experienced with sharp changes. The lag follows the rate of change in the profile. In the U component (Figure 3.6.12) the difference switches from signs as the velocity switches from increasing to decreasing and in the V component it tends towards zero once the stable velocity is established. In all cases there is a problem with the first range gate. This is due to the signal from the transponder not being emitted for the first part of this range gate so a bias is introduced into the SODAR measurement. Currently the lowest height at that the transponder echo emitted is 33m and therefore for a 15m range gate centred on 38m the first 3.5m of the averaging range has a zero result although this is not always measured as 0 ms^{-1} wind speed.

3.6.2.4. Test Four – Constant Wind Speed Profiles in Presence of White Noise

Figure 3.6.14 shows the differences between the SODAR and the transponder input speed for each range gate with different levels of white noise added to the signal from 1% to 80% in relation to the peak amplitude of the transponder echo signal.

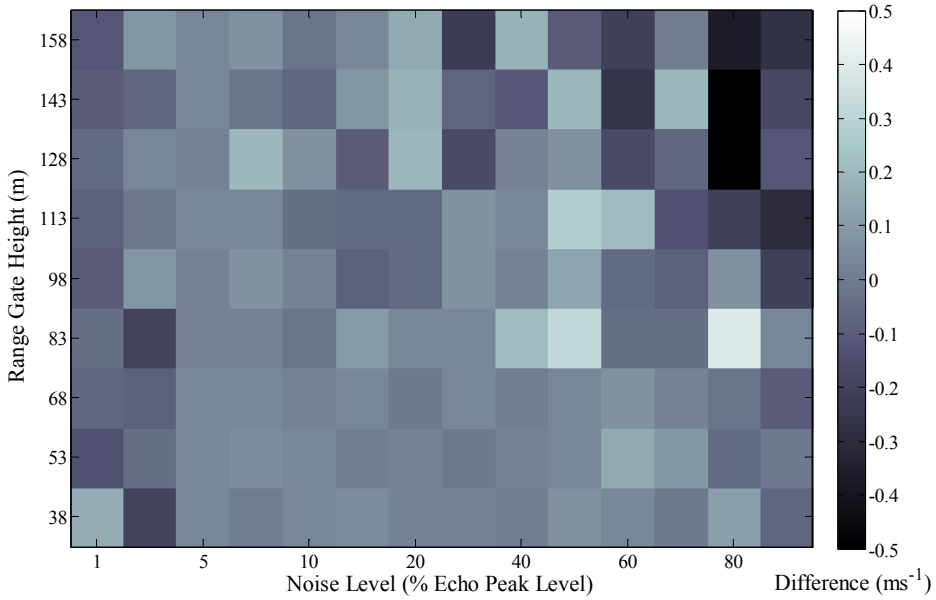

Figure 3.6.14 – Difference between SODAR measured speed and transponder input speed for averages with white noise added to the transponder signal with amplitudes of 1% to 80% in relation to the peak echo amplitude.

For low levels of white noise there is no degradation of the measurement. As the noise level is increased the difference between the transponder and the SODAR increases starting with the highest range gates. From 40% the SODAR data also recorded error messages stating that there was the presence of white noise signal. This reporting is individual to the METEK SODAR but it shows that the SODAR can measure beyond the level at which it has detected a noise signal. Tests were continued with the noise level set at 100% and 120% but at these levels almost no meaningful data was recorded by the SODAR. The drop off rate between the SODAR recording data with an error code and not recording any data is steep occurring in less than a 20% amplitude change which is 2 dB in SPL terms.

3.6.3 Measurements with the AQ500 SODAR

The transponder was tested with an AQ500 SODAR in semi-anechoic conditions. The AQ500 SODAR operates with three tilted beams horizontally separated by 120º. It employs two pulses for each beam, one short and one long, for each measurement. This is to give a better resolution at lower heights while offering a range extension with the longer pulse. In order to use the transponder system with the AQ500 SODAR the processing is changed to take into account these operational factors. Changing the processing to account for the different beam orientations requires a change to the frequency shift calculations. The short pulse employed by the AQ500 SODAR is designed to measure for 50-80m from 20m. This presents a problem for the transponder processing as it starts from 35m, 15m after the SODAR, and the length of the pulse is to short to generate sufficient power in the return over the remaining time window that the AQ500 does not record this echo consistently if at all. Some results were recorded for the longer pulse that represent the higher part of the measurement range. These results were limited to spectrum plots as shown in Figure 3.6.15 and no meaningful data was recorded.

It is thought that the SODAR rejects the transponder's echo as it doesn't match conditions it imposes in its data quality processing. This highlights a flaw in the

transponder system that needs to be overcome in order to use the system for all SODARs. Previous testing with the METEK SODAR has resulted in accepted wind speeds but an error message in the SODAR data is often found that states that the spectral width of the transponder echo is narrower than a real echo is expected to be. This problem could be solved by convolving the signal with a Gaussian or using a more complex wind profile model that offers many small frequency changes around the intended speed. The latter is computationally expensive and difficult to implement without causing significant digital signal processing errors.

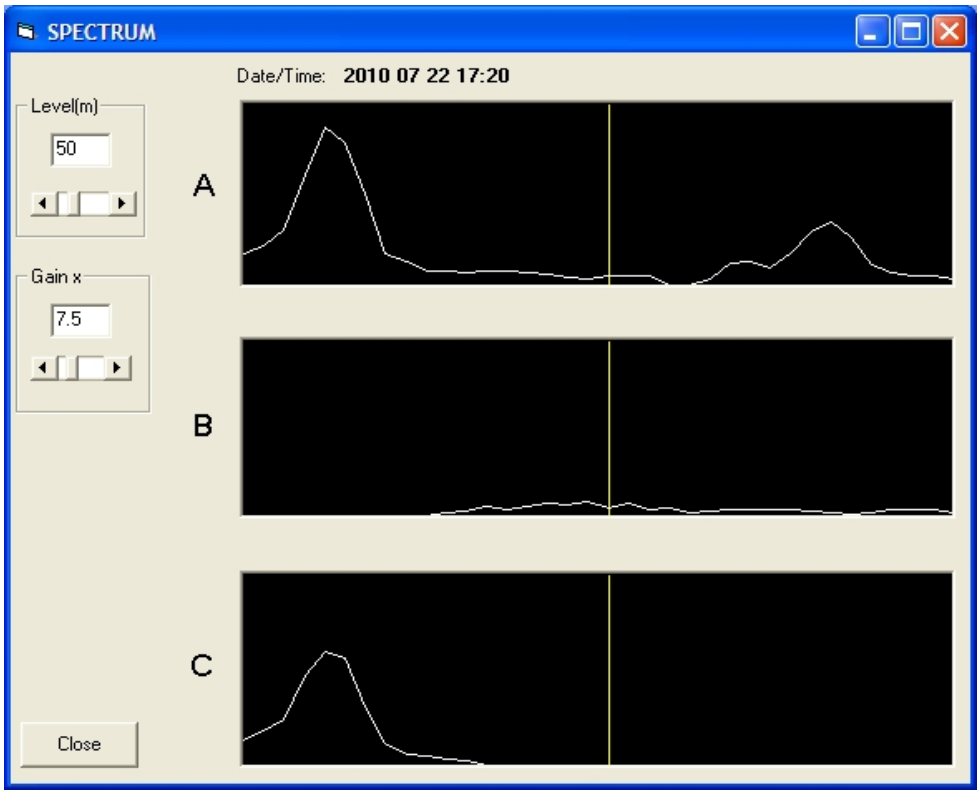

Figure 3.6.15 – Example of spectrum recorded with AQ500 SODAR when testing with transponder system.

3.6.4 Discussion

The transponder has been shown to work in laboratory conditions with one SODAR although there are significant error levels when that SODAR uses a cluster averaging technique. Further understanding of this effect is needed although it is

thought to be a systematic bias introduced by the transponder that is carried through the measurement due to the speed expectation inherent to the cluster algorithm. With a second SODAR the transponder system failed to work as expected and there is an issue with the spectral width of the signal that needs to be overcome. The transponder system can identify which Doppler shift equation is being used by a SODAR when the system is operating with the SODAR correctly. There is also the potential that it will be able to detect the type of peak detection – averaging method used by a SODAR but further reliable measurements are required on a range of SODARs before this is confirmed.

3.7 Field Testing of Transponder System

It is desirable to test SODARs in a field situation with the transponder system. There are several problems that need to be solved in order to be able to use the transponder system in the field. These are the presence of a real atmospheric echo, increased levels of background noise compared to measurements made in a semi-anechoic chamber, impulsive wind noise on the microphone and the need for a physical structure to mount the transponder components on. The different possible options for this adaptation are described here and then measurements made at two sites with two different SODARs using the transponder in this way are given.

3.7.1 Details of the Specific Problems Faced by the Transponder in a Field Situation

3.7.1.1 The Real Atmospheric Echo

The measurements made in the anechoic chamber had no real atmospheric echo present since the sound emitted by the SODAR was absorbed by the ceiling and walls of the chamber. In the field any sound emitted by the SODAR is reflected back to the SODAR with frequency changes according to the actual wind speed at the time. This creates an error in the Transponder-SODAR measurements in the same way a fixed

echo affects a normal SODAR measurement but the error is towards the actual wind speed rather than $0ms^{-1}$.

3.7.1.2 Background Noise

The level of background noise in the semi-anechoic chamber was very low compared with the level found outside. The general background noise level reduces the overall signal to noise ratio of the SODAR measurement and therefore the highest range gate from which measurements can be reliably made is lower. For the measurements with the transponder the result is that the higher uncertainty found at the highest range gates in the laboratory measurements occurs at much lower heights so overall the variance of the results will increase.

3.7.1.3 Impulsive Wind Noise on the Microphone

Wind and specifically gusts that are incident on a microphone cause high levels of noise to be recorded by the microphone. For the recording part of the transponder processing this results in a poor quality signal being recording. The impulsive nature of the gusts could cause the triggering in the playback part of the transponder to trigger out of synchronisation with the SODAR and therefore ruining a whole measurement.

3.7.1.4 Physical Structure

In the semi-anechoic chamber the components of the transponder can be fixed to the ceiling in known and repeatable positions. In the field a structure is needed that can replicate this. The structure needs to be big enough to satisfy the requirement of being at least 2.2 metres taller than the SODAR's array.

3.7.2 Adapting the Transponder for Use in the Field

Several possibilities for converting the Transponder into a field measurement system have been investigated. These are portable anechoic chambers, dome frames

and large dome shape tents such as Yurts, arched framework and gazebo frames. Some of these were also thought about as methods for the outdoor SODAR beam shape measurements that are described in Chapter 4. In some cases additional solutions are needed to deal with noise and the real atmospheric echo.

3.7.2.1 Portable Anechoic Chambers

This is the ideal solution in terms of acoustic performance since it would give very similar conditions to the laboratory with little background noise and no atmospheric reflections. Currently at least one company manufactures portable full and semi anechoic chambers. The sizes available are insufficient to house most SODARs along with the transponder components with the necessary separation. A bespoke chamber would be required, which is an expensive option. Logistically the chamber would have to be modular and a van or trailer would be needed to transport it.

3.7.2.2 Dome Frames and Tents

There are many different tent shapes available from the typical camping dome tent to large tents used for events. In principle an enlarged dome tent would be a good solution since it would be highly portable and has a curved structure that could be utilised for positioning components correctly and to make directivity measurements by running microphones along its structure. Yurt type tents as pictured in Figure 3.7.1 are less portable but their shape is better as they have an uncurved part at the bottom that makes them tall enough to accommodate most SODARs with full baffles. Geodesic dome type structures are also commercially available, an example is shown in Figure 3.7.1.

Figure 3.7.1 – Examples of dome tent structures that could be used to house the transponder system in a field situation (Left to right – Large Dome Tent, Geodesic Greenhouse, Garden Yurt)

The principle problem with using any of these structures is that the material that forms the walls is reflective of sound and therefore a reverberant field would be created by operating a SODAR inside one. This would influence the measurements made in the lower range gates and could cause components in the SODAR's signal chain to become damaged due to the excessive levels of returning sound. The material is part of the structure of all but the Yurt of the three examples discussed and therefore cannot be removed easily. The inside could be treated with acoustic foam but this reduces the portability of the solution.

3.7.2.3 Arched Framework

An arched frame could be created that allows exact positioning of the transponders components. This could be made from aluminium or steel. Figure 3.7.2 shows what this structure would look like.

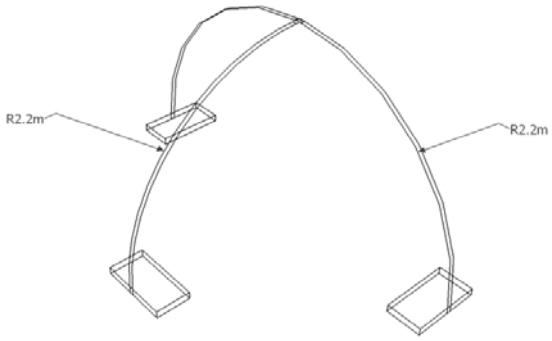

Figure 3.7.2 – Arch structure that could be used to hold the transponder components in position above a SODAR.

This structure would be very heavy and there are few manufacturers who can roll steel or aluminium bars to the correct shape. It is also a somewhat impractical shape to transport

3.7.2.4 Gazebo Frames

A very simple solution for a physical frame to hold the transponder components is the frame from a portable gazebo. This consists of a metal frame that unfolds to form a square area with a pyramid shaped roof. It is very portable as it is designed to be taken to camp sites and therefore could be transported and set-up by one person. It does not provide any acoustic qualities so methods to protect the microphone from impulsive wind noise and remove the effects of the real atmospheric echo and background noise are required. Microphone covers that protect from gusts have been used in the broadcasting industry for many years. They consist of acoustically absorbent foam and a loose fibrous outer cover. The outer cover breaks up the gust velocity near the microphone and the foam absorbs the excess noise. Removing the atmospheric echo is a more complicated problem. Attempts to use a acoustic foam layer above the

transponder components has been trialled but the effects are still noticeable as shown in the following section.

3.7.3 Field Measurement Results With a METEK DSDPA.90-24 at Carrington (UK)

Measurements were carried out using the Gazebo frame to hold the transponder system in place using the same methodology as the laboratory based measurements. However, due to time constraints and wet weather not all of the tests were carried out. The first test that measures just the vertical beam and the fourth test where noise is added to the signal were neglected. The focus of these measurements was to ascertain how the transponder system performed outdoors. It should be noted that the signal to noise ratio was initially found to be very low compared to the measurements made in the semi-anechoic chamber and therefore the output of the transponder was amplified to achieve a reasonable signal to noise ratio. It was later found that this occurred because the amplification stage of the SODAR's input was not functioning correctly.

3.7.3.1 Test Two – Constant Wind Speed Profiles

It was established during the laboratory measurements that the Doppler shift equations used by the transponder and the METEK SODAR were different and therefore the correction for the difference is automatically implemented for these measurements. Figure 3.7.3 shows the data collected for these measurements.

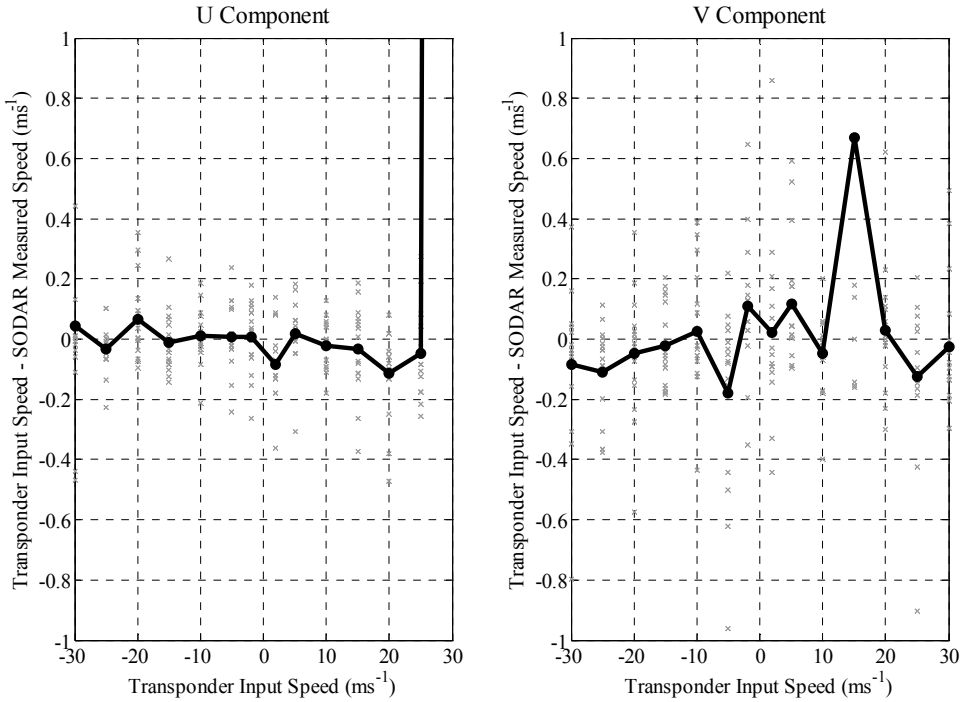

Figure 3.7.3 – Difference between transponder input speed and SODAR measured speed for measurements of the components of the horizontal wind speed made outside at Carrington with the METEK SODAR using spectral averaging only.

The differences between the transponder and the SODAR measurements are similar to those measured in laboratory conditions. The data spread is slightly larger and there are some obvious inconsistencies such as at 15ms^{-1} in the V Component. This is caused by the presence of interference from the surroundings during the averaging period. It was noted that a lorry reversing signal was audible at the time of this average. This highlights the need to protect the signal from such influence by either using a method of noise reduction or by repeating measurements when occurrences of tonal noise interference are noted. It also highlights the need for understanding of how noise features at a measurement site will reduce the amount of valid data collected within a measurement average as discussed in Chapter 2.

3.7.3.2 Test Three – Changing Wind Speed Profiles

Tests where the transponder used linear and Ekman shaped profiles were carried out.

Figure 3.7.4 shows the profile shapes and the difference between the transponder and the SODAR measurements.

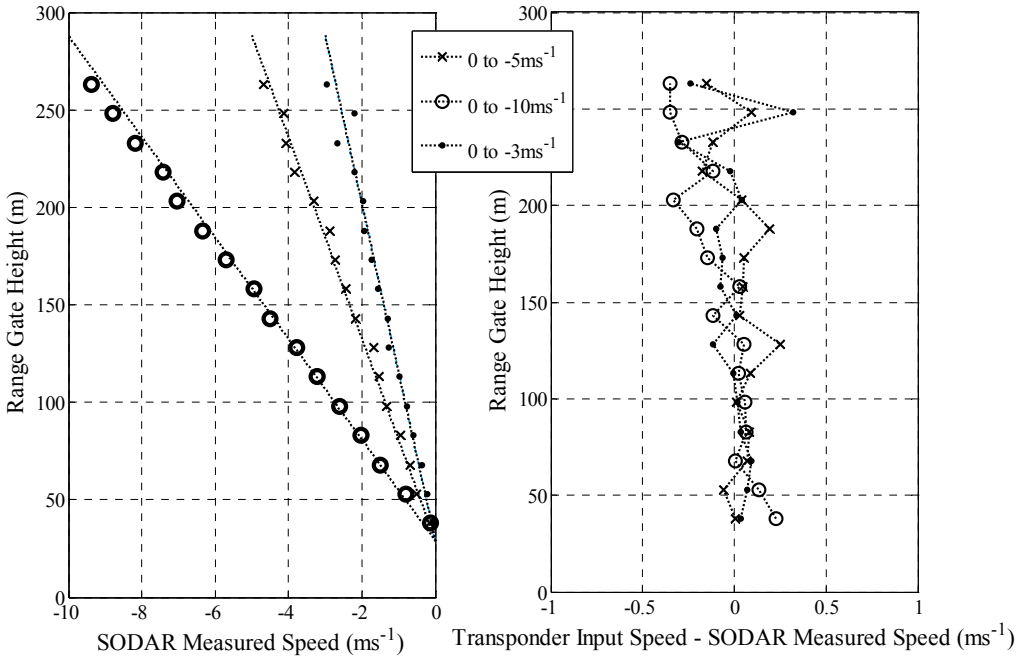

Figure 3.7.4 – Mean measured wind profiles and the difference between the transponder input speed and the SODAR measured speed for the U component of the horizontal wind speed.

These results are similar to the results from measuring in the laboratory using the same profile shape although the variability is higher especially in the higher range gates and this is expected since the background noise levels are much higher at the Carrington test site. It is a similar data consistency drop off that was shown for 60% white noise levels in Figure 3.6.14.

3.7.3.3 Summary

The measurements made at Carrington using the METEK show good agreement with those made in the semi-anechoic chamber using the same SODAR and transponder set-up. There is some noticeable influence from the surroundings such as periods where tonal noise affected the measurements. The results are artificially good due to amplification stage of the SODAR's input not functioning correctly. This is a

convenient way of removing the effects of the real atmospheric echo and background noise. The transponder is intended to be a 'black box' tool that does not require the user to interfere with the inner workings of the SODAR that is being measured and therefore this is not a method that should be actively implemented.

3.7.4 Field Measurement Results With an ASC4000 at Grevenbroich (Germany)

Measurements were made at Wind Test Grevenbroich's wind turbine test site using the transponder system with an ASC4000 SODAR over a two week period. The ASC4000 SODAR tested uses an autonomous set-up featuring a trailer to house the SODAR and its electronics and a GPS modem to transfer data. As a result of this set-up a certain amount of automation was used in the transponder systems processing to maximise the amount of data collected. Making sure this automation functioned correctly used up several days of measurement time reducing the actual testing period

time to only three days. Figure 3.7.5 shows the SODAR trailer at its location.

Figure 3.7.5 – ASC4000 Wind Explorer SODAR set-up at Wind Test Grevenbroich's turbine

testing field in Germany.

As shown in Figure 3.2.6, the ASC4000 requires that the transponder components are positioned 3.2m above the SODAR. This is not achievable with the gazebo frame set-up that the transponder uses. It was possible to raise the transponder 2.5m above the SODAR by fixing the frame to the outside of the SODAR's trailer. The temperature was sub-zero throughout the measurements causing ice to form on some of the transponder components and thus reducing the performance of these components. This meant that data was only collectable for range gates between 90 and 140m. Two sets of measurements were made with the SODAR orientated in a different direction for each. The change in orientation was made because previously recorded data showed the presence of fixed echoes. Figure 3.7.6 shows the set of results recorded before the change in orientation.

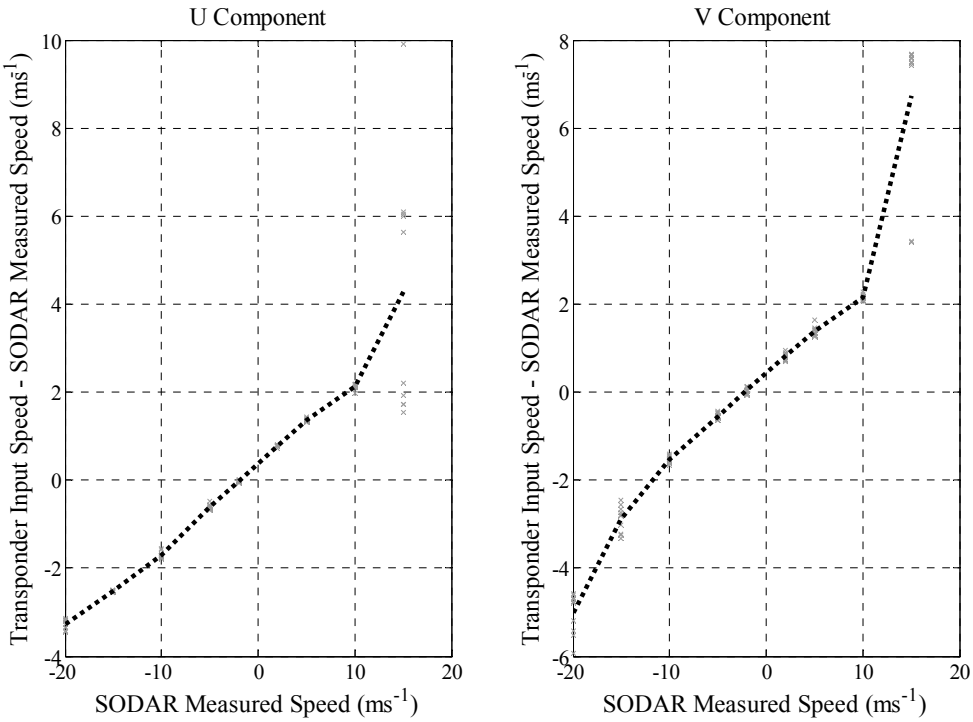

Figure 3.7.6 – Differences between transponder input speed and SODAR measured speed using an ASC4000 SODAR in its initial orientation.

The first set of results show very large differences between the transponder input and the SODAR's measured speed although the variance is similar for all speeds. This suggests the consistent influence of a real atmospheric echo as well as the possibility of fixed echoes. It was identified by the operators of the SODAR before these measurements that there was a fixed echo problem and this is the likely cause of the large differences encountered since the SODAR data is significantly slower than the transponder input speed. The data shows a bias towards larger positive speeds. This highlights that the real atmospheric echo is showing some influence on the data since this is consistent with wind speeds measured by the SODAR when the transponder was not in use. Figure 3.7.7 shows the results recorded after the change in orientation.

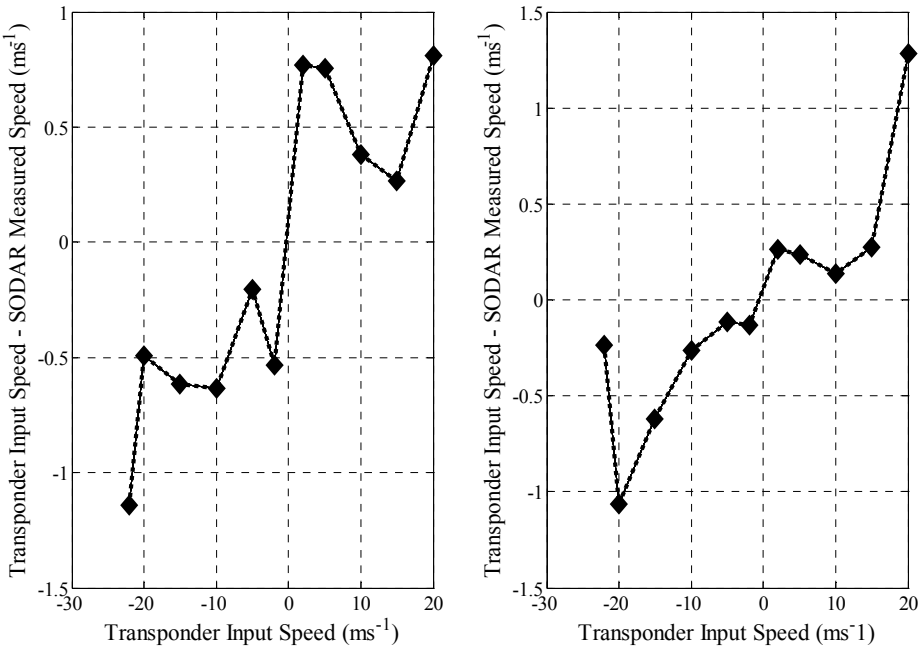

Figure 3.7.7 – Differences between transponder input speed and SODAR measured speed using an ASC4000 SODAR in its altered orientation.

The second set of results show smaller differences than the first set although still significantly larger than those found in the tests with the METEK SODAR. The results highlight that the foam covering on the top of the transponder is insufficient for removing the effect of the real atmospheric echo when the SODAR is fully operational.

3.8 Further Work Required for Transponder System to Become a Useful SODAR Calibration Tool

There are two problems with the transponder in its current form. These are that the return echo is not realistic enough so is often rejected by a SODAR's quality control methods and that in the field the presence of the real atmospheric echo is too strong to allow for conclusive measurements.

3.8.1 Making the Return Echo More Realistically

The current method of producing a return echo creates a signal with a narrow spectrum as it only uses one Doppler shift. SODAR echoes are volume averages where there is some wind speed variability within the volume. One possible method would be to convolve the recorded SODAR echo with a realistic atmospheric model. Some work has been done in Kendrick (2010) using finite difference time domain methods (FDTD) although this is computationally expensive and therefore some work would be required to make the result into a set of variables that could be easily employed within the transponder processing.

3.8.2 Removing the Real Atmospheric Echo

The layer of acoustic foam used to reduce the effects of the real atmospheric echo proved to be insufficient. A more effective method is required. This could involve a thicker layer of acoustic foam that is backed with a solid sheet material forming a complete roof above the transponder. This idea creates two further problems. Logistically this would be difficult to transport although if the transponder is to be taken further as a field tool then it should be housed in its own van or trailer anyway to protect it from extreme weather conditions. The second issue with building a roof is that while the atmospheric echo is reduced diffraction at the edges of the structure may

lead to fixed echoes. The only real solution is to create a fully enclosed structure to house the transponder and the SODAR. Since many SODARs are now housed in trailers as part of an autonomous set-up this structure would have to be large enough to fit over a trailer as well as the SODAR itself.

3.9 Summary

In this Chapter the details of a transponder system for exploring the influence of a SODAR's hardware and set-up on measurements made by the SODAR are given including the full details of its design and the results of testing in several different scenarios. The transponder system is made up of several speakers, a microphone and a laptop computer, which carries out all the processing required to create the desired return echo signal. The majority of the testing has been carried out on a METEK DSDPA.90-24 SODAR with promising results in semi-anechoic conditions despite a signal that lacks a realistic spectral width.

Methods for converting the transponder system into a field tool have been explored with a Gazebo frame and some acoustic foam being tested as an inexpensive and logistically convenient solution. while results of using this system with the METEK SODAR showed good results it was found that through testing with an AQ500 in a semi anechoic that the spectral width of the echo is too narrower for some SODARs to make an wind speed estimation an and through testing with an ASC4000 SODAR in a field situation that the real atmospheric echo has a significant influence on the results of testing.

In order to make the transponder system into a usable measurement tool the spectral width of the return signals it creates needs to be increased and the atmospheric echo needs to be fully removed. Information learnt through the use of a fully functional transponder system can be used to increase the accuracy of theoretical predictions of how SODAR measurements will represent the wind speed in a particular measurement site in relation to a wind turbine position or other point of interest. This

will be discussed in Chapter 5 of this thesis with reference to the required wind speed accuracy for wind energy measurements.

4. Methods to Measure the Beam Shape and Tilt Angle of SODARs

Chapter 4 – Methods to Measure the Beam Shape and Tilt Angle of SODARs

4.1 Introduction

The directivity pattern and the beam tilt angle have a large effect on the measurements made by a SODAR. This was given some theoretical exploration in Chapter 2 of this thesis based on models created using perfect sources where the effective measurement volume was estimated. Real SODARs contain imperfect sources that have a range of directional behaviour. It is therefore necessary to explore methods to measure the directivity of SODARs. In this Chapter various methods are discussed in order to assess the accuracy and usability of each for obtaining estimates of beam width and tilt angle. These methods are anechoic acoustic measurements of individual elements of a speaker array coupled to an array model, anechoic acoustic measurements of a SODAR array, anechoic measurements of a SODAR array using Near-field Acoustic Holography, outdoor acoustic measurements of a SODAR array using a tilting platform and outdoor measurements of a SODAR array using the Bradley (2008) method. The aim of this is to identify the most appropriate methods for exploring the beam shape and tilt angle of a SODAR so that the uncertainty in the SODAR measurement that is related to the acoustic beam can be quantified.

4.2 Anechoic Measurements of SODAR Horns

If the characteristics of a single source from within a SODAR array are known then the models created in Chapter 2 can be adjusted to create a more realistic model by replacing the directivity arising from the piston assumption with the measured directivity. The standard method for measuring the directivity of a sound source is to place the sound source in an anechoic chamber attached to a turntable. Measurements of the sound pressure at a range of angles can then be made.

4.2.1 Measurement Methodology

Two horn loudspeakers from the SODAR array were selected for the measurement. The loudspeakers were mounted on a stand using small metal clamps and the stand was positioned on a turntable with five degree increments marked on it. A measurement grade microphone was positioned 1m away from the centre of the turntable. Some foam absorption was placed on the turntable between the horn and the microphone in order to reduce comb filtering effects caused by sound reflections off the turntable. A frequency spectrum was recorded for each 5º rotation of the horn. The error in the position for each measurement was +/- 0.5º. This is a large error and the resolution of the measurement is coarse. In order to carry out these measurements more accurately an automated turntable would be required so that a resolution of 1º or better would be achievable with a small position error.

4.2.2 Measurement Results and Analysis

Figure 4.2.1 shows the measured directivity patterns of the two speakers compared with a prediction based on the piston source type used in the models detailed in Chapter 2.

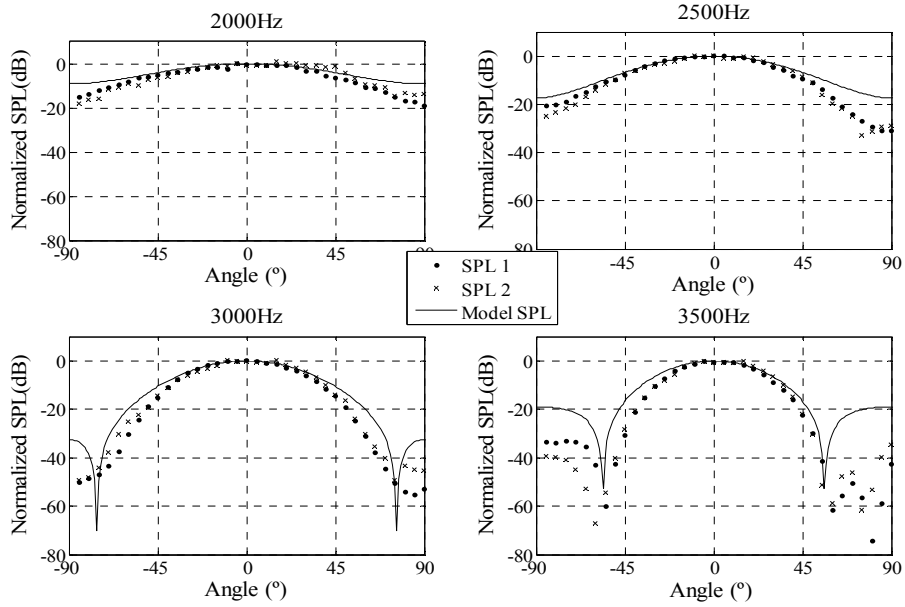

Figure 4.2.1 – Measured directivity patterns of two loudspeakers compared to a prediction

from a piston function based model.

The measurements made of the two horn loudspeakers show good similarity to the model prediction. The measured SPL is generally lower at the larger angles. This is because the piston source prediction assumes that a volume of air at the end of the piston moves in phase and has a disc shaped geometry. The variation is due to inhomogeneities across the surface of the horn loudspeaker. As the horns are folded part of their physical structure exists in the centre and this is the likely to contribute strongly to this effect. The measured directivity can be used in an array model where the piston function is replaced with the absolute measured pressure scaled to be between +/- 1 Pa. This is shown in Figure 4.2.2 where the directivity of the METEK DSDPA.90-24 SODAR is modelled using the piston function and replacing this with the measured data.

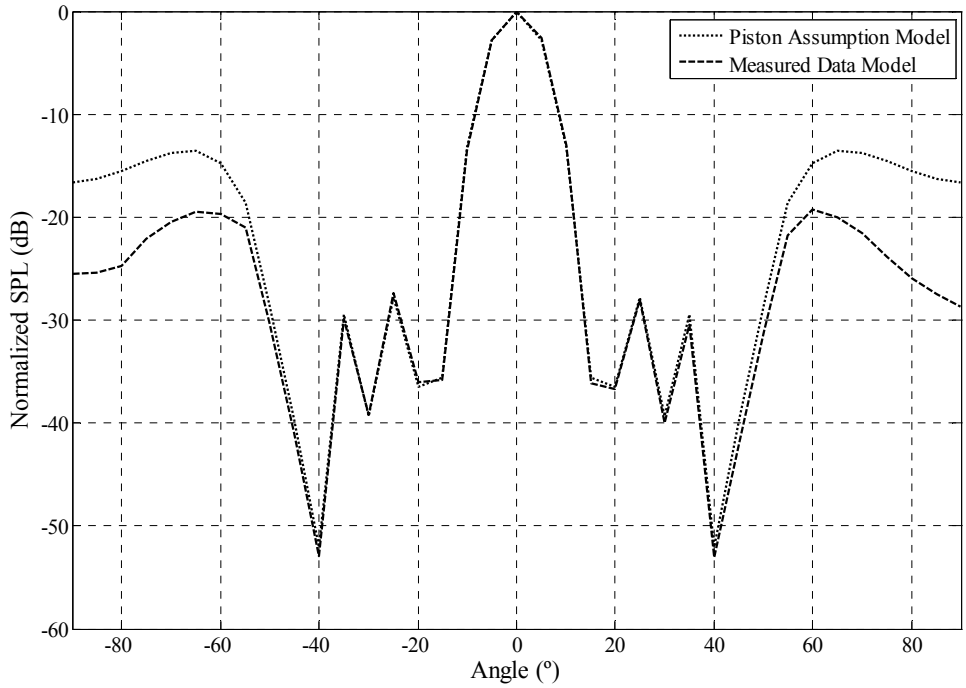

Figure 4.2.2 – Comparison of the modelled directivity of a METEK PCS2000-24 SODAR speaker array using the measured directivity of two of its component speakers and a piston assumption.

The only noticeable difference is the energy at the largest angles for the measured data

based model is significantly lower than in the piston based model. This is expected due to the inhomogeneities in real loudspeakers.

4.2.3 Summary

Measurements of elements from a SODAR array have been carried out in anechoic conditions in order to improve the accuracy of a model of the whole array. The measurements give reasonable agreement with a model of a single piston. The directivity of the horns was found to be slightly stronger than predicted. When the data is used to replace the single piston in a model of a whole array of horns it was shown that the change in the FWHM is less than 0.01º and therefore is negligible. A conclusion that can be made is that the side lobe energy in real SODAR arrays will be less than the energy predicted in models using the piston assumption whilst the the main lobe width can be predicted accurately. This measurement technique offers no possibility for finding the tilt angle of the SODAR in a given set-up. The magnitude of the directional characteristics of the individual transducers is weaker than the contribution caused by the combination of several sources in a particular geometry. Therefore this method is useful in the design of a SODAR array but is not complete enough to find all the details required to quantify how the SODAR's directivity affects the wind speed estimation.

4.3 Anechoic Measurements of SODAR Arrays

Measurements were made of the speaker array from the METEK DSDPA.90-24 SODAR in an anechoic chamber based on the same principle as in the previous section. Comparison is made to the same model as in the previous section. These measurements were carried out to explore how the directivity of the whole SODAR array compares with the model predictions.

4.3.1 Measurement Methodology

Due to the SODAR arrays large size and weight it was preferable to move the microphone along an arc rather than rotating the SODAR array. A wire arc with a radius of 1.5m was set up around the SODAR array with four degree increments marked on it. This allowed for the sound field between minus eighty eight and eighty eight degrees to be measured in 4º increments with an accuracy of +/- 0.2º. This is shown in figure 4.3.1.

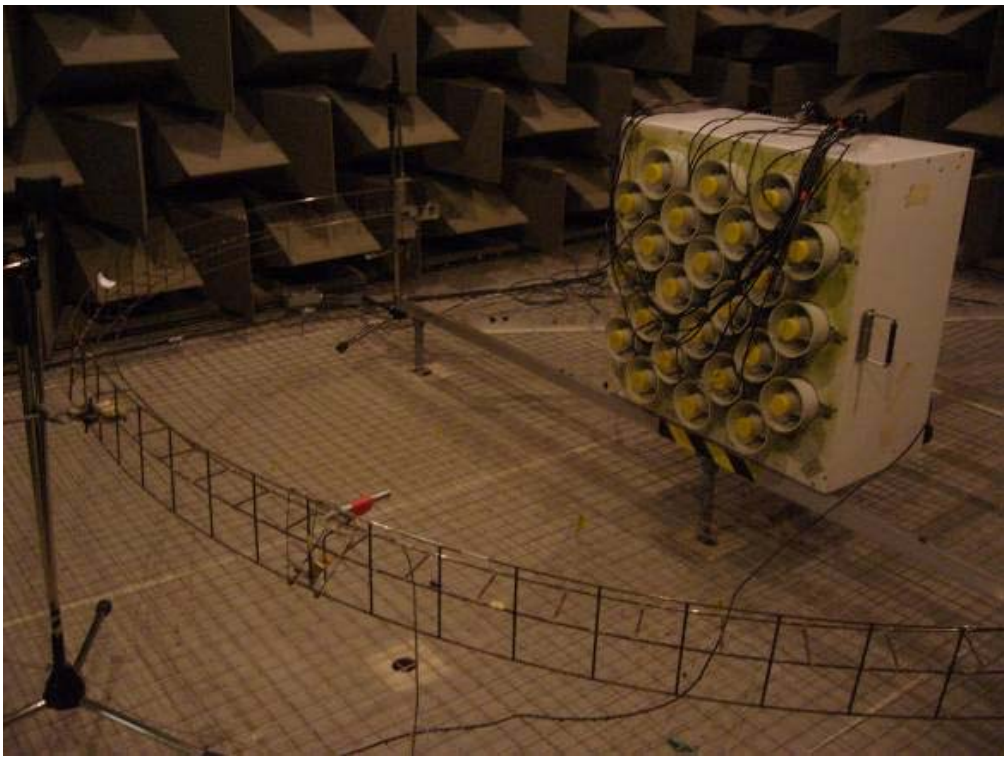

Figure 4.3.1 – Set-up of SODAR array for anechoic directivity measurements.

The horns within the array were disconnected from the SODAR electronics and instead connected in parallel to a power amplifier carrying a white noise signal from a Bruel and Kjaer Pulse analyser system. The SODAR array was measured without its baffles. In order to check that no significant phase or amplitude differences existed between the horns within the array each speaker was checked using an oscilloscope and a sine wave input signal. Measurements were then carried out using a GRAS

40AF measurement microphone. At each microphone position a 1601 line auto-spectrum was recorded. The SODAR array was measured across both the horizontal plane and diagonal plane.

4.3.2 Measurement Results and Analysis

Figure 4.3.2 shows the measured beam pattern of the SODAR at 2200 Hz and 4500 Hz.

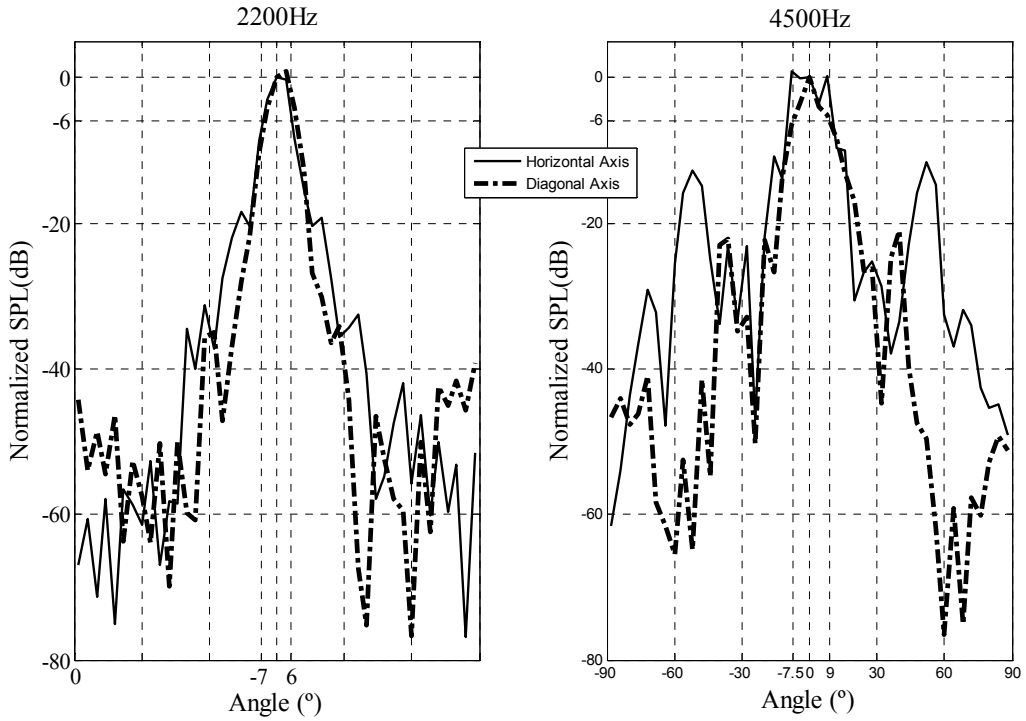

Figure.4.3.2 – Measured directivity patterns of METEK DSDPA.90-24 SODAR array for 2200 Hz and 4500 Hz in horizontal and diagonal axis.

As frequency is increased the main lobe reduces in width. Due to the quality of the power amplifier used side lobes are only clearly visible when they exceed the amplifiers self noise level which is shown at approximately -50 dB. The definition of the side lobes is poor due to the high noise floor introduced by the amplifier used in the measurement system and the coarse angular resolution of 4º, however larger side

lobes are clearly defined. The FWHM at 2200Hz is 13º and at 4500 Hz is 16.5º . The measurements at 4500 Hz are unreliable due to the influence of the near field and reflections of the metal measurement arc leaving the beam shape visible but distorted. The limit of reliable measurements for this set up was found to be 3500 Hz. The measurements at 2200 Hz are compared to predictions made based on the far field model developed in Chapter 2. This comparison is shown in Figure 4.3.3.

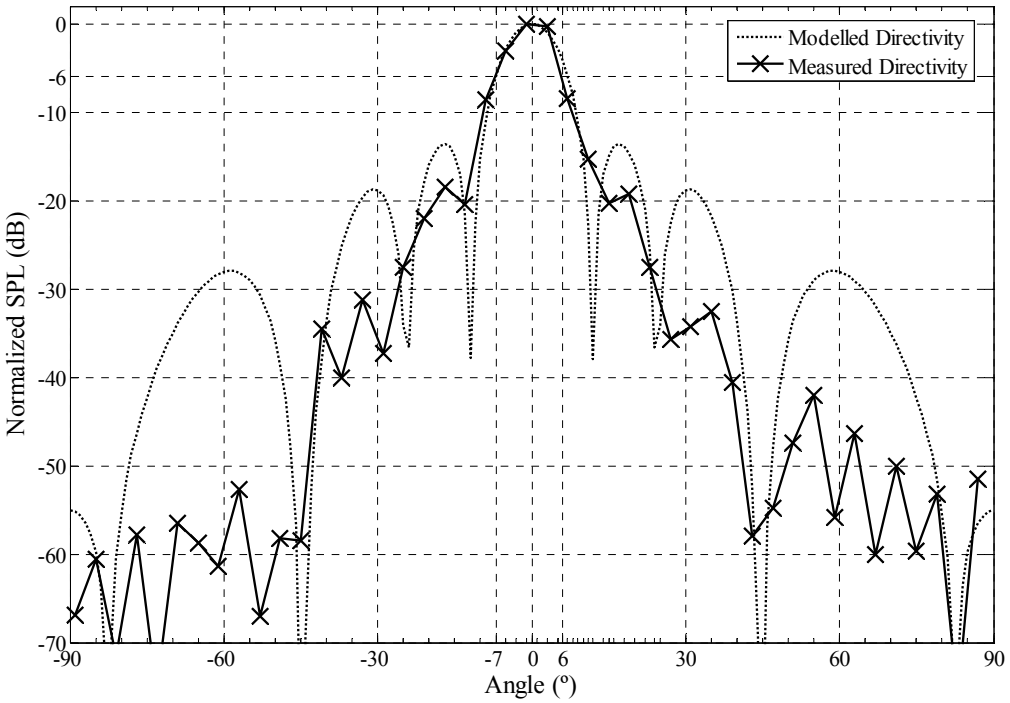

Figure 4.3.3 – Anechoically measured SODAR array directivity compared with modelled directivity across horizontal axis for a frequency of 2200Hz.

Whilst there is reasonable agreement between the model and the measurements for the FWHM, approximately 13.5º, the measured side lobe behaviour does not consistently match the model. The reason for this is that at larger angles the microphone was positioned inside of the SODAR array's acoustic near-field resulting in unpredictable behaviour. This is due to the physical size of the SODAR array. A larger anechoic chamber is required to make true far-field measurements of the SODAR array's directivity and if the SODAR's baffles are included in the measurement the size of the

chamber is increased further. For the METEK SODAR tested here a semi circular arc with a radius of 4.5m is the smallest required to make measurements of the entire SODAR array including its full set off baffles. If the baffle edge is considered the source aperture then chamber is required to have at least two 9m dimensions of usable space.

Measurements of tilted beams were not carried out with this measurement set-up because the intention was to measure the directivity at all useful frequencies. If measurements were focussed on the normal operating frequency of the SODAR in question then measurements of a tilted beam could be carried out using a peak finding method similar to the method employed in Section 4.5.

4.3.3 Summary

Measurements of the SODAR array from a METEK DSDPA.90-24 SODAR have been carried out in an anechoic chamber. Measurements were carried out using white noise in order to record directivity information for all frequencies of operation. It was found that the measurements near the 0º axis agreed reasonably well with a far-field model of the SODAR array. Measurements far from the 0º axis showed little agreement with the model. This is due to the microphone being positioned in the near-field of the acoustic array at these angles. A larger chamber is needed in order to make full measurements and to include the SODAR's baffles. The positioning error was +/- 0.2 as it was positioned manually. Use of an automated system for positioning the microphone would reduce this error and allow for a higher angular resolution .

4.4 Near Field Acoustic Holography (NAH) to Measure SODAR Directivity

The measurements presented so far in this chapter all rely on the assumption that a microphone is placed sufficiently far away from the speaker(s) to be considered in the acoustic far-field. The acoustic far field limit is described in Equation 3.2.1 taken from Kinsler (2000) and the area inside this limit is considered acoustically

complex due to the close interactions of the different parts of the sound source(s) and the presence of evanescent waves. Therefore measurements using a single microphone inside this limit are not thought to be reliable and this effect was noticeable on the measurements at larger angles of the whole SODAR array in the previous section. An alternative to increasing the size of the anechoic chamber is to use a method designed to measure in the near field. Near Field Acoustic Holography(NAH) is a method based on high resolution sampling of the acoustic near-field and extensive FFT analysis to solve forward radiation problems with the use of Rayleigh's first integral. NAH was principally developed for use in vibration analysis for complicated structures such as engines. Details of the development and application of NAH can be found in Williams (1982 & 1991) and Maynard (1985). The aim of the development of this method is to increase the speed of computation whilst maintaining the accuracy of the measurement system. The latest commercial implementations of NAH, such as 01dB-Metravib's dBVision software offer algorithms for predicting far field directivity patterns based on the near-field measurements. This feature can be used for predicting the beam shape and tilt of a SODAR array and an investigation into the potential of this method has been carried out. There is also the potential that the interference pattern caused by the SODARs baffles edges can be measured. This is also investigated in this section.

4.4.1 NAH Principle

NAH takes a number of microphone measurements on a plane close to the sound source of interest and performs analysis on the cross spectra between each of these measurements and one or more reference points. A cross spectra is the FFT of the cross correlation function of two signals, in this case the reference point and each individual position on the measurement plane. From combining these cross spectra three dimensional pressure, intensity and particle velocity fields can be found. This can then be converted into a far-field directivity pattern. This would be a straightforward process if the sound source being measured was very simple. For large sources or sources with multiple parts a phase relationship between the parts of the source is

needed. To achieve this the sound field must be separated into evanescent waves, which are near field waves that decay exponentially, and plane waves. The plane waves travel away from the source and give the far-field directivity pattern whilst the evanescent waves exist close to the source creating complex near-field behaviour. The acoustic field at the measurement plane is back-propagated to the source position using Rayleigh's first integral equation that includes Dirichlet Green's function, which can be considered a transfer function between the sound pressure field at two planes. The frequency range that can be measured using an NAH system is dependent on the spacing of the transducers in the holography array and size of the measurement plane. The maximum frequency, f_{max}, can be found from Equation 4.4.1, from Maynard (1985), where c_0 is the speed of sound and Δ is the transducer spacing distance.

$$f_{max} = c_0 \frac{1}{2\Delta} \quad \text{(Equation 4.4.1)}$$

The minimum frequency is defined by the condition that at least one wavelength must exist within the measurement plane. The frequency range of interest for measurements of SODAR arrays is 1.5 kHz to 6 kHz. The maximum transducer spacing in the holography array is therefore approximately 2.5cm. However for SODARs using lower frequencies a larger spacing can be employed. For instance a 5cm separation is applicable to measurements below 3400 Hz. The minimum measurement plane dimension is 23cm. This is smaller than typical SODAR arrays and therefore is unlikely to impose any problem on this type of measurement. The equations employed by NAH systems compute integrals over infinite domains. All measurements have a finite domain but so long as this is sufficiently bigger than the source being measured the errors that occur at the edges of the domain can be minimized. Some windowing and filtering can be performed to enhance the treatment of these boundary errors.

4.4.2 Investigations into the Prediction of a SODAR's Far-Field Directivity Using NAH

Measurements were made of the speaker array from a METEK DSDPA.90-24

SODAR using the 01dB NAH software dBVision in Taylor (2009). This investigation was to explore the suitability of NAH for use in measuring the beam pattern of SODARs. The measurements made using NAH are compared to the directivity measurements detailed in Section 4.3 and to models from Section 2.2. The measurement set-up used a wire mesh as a position guide, similar to the type employed in Maynard (1985), that was similar in size to the surface of the SODAR array. Three frequencies were measured, 1.8 kHz, 2.1 kHz and 2.4 kHz. These frequencies are all within the 3400 Hz limit for the microphone array used, which had a transducer spacing of 5cm, and are typical operating frequencies for the SODAR model. The dBVision has the ability to transform the back propagated pressure field at the source into a far-field directivity pattern through the use of a Cartesian to spherical transform. Figure 4.4.1 shows the directivity patterns obtained from these NAH measurements.

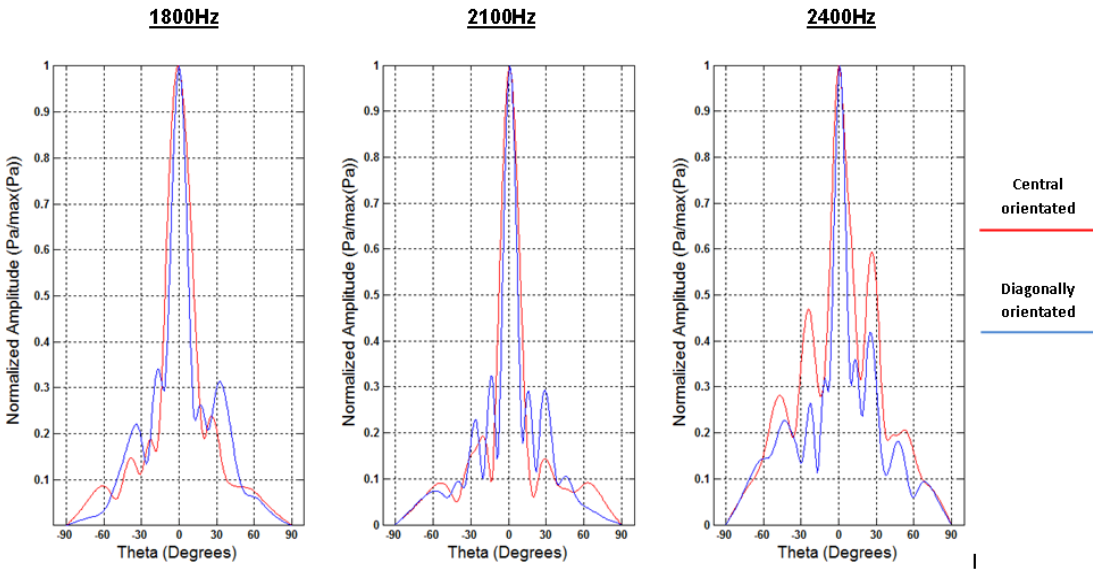

Figure 4.4.1 – NAH measured directivity patterns of METEK DSDPA.90-24 SODAR array from Taylor (2009)

The main lobe in at each frequency is clearly defined although it is noticeable that

measurements along the centrally orientated axis give wider main lobes than the diagonal axis. Comparison of the angle of the first null and first side lobe was then carried out. It was shown that the measured results using both NAH and the far-field method showed smaller main lobes than those predicted by the model. This is likely to be a result of an incorrect source size being used in the implementation of the model since the dimension required is the effective acoustic width and not the physical width of the horn. In this Chapter the FWHM is the focus of the measurements so analysis gives the FWHMs of the measurements along the diagonal axis, shown in Table 4.4.1. This analysis was performed by eye on the previous figure and therefore the accuracy is +/- 0.5º.

Frequency	FWHM
1800 Hz	16º
2100 Hz	13º
2400 Hz	10º

Table 4.4.1 – Estimated FWHM of SODAR beam based on Figure 4.4.1.

The measurements carried out using NAH used a measurement plane which was not significantly larger than the size of the SODAR array and therefore the measurements at the edge of the array introduce some errors to the overall measurement. As a result the side lobe information in the directivity pattern is increasingly unreliable at larger angles. Further measurements are required with an appropriately sized measurement plane.

4.4.3 Investigations into Measuring and Predicting Baffle Edge Interference Using NAH

If the edge of the SODAR's baffle is considered to be a secondary source NAH can be used to measure the diffraction effects that occur at this edge. A METEK DSDPA.90-24 SODAR with its baffles attached was set up in an anechoic chamber and NAH measurements were made in the area close to the baffle edge. The

microphone array was positioned with the aid of a frame fitted with reference wires to improve accuracy. Figure 4.4.2 shows the holography measurement plane and

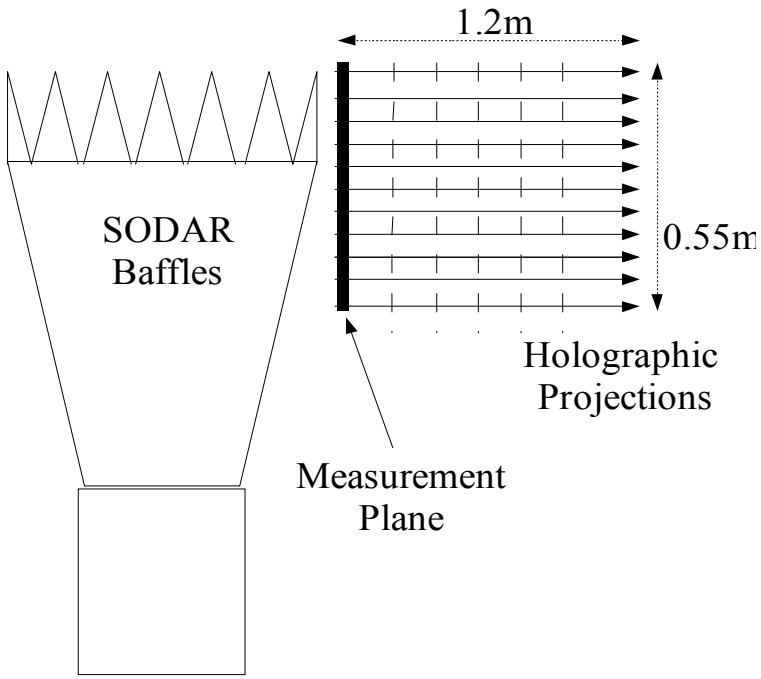

projection planes in relation to the SODAR baffles.

Figure 4.4.2 – Position of NAH measurement plane and projection planes in relation to SODAR baffle.

Measurements were made of the SODAR operating a vertical beam only. Figure 4.4.3 shows the extracted sound radiation away from this baffle edge in a horizontal plane for different heights from 50cm below the baffle edge to 5cm above it.

Figure 4.4.3 - Sound radiation patterns from a SODAR baffle edge predicted from NAH

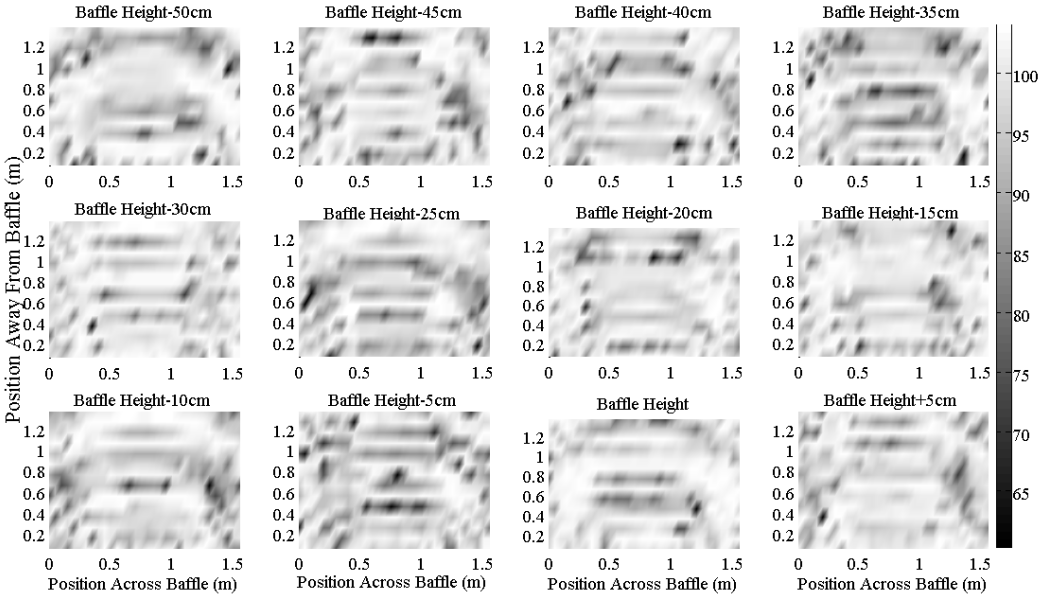

measurements at different heights in relation to the baffle edge height.

Whilst there are some noticeable patterns shown from these measurements it is clear that there are some accuracy problems which arise from movements of the reference frame and too small an extension of the measurement plane above and to the side of the SODAR baffle edge. The results show that with a stricter measurement method it may be possible to explore the details of the baffle edge diffraction. It should be noted that these measurements were only a preliminary investigation into whether NAH could be used to investigate the behaviour of SODAR arrays and baffles. They should be repeated focusing on the beam that is tilted towards the baffle edge as well as the vertical beam with a wire mesh as a guide in the same way that the measurements of the SODAR array were carried out.

4.4.4 Summary

Measurements of a SODAR array have been made using NAH with a focus on far-field directivity predictions and of a SODAR baffle edge, assumed to be a secondary source, focussing on the sound pressure patterns close to the baffle edge. The measurements of the SODAR array show promising results although it is clear

that there are problems at the edges of the measurement caused by the lack of extension beyond the source geometry. Estimations of the FWHM can be made with this technique and those found in these measurements show reasonable agreement with models and measurements using far-field assumptions. The short investigation to explore the diffraction effects at the baffle edge show less promising results predominately due to measurement inaccuracies. Ideally a measurement of a whole SODAR including baffles would be made. The geometry for such a measurement needs careful consideration since treating the top of the baffle as the sound source aperture would leave a large area where the NAH microphone array is to far away from any sound source. This would also be a problem if the measurement was split into two planes. It might be possible to measure across the speaker array and also in a ring around the baffle edge as shown in figure 4.4.4. This depends on whether the software used to carry out the analysis has the ability to handle multiple sources with comparatively large separation distances.

Figure 4.4.4 – Proposed NAH measurement geometry for measuring aspects of SODAR

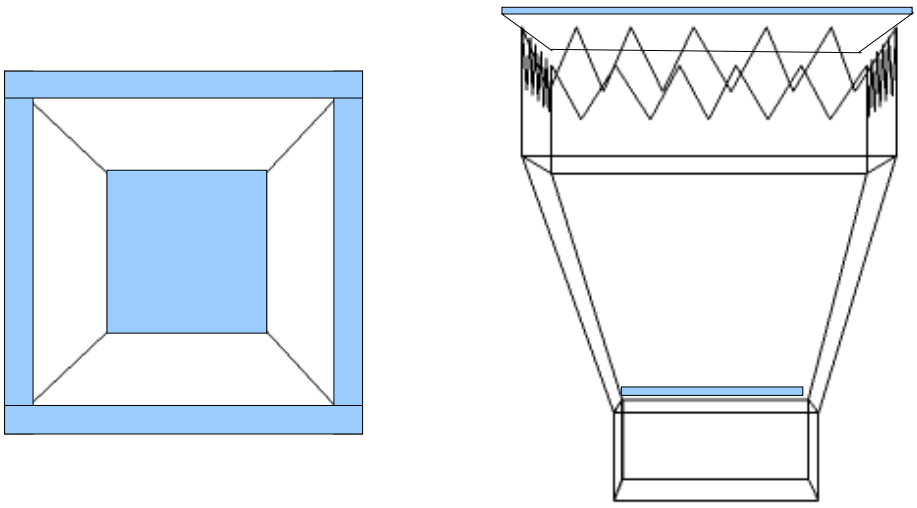

directivity including baffle diffraction effects with holography measurement planes shaded.

4.5 In-Field Directivity Measurements Using a Tilting Platform

Measuring SODAR directivity in laboratory conditions can be carried out using

the methods described earlier in this Chapter. Making these types of measurements in the field can save on the logistics of moving a SODAR to a laboratory, reduces the chance that the measured directivity is likely to change as minimal movement of the SODAR is carried out and allows the measurement to be a true far-field measurement since there is, in principle, no space limitation. From a calibration perspective the FWHM and the acoustic beam tilt angle are the most important aspects of the SODAR directivity that need to be measured. Therefore only a 30º section of the directivity needs to be measured. This type of measurement can be achieved with a tilting platform and a small mast or tower with a microphone device fixed to the top. Measurements can be made of the SODAR array with and without baffles. This can give some insight into how the baffles affect the SODAR's beam pattern. Figure 4.5.1 shows the a model of the arrays directivity with the measurement points marked.

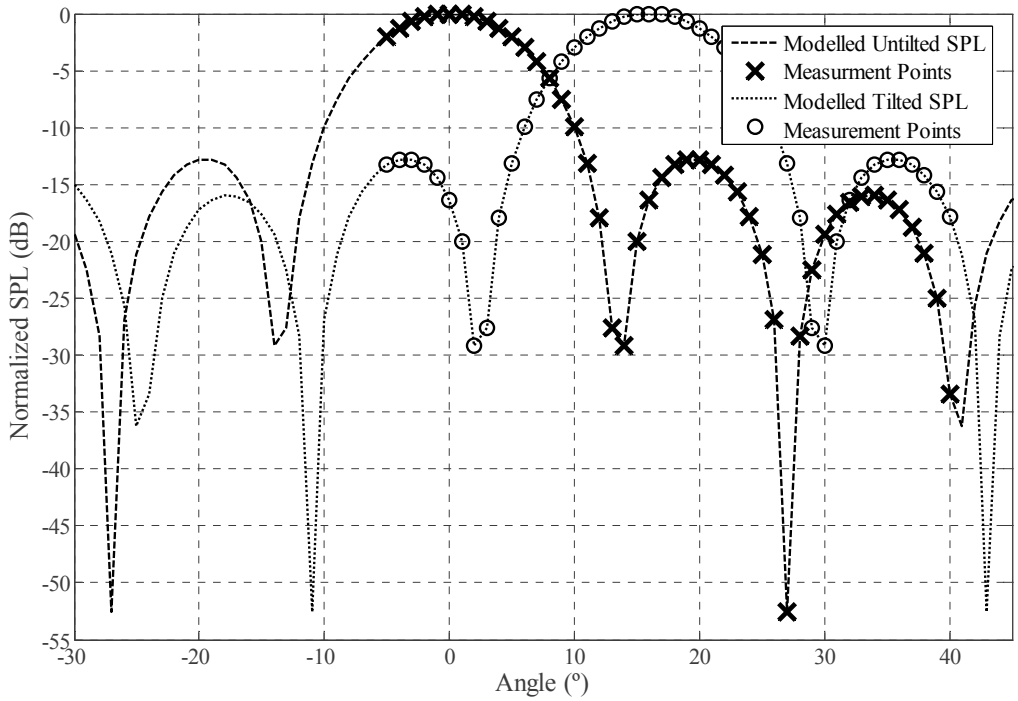

Figure 4.5.1 – Modelled directivty with the measurement points marked.

In a real measurement there is likely to be some random deviations due to the individual characteristics of the SODAR array and the nulls will not be so defined as they are limited by the level of background noise. The results are also subject to comb

filtering effects caused by reflections from nearby objects and the ground. It should be possible to show that the FWHM and tilt angle can be measured in this way.

4.5.1 Methodology

Measurements of this type require the SODAR to be physically tilted in small increments. This is achieved by constructing a hinged platform that is driven by a tilting mechanism such as a linear actuator. This is positioned beneath the platform with rollers attached so that it can push one end of the platform upwards freely. An example of this type of actuator is a Hiwin-LAM actuator which is an inexpensive mechanism that can be driven by a car battery, can handle a high loading of up to 5000N depending on the model and allows for small movements giving high tilt angle resolution. A device to measure the tilt angle is also required. Digital spirit levels are available and for an automated measurement system a spirit level with a 0.1º resolution would be suitable. For a non-automated measurement a lower resolution is possible due to the lower level of accuracy achievable by human control and therefore a spirit level with a 1º resolution is sufficient. Smart mobile phones contain accelerometers and software that can act as a spirit level so a phone of this type was employed as part of the measurement set-up. The accuracy of a phone using this software can be checked using a protractor and tilting the phone with respect to a surface to see if the readings measure those of the protractor. Figure 4.5.2 shows the set-up for measurements made with the METEK DSDPA.90-24 SODAR. The actuator and the front of the platform are set in the ground in a concrete casing as the forces exerted on the frame require this high foundation strength.

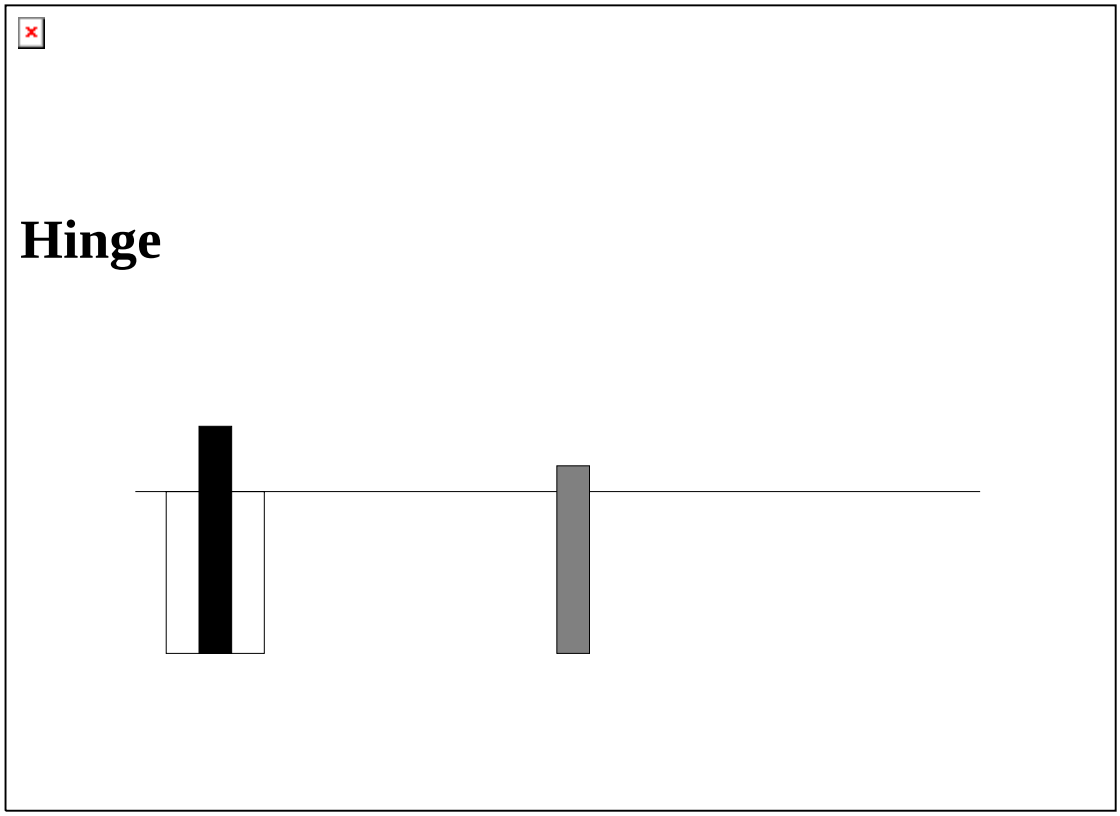

Figure 4.5.2 – Set-up of tilting platform for measurements of the SODAR array beam shape.

The range of tilt angles allowed by this set-up is 8º to 35º. A larger range would be possible with an actuator that has a larger excursion but for the initial measurement this range is considered large enough to capture the required details of the SODAR beam pattern. A Sound Level Meter(SLM) with the ability to record frequency data in small time increments and store this information for a long recording period is used to capture the SPL for each tilt angle. In this case the SLM used was a SVANTEK-957 sound and vibration analyser. The SLM is attached to the top of a small hydraulic mast. The mast is raised so that the angle between the SODAR array surface and the SLM is 30º with a minimum separation of 7m. Figure 4.5.3 shows physical positioning of the mast in relation to the SODAR for the measurements shown in this thesis.

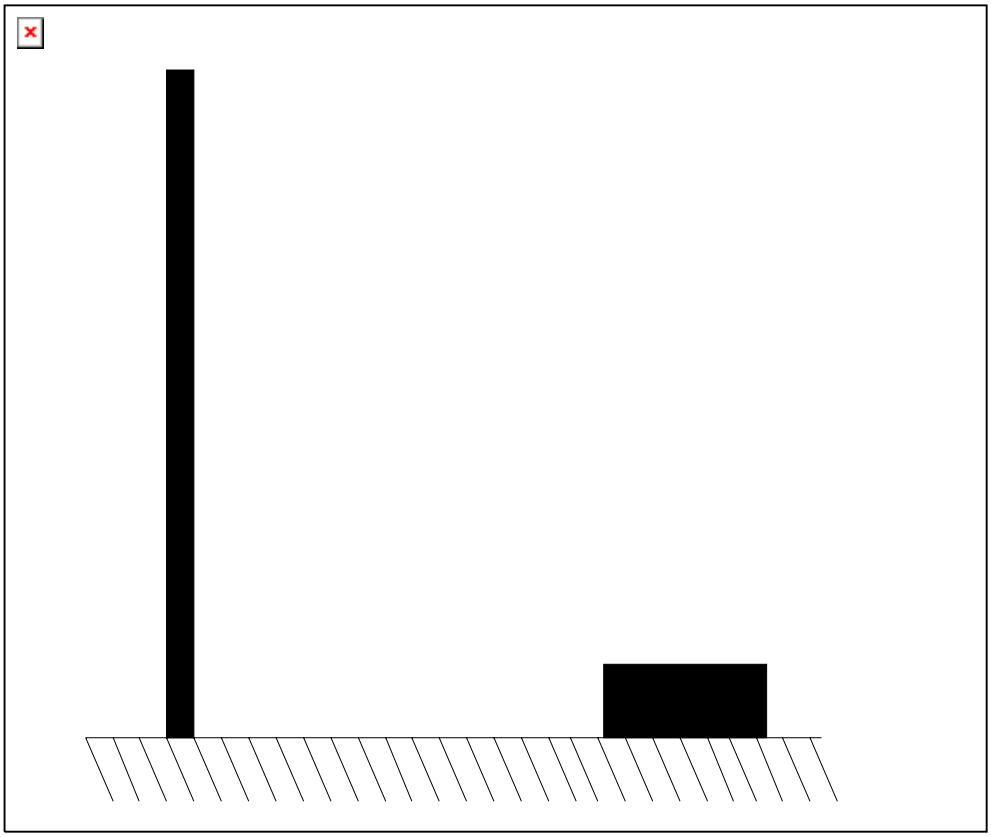

Figure 4.5.3 – Position of SLM in relation to SODAR array mounted on tilting platform.

The distance between the Mast and the centre SODAR array whilst untilted is measured using a laser distance sensor with an manufacturer stated accuracy of +/- 2mm. From this distance the required height of the mast is calculated in order to give a 30º angle between the SLM and the centre of the SODAR array. Once set-up the height is checked using the laser distance sensor. The distance between the SLM and SODAR array changes as the tilt angle is increased because the centre of the platform moves towards the SLM. A correction for this change in distance is required during the data analysis based on this geometry. The top of the mast has some movement due to wind incident on it and therefore the uncertainty of the exact angle and distance between the SODAR array and the SLM is increased. Averaging several recorded pulses for each tilt angle can reduce the degree of this uncertainty.

Once the SLM is in place the SODAR should be set to emit the vertical beam and the beam tilted towards the SLM at maximum amplitude with a third beam titled

away from the SLM set to a low amplitude in order to act as a reference point in the recorded data. The digital spirit level should be calibrated on a known flat surface and then fixed in position on the platform. The measurement can then be performed with several pulses recorded for each tilt angle in order to reduce the influence of random variations caused by movement of the mast and impulsive background noise incidents.

4.5.2 Results and Analysis

Data was recorded using the set-up detailed above for the METEK DSDPA.90-24 SODAR. Measurements were made with and without the SODAR's baffles although for measurements made with the baffles attached the angle range was reduced to 8-30º as stability is an issue when using full baffles. For future measurements a stronger platform made from a metal frame and a method for supporting the top of the tilted SODAR would be required to make measurements of the whole SODAR for a larger range of angles.

4.5.2.1 Results Recorded without the SODAR's Baffles.

The first set of results was recorded without the baffles attached to the SODAR. For each tilt angle ten pulses were recorded for each beam. The measurement period was approximately an hour long as a result so increasing the number of pulses recorded should not be a time problem for future measurements. The SLM recorded an FFT every 0.1s. This is the shortest integration time allowed by the SLM software and was used to minimise the comb filtering effect caused by reflections from surrounding objects. Filtering was carried out on the data to remove all the points that occur in between the SODAR pulse peaks resulting in a reduction of the number of data points from approximately 30000 to 280 giving ten points for each angle from 8º to 35º. Figure 4.5.4 shows the data in this form.

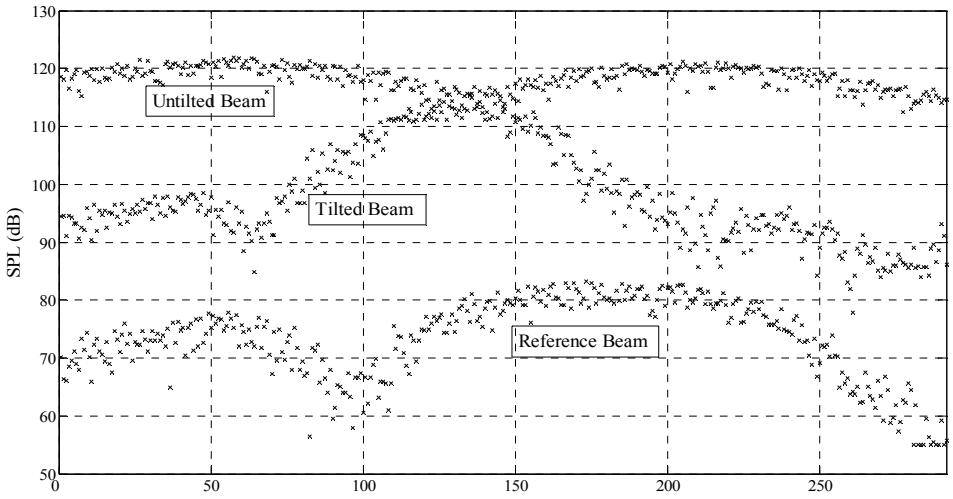

Figure 4.5.4 – Raw data from measurements of METEK DSDPA.90-24 SODAR directivity using a tilting platform and without baffles attached.

In order to improve the quality of the data further the two largest and smallest values for each tilt angle were removed and the remaining six points averaged. Due to the movement of the SODAR array towards the SLM, as the tilt angle was increased, a correction to the data to account for the small changes in distance and angle is applied. This correction is calculated using trigonometry to find the change in angle and distance and the inverse distance law to calculate the change in SPL due to the distance changes. Figure 4.5.5 shows this data with a comparison to the predicted directivity based on the model shown in Chapter 2.

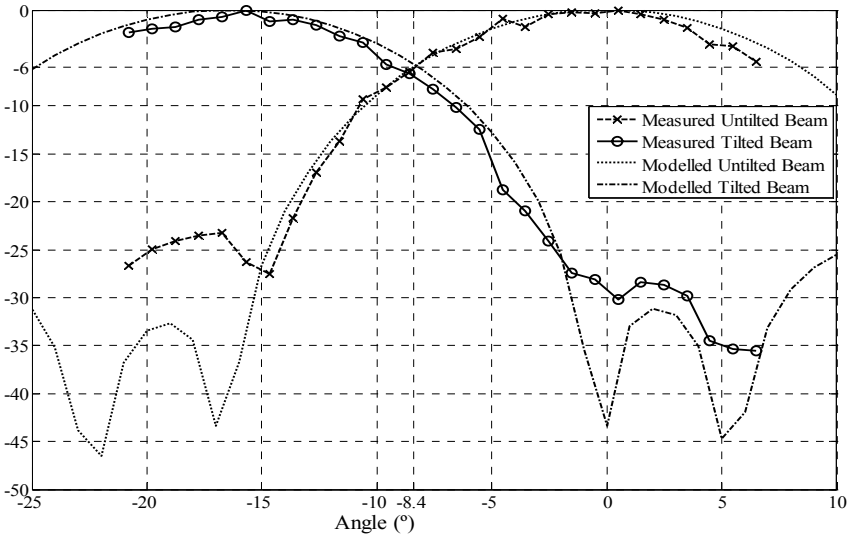

Figure 4.5.5 – Measured directivity of METEK DSDPA.90-24 SODAR array using tilting platform method for a tilted and untilted SODAR beam compared with modelled beam patterns of the same array shape.

From these result it can be seen that the FWHM is 16.3º for both the model and the measured data. There are some discrepancies between the data and the model. For the untilted beam the first side lobe energy is more than 10dB higher than in the model and the first null occurs at a narrower angle. This is due to the reflection of the pulse from the ground near the tilt platform. The SODAR computer stated that the tilt angle used for the second beam was 16.8º. It is unclear from this plot whether this is true or not however it is likely that the angle is slightly different since the SODAR computer assumes that the SODAR's baffles are attached. A quadratic fit can be applied to the section of measured data that represents the main lobe of this beam in order to find to tilt angle. Figure 4.5.6 shows the data from the tilted beam fitted with a quadratic curve.

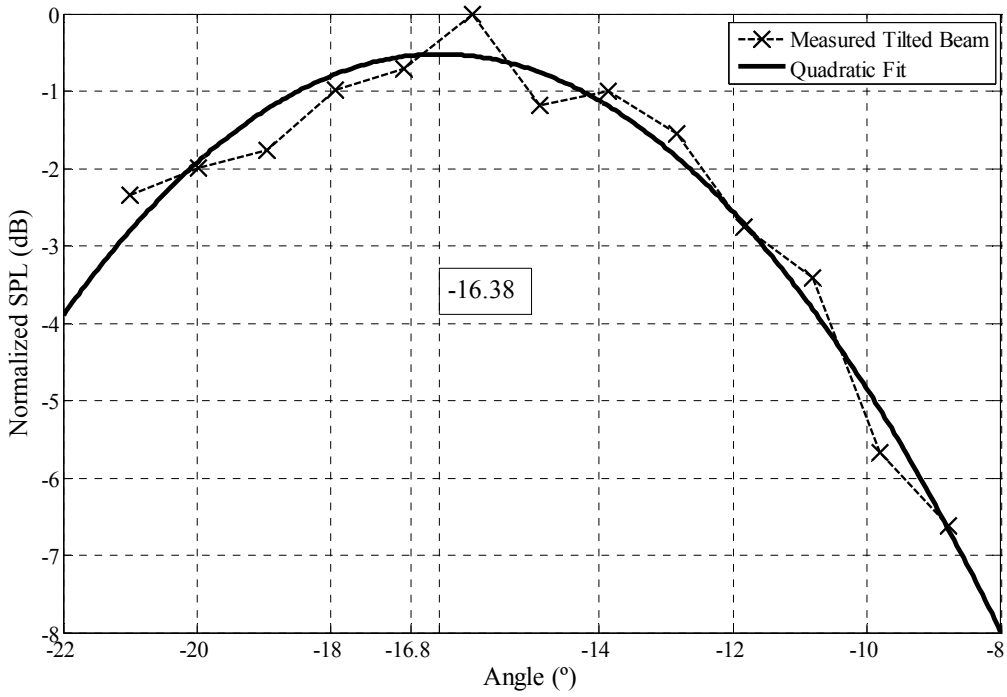

Figure 4.5.6 – Measured data for tilted SODAR beam fitted with a quadratic curve to estimate the acoustic tilt angle.

The peak of the quadratic curve is found to be 16.38º which is 0.42º lower than the angle stated by the SODAR computer. This is a significant difference that could be caused by the presence of echoes from the ground and nearby buildings distorting the beam at the position of the SLM. It does show that it should be possible to find the acoustic tilt angle of a SODAR for a given set-up using a tilting platform and a SLM attached to a tower.

4.5.2.2 Results Recorded with the SODAR's Baffles.

A second set of results was recorded with the SODAR's full baffles attached. This set of data was recorded in cooler temperatures than the first set and the beam tilt angle employed by the SODAR was 14.7º instead of 16.8º. The range of angles measured was from 7º to 28º as the SODAR with baffles on the platform becomes unsteady above 28º. Figure 4.5.7 shows the data recorded with the baffles attached. There is no comparison to the modelled behaviour of the array since the model does

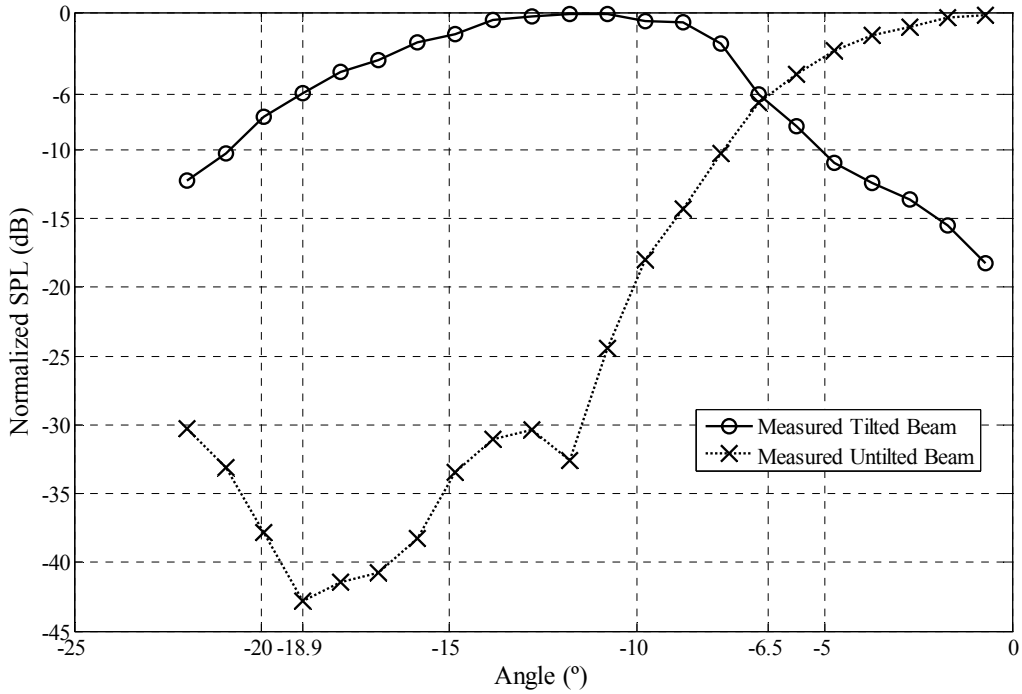

not include the baffle effects.

Figure 4.5.7 – Measured directivity of METEK DSDPA.90-24 SODAR array with full baffles using tilting platform method for a tilted and untilted SODAR beam.

From these measurements the FWHM of the untilted beam is 13º. All the recorded side lobe energy is at least 30 dB below the main lobe peak, although the exact peak of the main lobe was not recorded due to the physical restrictions of the platform. The FWHM of the tilted beam is 12.4º. The reduction in width is due to the baffles reflecting the edges of the beam back into itself resulting in a narrower width. Figure 4.5.8 shows the tilted beam fitted with a cubic in order to estimate the beam tilt angle. A cubic fit is preferred this time due to the more complex shape resulting from the baffle influence. Both quadratic and cubic fits were tried for the unbaffled results with no change to the tilt angle identified.

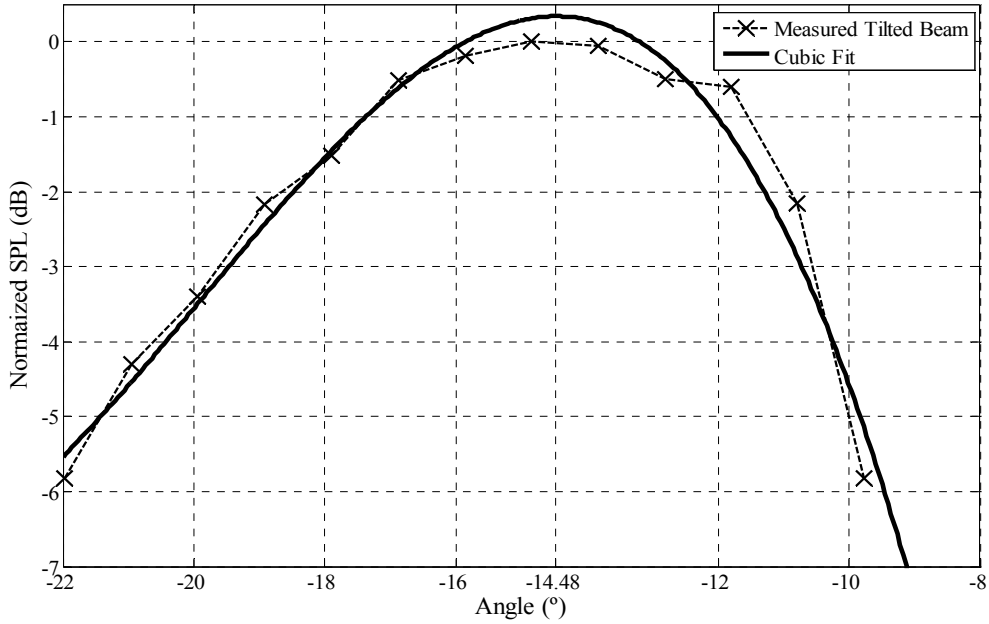

Figure 4.5.8 – Measured data for tilted SODAR beam with baffles fitted with a quadratic curve to estimate the acoustic tilt angle.

The peak of the cubic fit is found at 14.48º which is 0.22º lower than the angle stated by the SODAR computer. This could be due to measurement position errors and errors in fitting along with reflections from the surrounding buildings. The positioning error due to the human control of the tilt platform is 0.2º so this result is close to the SODAR angle if position error is a contributing factor to the measurement result. There is significant distortion of the beam shape between -7º and -11º which would have altered the fitting although it is clear that the peak of the measured data is lower than 14.7º. The angle reported by the computer is a theoretical angle rather than the true acoustic angle so this may also contribute to the difference measured here.

4.5.3 Conclusions

The method of measuring a SODAR's directivity over a limited range of angles in order to find both tilt angle and FWHM shows good potential. The measurement of the untilted beams FWHM in both cases seems plausible. The measurement of the tilt angle shows larger uncertainty. The error in the platform tilt angle is found to be +/- 0.2º due to the use of human control although this could be reduced to 0.01º through

the use of computer control. The use of computer control would also allow a larger number of data points to be collected for each tilt angle and therefore improving the final estimation of the tilt angle and FWHM. The position of the mast in relation to the platform and the height of the mast had an error of +/- 2mm however the sway of the top of the mast was approximately +/-0.05m altering the distance by +/- 0.025m and angle by +/-0.28º of the SLM in relation to the SODAR. To improve this method a stronger platform and tilt mechanism is required so that the entire SODAR can be measured including the baffles for a larger range of angles than currently possible and a stiffer mast or mounting for the SLM should be used to limit the position blurring caused by the swaying of the mast top.

4.6 Beam Tilt from SODAR data (Bradley Method)

A review of a method for in-situ effective beam tilt angle is described in Bradley(2010) and reviewed in Chapter 1 of this thesis. Measurements using this technique are carried out to confirm this technique and provide comparison to the acoustic based measurement described in the previous section. A key difference between the two is that the Bradley method gives a measurement of the effective beam tilt angle using differential wind measurements whilst the tower and tilt method measures the acoustic beam tilt angle. Table 4.6.1 shows the results obtained in a previous measurement made using this technique where the subject was an AeroVironment 4000 SODAR where θ_1 is the tilt angle of the beam emitted in the direction of the tilt, w is the measured vertical wind speed and $\sigma_{mean\theta}$ is mean uncertainty in the tilt angle estimation.

	Mean θ_1	$\sigma_{mean\theta}$	Estimated-calculated θ_1
Calculated θ_1	18.32º		
θ_1 estimated with w=0	18.27º	0.23º	-0.05º
θ_1 estimated with w≠0	18.55º	0.54º	0.23º

Table 4.6.1 – Comparison between estimated beam zenith angles and the calculated zenith angle for results presented in Bradley(2010).

4.6.1 Methodology

The SODAR to be tested is fixed to a tilting mechanism or platform and set up to perform measurements with the desired operation parameters. An digital spirit level is attached to the tilt mechanism or SODAR to give a readout of the perturbation angle for each measurement. Measurements of the wind speed are made for two averaging periods and the angle perturbation is then significantly changed through the use of the tilting mechanism. For each pair of averaging periods the change in angle should occur in only one leaving one unaffected averaging period at each angle. This process is repeated for a number of averaging periods and the wind data is then analysed to find an estimate of the effective beam tilt angle of the SODAR through comparison of pairs of differently perturbed averages. The tilt mechanism is the same as used in the previous section and is shown in Figures 4.5.2 and 4.5.3.

4.6.2 Results

Figure 4.6.1 shows the measured wind speed averaged over all heights for the time period of the measurement with the platform tilt angle for each ten minute average shown by the bar plot.

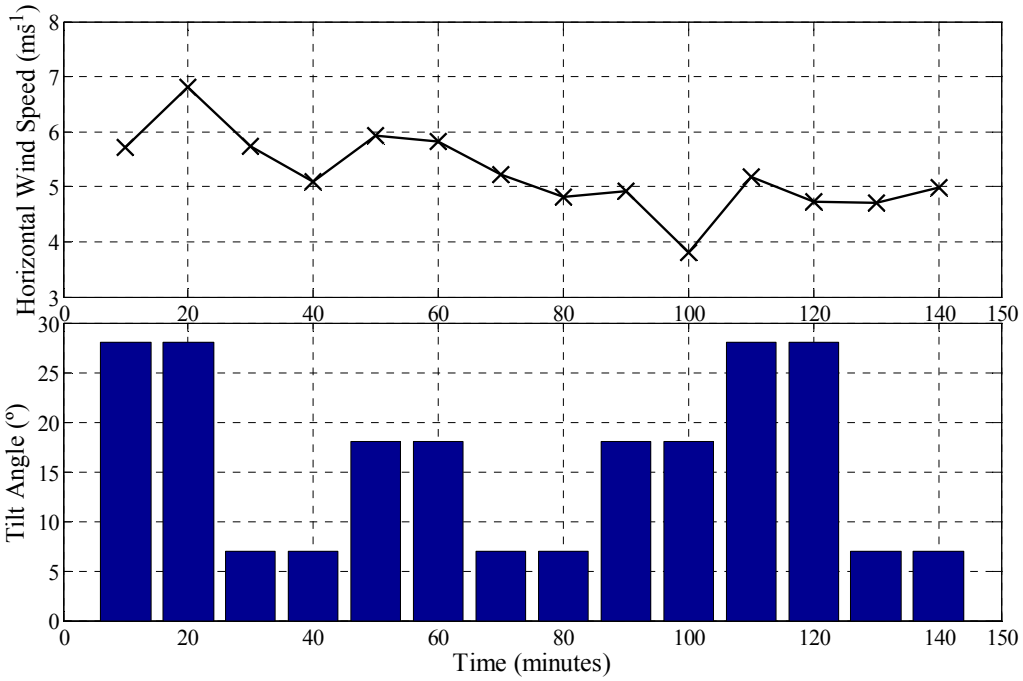

Figure 4.6.1 – Measured wind speed and platform tilt angle for 14 ten minute averages.

The wind speed measured shows variations that follow the tilt angle changes for all but the last average. The calculation of the tilt angle for each SODAR beam, where θ_1 is tilt angle of the beam 1 which is pointed in the direction of the tilt and θ_2 is the tilt angle of beam 2 which is pointed 90 to the tilt direction, is performed using Equations 4.6.1 and 4.6.2 from Bradley (2010) where V_{r1}, V_{r1}*, V_{r2}, V_{r2}*, V_{r3} and V_{r3}* are the radial speeds measured along beams 1,2 and 3 with the * denoting beams with the change in tilt angle and $\Delta\theta$ is the change in tilt angle of the platform.

$$\sin \theta_1 = \frac{V_{r1} V_{r3} - V_{r1} V_{r3}}{V_{r3}^2 - 2 V_{r3} V_{r3} \cos \theta \; \theta \; V_{r3}^2} \quad \text{(Equation 4.6.1)}$$

$$\cos \theta_1 = \frac{V_{r2} - V_{r2}}{V_{r3} - V_{r3}} \quad \text{(Equation 4.6.2)}$$

14 averages were recorded during the measurement period, 2 for each platform tilt angle. The first of each pair is discarded as it will be contaminated by data collected whilst the angle change was taking place. The beam tilt angle can then be found by

using adjacent averages resulting in 6 estimations of the SODAR beam tilt angle. Figure 4.6.2 shows the angle calculated in each estimation for both beams 1 and 2.

Figure 4.6.2 – Estimations of the beam tilt angle for beams 1 and 2 for individual pairs of

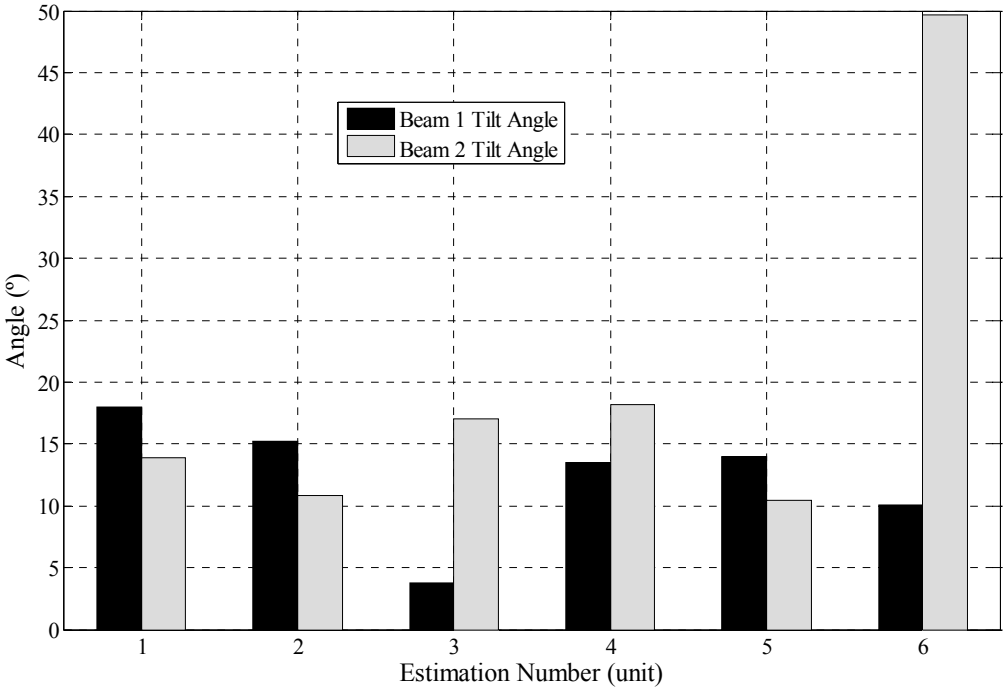

averages.

There is some variability to these results and this is likely to be due to changes in the overhead wind speed and some influence of fixed echoes due to the surrounding buildings at the measurement site. Estimation 3 for beam 1 and estimation 6 for beam 2 are two obvious outliers that should be removed before calculating the final average. Table 4.6.2 shows the calculated mean tilt angles for each beam with the difference from the SODAR reported angle which is a theoretical calculation based on the source separation and the wavelength that is temperature dependent.

	Mean θ (°)	Estimate – SODAR θ (°)
Beam 1	14.16	-0.63
Beam 2	14.09	-0.7

Table 4.6.2 – Mean beam tilt angle and difference between SODAR reported angle for beams 1 and 2.

The mean and difference of the tilt angles for the two beams are similar. Beam 2 is slightly smaller and it is expected that the accuracy of this estimate is less than the estimate for beam 1 as the relative movement of the beam is smaller. These estimates of the beam tilt angles are of the effective beam tilt angle, which takes into account the volume averaging effects that occur in the SODAR measurement, whilst the SODAR reported angle is a theoretical calculation of the beam pointing angle. The results from the previous study showed closer agreement between the theoretical and the estimated angles and this could be due to the measurement site having a lower influence from fixed echoes due to fewer surrounding obstacles and that the beam shape and therefore volume averaging effects are different. The number of measurements made in this experiment was less than the previous one and therefore the uncertainty will be higher. The agreement between the two separate beams is a promising result.

4.6.3 Conclusion

A technique for calculating the effective beam tilt angle that is presented in Bradley (2010) has been shown here to be easily repeatable for a different SODAR at a different test site. The results show larger differences to theoretical estimations of beam pointing angle but this is due to a number of factors including increased influence of fixed echoes, less data points and a different beam shape. The angles measured for the two beams show good agreement. The uncertainty in this measurement is 0.41º compared to 0.23º in the previous measurement due to the fewer number of observations used. As the mathematics behind this technique relies on trigonometry it is applicable to all SODAR types.

4.7 Discussion

Several different approaches have been examined in this Chapter for measuring the FWHM and beam tilt angle of a SODAR array. These measurement approaches

have various advantages and disadvantages with not all capable of measuring both the beam tilt and the FWHM.

Anechoic measurements of a single sound source from a SODAR array can be carried out with a high degree of accuracy and resolution if automated platforms are used and the size of the chamber required is small. It can only be used to make models of the whole array more realistic giving an indication of the FWHM and does not allow for exploration of the tilt angle or the influence of any baffles. It does allow for identification of the effective size of the sound source through averaging and comparison to a piston directivity function which makes it useful as a tool for theoretical calculation of the beam tilt angle which is can be employed in the analysis of measurements made with the Bradley technique as well as in SODAR design.

Anechoic measurements of the whole SODAR array can be carried out with a lower degree of accuracy than the measurements of the single sound source as the SODAR array is too large to be mounted on most rotating platform types. Instead measurements must be made using a metal guide arc which decreases the position accuracy of the microphone. In a normal size anechoic chamber there is insufficient space for the microphone to stay outside the acoustic near field of the speaker array at the largest measurement angles and there is not room to include the baffles in the measurement. The measurements can give a verification of a model of the SODAR array. This measurement allows for measurement of the FWHM and, although not carried out in this thesis, it is possible to measure the acoustic beam tilt angle using this method. A much larger chamber is required to make true far field measurements of the whole array including the baffles making this method expensive and logistically difficult to implement. An alternative where measurements are carried out in the field is preferable.

NAH shows the possibility for exploring not only the FWHM and the beam tilt angle of the SODAR but also the influence of the baffle edge and could be carried out in the field as the microphones are placed close to the sound sources reducing the

potential background noise influence. The measurements shown in this chapter are from two preliminary experiments carried out in anechoic conditions. The first shows that a beam pattern similar to those modelled theoretically and measured in the far field can be calculated from the NAH measurements although it is difficult to confirm the accuracy of this. These measurements suffered from insufficient extension of the measurement plane resulting in high errors at the outer edges of the measurement. The second measurement attempts to show the diffraction effects caused by the baffle edge and whilst there is a noticeable pattern to the results it is too inconsistent to gain any real insight. The drawbacks to using this approach for further measurements are that it is time consuming and that the measurement plane can not be extended when the SODAR baffles are attached unless the measurements are continued over the entire inner surface of the array and baffles. It would be very difficult to ensure the accuracy of this and the preliminary results show no obvious advantage over far-field measurements which is less likely to suffer from positioning errors and is less time consuming.

True far-field measurements of the SODAR beam can be achieved using a tilting platform and a SLM on a 10m mast. This method is a field realisation of the anechoic array measurements that overcomes the space limitations of an anechoic chamber allowing for the microphone to be placed in the far field for all measurement angles and allowing for the inclusion of the baffles. The measurement arc is smaller than carried out in the anechoic measurements covering only 35º for the METEK DSDPA.90-24 SODAR or up to 45º for a smaller SODAR. Therefore only details of the main lobe and parts of the first side lobe of the vertical beam and the tilted beam that is orientated in the direction of the SLM can be obtained. This measurement range allows for estimation of the FWHM and beam tilt angle so is sufficient for that purpose. The two main sources of error occur from movement of the microphone at the top of the mast and the control of the platform tilt angle. The latter can be reduced by an order of magnitude through the use of an automated control system. Limiting the movement of the microphone requires a stiff tower and low winds, which are also

required to carry out the measurements safely. Measurements can also be carried out without the baffles attached which allows for some insight into the effect of the baffles on the edges of the tilted beam and the side lobes of the main beam. The measurements in this thesis suggest that there is a broadening of the tilted beam on the side of the baffle. Generally the accuracy for estimation of the FWHM is sufficient for calculating the effective measurement volume as this is an approximate value. The measurement of the tilt angle with and without baffles was within 0.5º of the angle reported by the SODAR software with the baffled case showing a closer match suggesting that the presence of ground reflections in the unbaffled case influenced the measurement.

The final approach tested was the Bradley technique, which is a measurement of the effective beam tilt angle rather than the acoustic beam tilt angle as it takes into account the volume averaging processes that occur in a SODAR measurement. This method only measures the tilt angle and not FWHM. Measurements had been previously carried out using this technique with the uncertainty shown to be 0.22º The measurements presented here were carried out over a shorter period than previously reported due to time constraints and therefore the uncertainty in the measurement is increased but it is still similar to the uncertainty in the tilt platform far field measurements. The calculated tilt angles were around 0.65º below the angle reported by the SODAR and this could be because of the difference between effective and theoretical tilt angle. The far field tilt measurements also underestimated the tilt angle so there is also the possibility that the SODAR reported angle is not correct or that fixed echoes at the measurement site compromised these measurements. This method assumes constant wind speed between measurements and variability of the wind may have been lower during the first measurement campaign. This is the only assumption made in this method and therefore a reference wind measurement could be useful for identifying averages where the wind speed changes significantly. A simple solution would be to use a sonic anemometer attached to a 10m mast. The measurements from the Bradley technique and the far-field tilt approach are within 0.4º of each other

showing that these measurements give similar results through different processes.

Of the five approaches examined in this chapter the most promising are the two methods that are carried out in the field using a tilting platform. Neither show lower accuracy than measurements made in laboratory conditions and measurements made in the field reduce the logistics of the measurement process as the equipment required is significantly easier and cheaper to transport to the SODAR than the SODAR to a laboratory with a suitably sized anechoic chamber. As they both rely on a tilting platform and due to the short time required to carry them out both can be achieved within a single day using the same set up. Although this is weather permitting since the SLM measurement requires low wind speeds and the the Bradley technique needs steady winds speeds.

These measurements should form a part of the set-up procedure when beginning a SODAR measurement campaign and could also be repeated at the end of the campaign or at intervals within it. So far the tilt mechanisms have been designed around specific SODARs and a universal approach to this is required. This should be fairly straight forward so long as materials and a structure capable of carrying a heavy load are used. Newer SODARs are often housed in small trailers to allow for autonomous deployment which means that a different tilt mechanism would be needed in order to tilt the whole trailer without creating instability.

Further NAH measurements could be carried out to explore baffle diffraction effects but there is little point in making further beam shape measurements since the accuracy is not better than far field measurements achieved through the use of the tilting platform. Measurements of single transducers in an anechoic chamber are important for SODAR design since they allow the effective sound source diameter to be found. This gives better calculations of the theoretical tilt angle and beam width. Measurements of whole SODAR arrays are not useful since similar accuracy has been shown in outdoor measurements.

4.8 Summary

Five methods for measuring aspects of a SODARs directivity have been examined with the different strengths and weaknesses of each compared. Anechoic measurements of single sources have been shown to be simple to perform and useful for calculation of theoretical aspects of the SODAR directivity. Measurements of whole SODAR arrays in anechoic conditions have been shown to be cumbersome and the accuracy is not better than the other methods tested. NAH is an interesting method for measuring different aspects of the SODAR directivity and whilst measurements of the beam shape are not as reliable as other methods it has potential as a method for exploring baffle edge diffraction effects. Outdoor far field measurements using a tilting platform have been shown to be a viable option for finding the FWHM and an estimate of the acoustic tilt angle with at least the same degree of accuracy as the anechoic measurements whilst saving on the logistical problems of measuring SODARs in anechoic chambers and giving a true far field measurement. The Bradley technique allows for calculation of the effective beam tilt angle with low uncertainty and easy repeatability and can be carried out on the same tilting platform as the far field measurements. A comparison study should be carried out to see if measurements calibrated with the effective beam tilt angle and the acoustic beam tilt angle give better correlation with other instruments. The differences between the comparison instrument and the SODAR should be taken into account in this study.

5. Method Integration and Further Work

5. Method Integration and Further Work

5.1 Introduction

In this thesis three different approaches have been taken to reduce uncertainty and give meaning to SODAR measurements. These separate aspects are brought together in a hypothetical example to show how they can be integrated to create an approach to SODAR measurements that reduces overall uncertainty. The context of the research with respect to the requirements and current trends in the wind energy industry is given and the further work required to realise the full method is detailed.

5.2 Hypothetical Example of the Application of the Research Findings

Here the application of the findings of this thesis is given to a hypothetical example of a SODAR measurement set-up based on an arbitrary SODAR array and little or no knowledge of the exact processing. This is carried out to show how the separate parts can be integrated into an examination of the meaning and uncertainty of a SODAR measurement campaign. The process involves measuring the directivity of a single element from the SODAR array to find the effective source size, creating models based on the array geometry and the source size to find the effective measurement volume and directions where diffraction is mostly likely to occur, carrying out measurements of the whole array in the field to find the true beam tilt and FWHM values so that the wind speed and measurement volume estimates can be altered accordingly and carrying out transponder measurements to identify any systematic influences from the processing. As this is a hypothetical example no real measurements have been made however the example results will follow results found in real measurements.

5.2.1 The SODAR, Turbine and the Measurement Site

The SODAR in this example has an array layout as shown in Figure 5.2.1 made up of horn type loudspeakers with a physical diameter of 12cm, features a circular baffle with the top edges being at 35º in relation to the centre of the array. It operates at a frequency of 3600Hz with a range gate resolution of 10m meaning that the height span of each range gate is 20m and it has an average cycle of 4 seconds giving 150 measurements per 10 minutes. The tilt angle reported by the SODAR for the example is 15º. The details of the processing inside the SODAR uses are unknown.

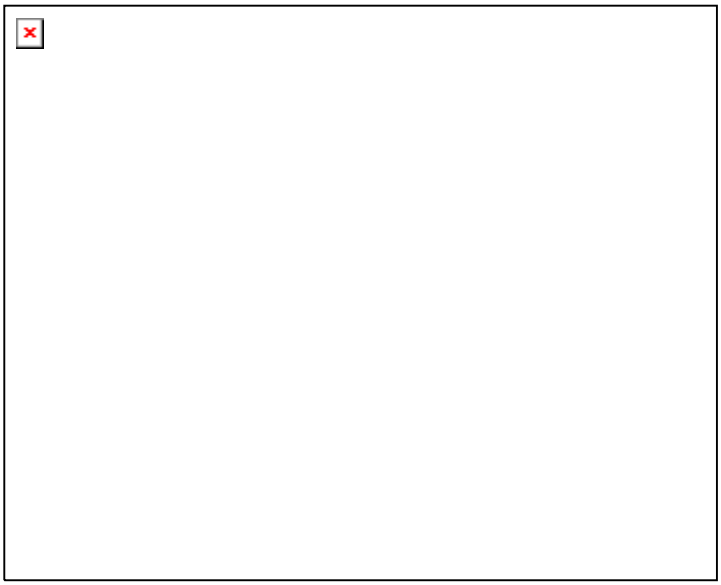

Figure 5.2.1 – Array layout of example SODAR array.

The turbine used in this example has a hub height of 100m and a blade span of 50m. The measurement site is relatively simple terrain with some reflecting objects featured. Figure 5.2.2 shows the layout of the measurement site with the SODAR wind turbine locations highlighted.

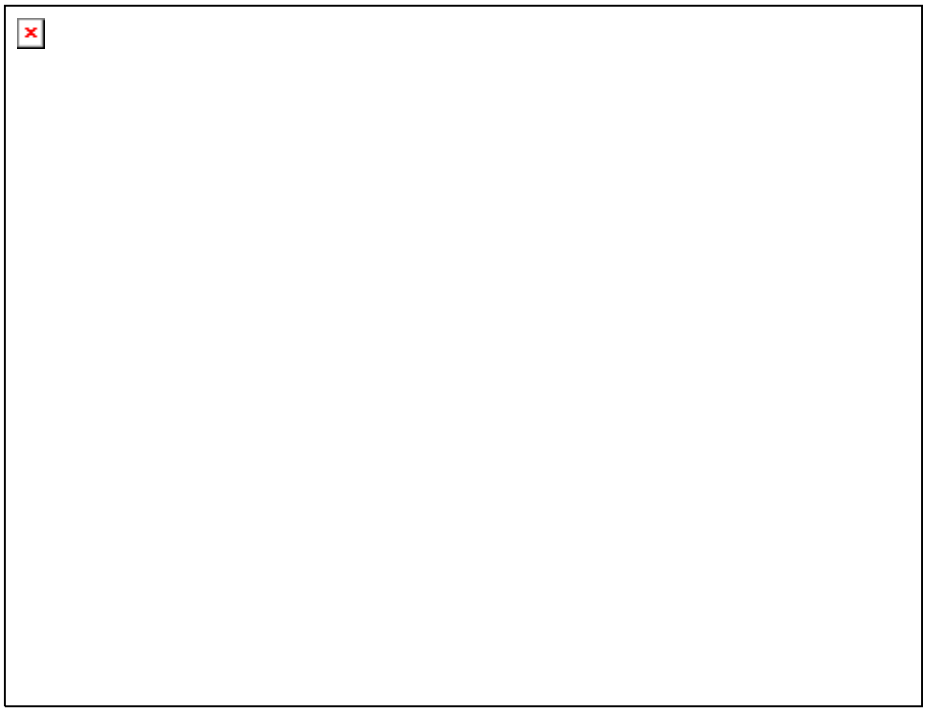

Figure 5.2.2 – Example measurement site layout.

In this layout the buildings and turbine present the directions which strong side lobes should not be pointed in. The ground variation is small but will change the wind between the two positions of interest.

5.2.2 Results

The diameter of the loudspeakers used is 12cm. If these are measured in an anechoic chamber to a high level of accuracy and with a angular resolution of at least 1º then the measured shape can be fitted to a piston function described by Equation 2.2.1 where the source radius is varied to find the best fit. In similar measurements made in Chapter 4 it was found that the effective diameter of the source was slightly larger than the physical diameter and therefore this result will be used here with the effective diameter of the loudspeaker modified to be 12.2cm. A model of the beam pattern of the whole array can then be made using the method described in Chapter 2. Figure 5.2.3 shows the modelled directivity pattern of this array shape using the effective diameter of the loudspeakers.

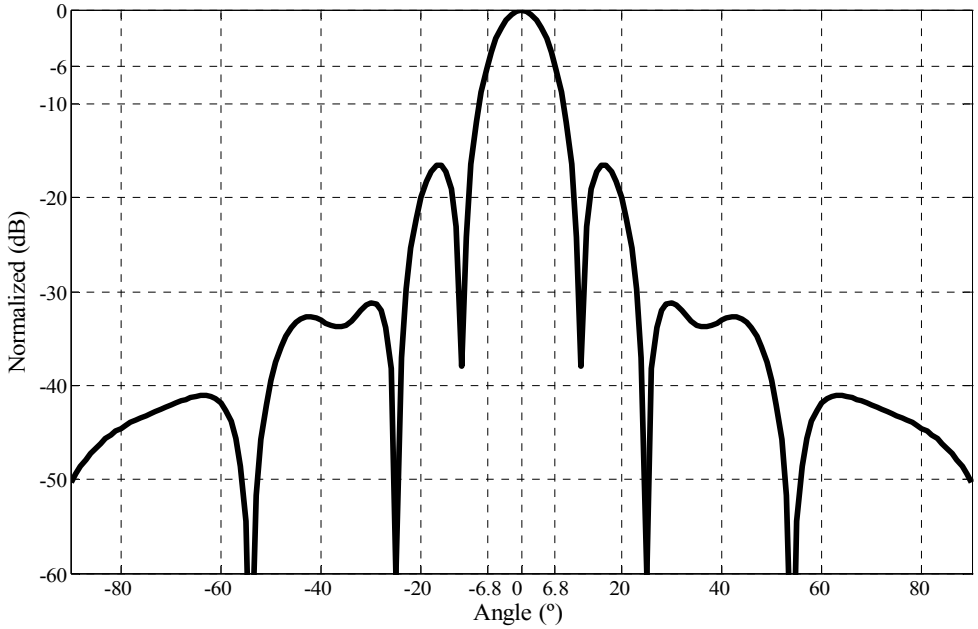

Figure 5.2.3 – Directivity pattern of example SODAR at 3600 Hz based on a source size of 12.2cm.

From the model of the array pattern it can be seen that the FWHM is 13.6º. The effective measurement volume is approximately 15% of a cone section with this width and a height span of 20m due to the range gate size. This results in an effective volume, for a range gate centred at 100m, of 2017 m^3. Using this the ratio of the effective measurement volume to that passing the same segment of a wind turbine blade span can be plotted against wind speed. This is shown in Figure 5.2.4 for all the range gates across the 100m span of the turbine blade with the combined total volume comparison shown with a bold line.

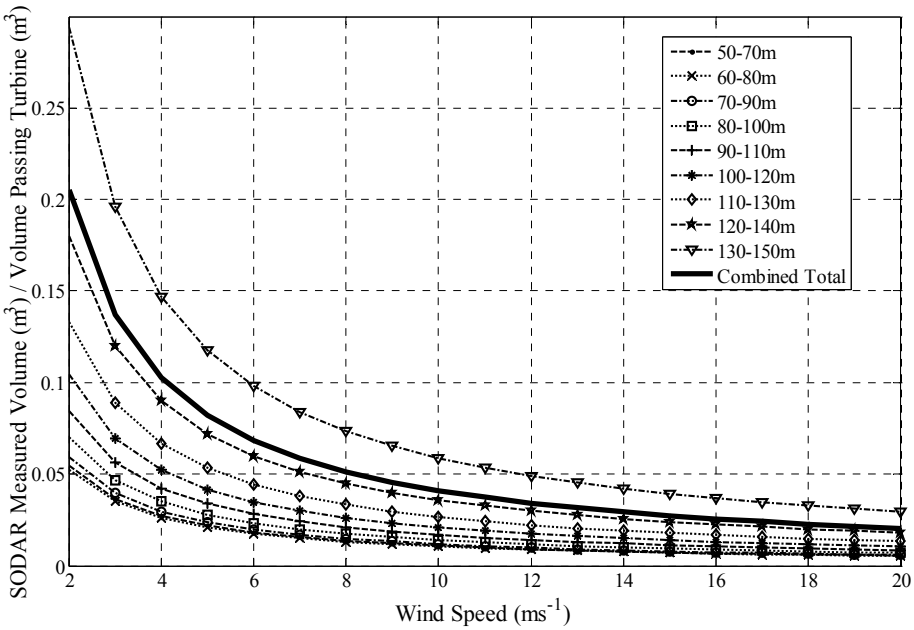

Figure 5.2.4 – Ratio of effective volume measured by the SODAR example to the volume passing the wind turbine over a 10 minute period assuming the SODAR makes 150 samples in the same period.

The SODAR samples between 3% and 15% of the turbine volume for the range of wind speeds that a the turbine operates at over the whole profile. At this point a CFD model is needed to describe the relationship between wind at the SODAR and the wind at the turbine. For instance if the CFD model shows that wind speeds at the turbine are 2% faster at $10ms^{-1}$ than the SODAR with a confidence interval of 0.2% and the turbulence is assumed to follow a normal distribution then the confidence that the SODAR speed plus 2% represents the speed at the turbine is a 5% sample of a normal distribution plus 0.2%. This is quite a complex calculation that requires further investigation but the possibility for finding the confidence interval of the SODAR representation of the wind speed at the turbine is evident. This is likely to change with the diurnal and seasonal cycles of the climate at the location. It should be noted that this full integration relies on the development of accurate CFD modelling for all terrain types. In its current form, as discussed in Chapter 1, it is accurate for simple terrain problems but less accurate for more complex terrain. In Bingöl (2009) and Behrens (2010) CFD modelling has been applied to remote sensing measurements to explain the underestimation in wind speed results in relation to cup anemometry. The

results are promising with the latter finding that the CFD modelling could predict the underestimation found.

The directivity model can then be used to find the angles of the strongest side lobe energy that occurs near the baffle edge. Figure 5.2.5 shows the 2D directivity pattern in Cartesian projection with the baffle edge position marked.

Figure 5.2.5 – 2D directivity pattern of the SODAR array tilted by 16º in Cartesian projection

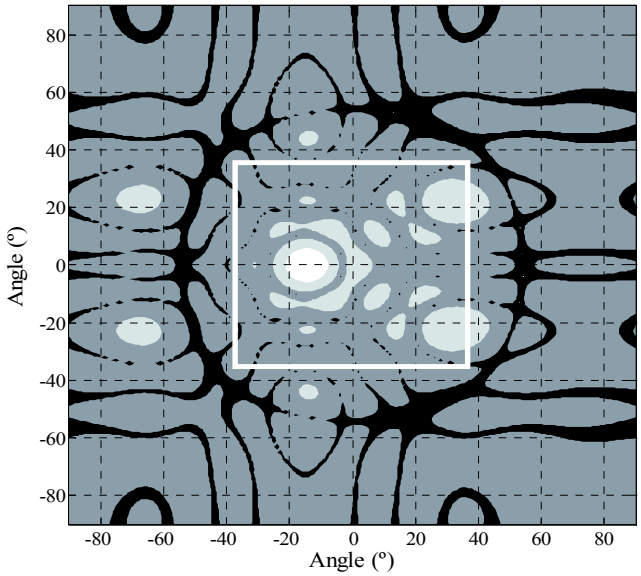

with the baffle edge position marked by a white square.

Two strong side lobes coincide with the baffle edge position centred at 162º and 202º in relation to the direction of the beam. The separation between the baffle edge and the main lobe is large so only the two side lobes are of real interest. This is converted into a side lobe direction guide that can be applied to the site map to determine the best orientation for the the SODAR as shown in Figure 5.2.6.

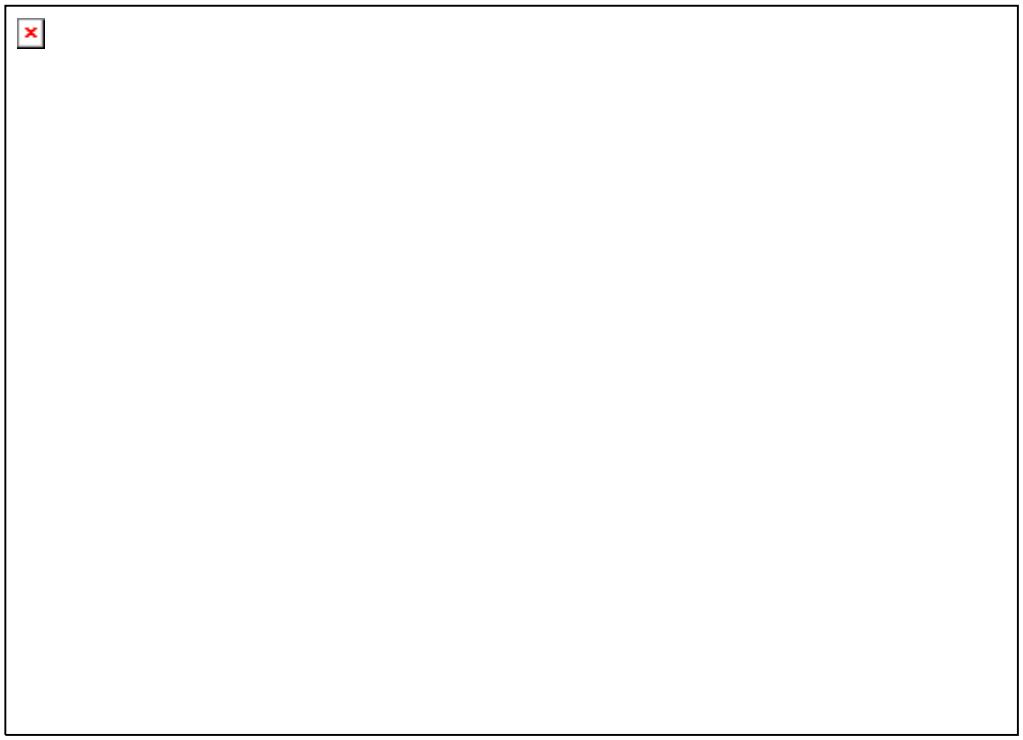

Figure 5.2.6 – Side lobe direction guide applied to site map with side lobes marked by bold dashed arrows.

With the best orientation for the SODAR identified and predictions of the ratio of the effective measurement volume to the turbine made with a wind speed relationship created based on CFD modelling measurements of the SODAR array can be performed at the site using both the tilting platform and the transponder to identify how the SODAR measurements should be interpreted to give a reliable estimate of the wind at the turbine.

Assuming that the issues with the transponder system have been solved such that the spectral width of the signal is realistic and the real atmospheric echo is effectively removed the system can be used to find the Doppler shift equation employed by the SODAR and any systematic bias resulting from the internal processing. In this example it is found that the SODAR is operating the Doppler Equation 2.8.1 so any wind speeds should be recalculated to take this into account, so long as it is proven that Equation 2.8.2 is more correct. Further to this the transponder system identifies a 0.1% slope across all wind speeds so this should also be taken into account.

Measurements using the tilting platform and the far field approach identify that the FWHM is within measurement error of the model and therefore no adjustment to the effective volume calculation is required. The acoustic tilt angle is found to be 14.88 which is 0.12º less than the SODAR reported tilt angle. Measurements using the Bradley technique find the effective tilt angle to be 14.71º which is 0.29º less than the SODAR reported angle.

Using the results of the transponder, tilt measurements and the CFD model the wind measured by the SODAR can be corrected to give the wind estimation at the turbine with the uncertainty found from the uncertainty of the CFD model and the statistical relationship between the volumes. Figure 5.2.7 shows the correction curve for this example assuming a 0ms^{-1} vertical velocity.

Figure 5.2.7 – Corrections to SODAR measured wind speed to give estimation of the wind

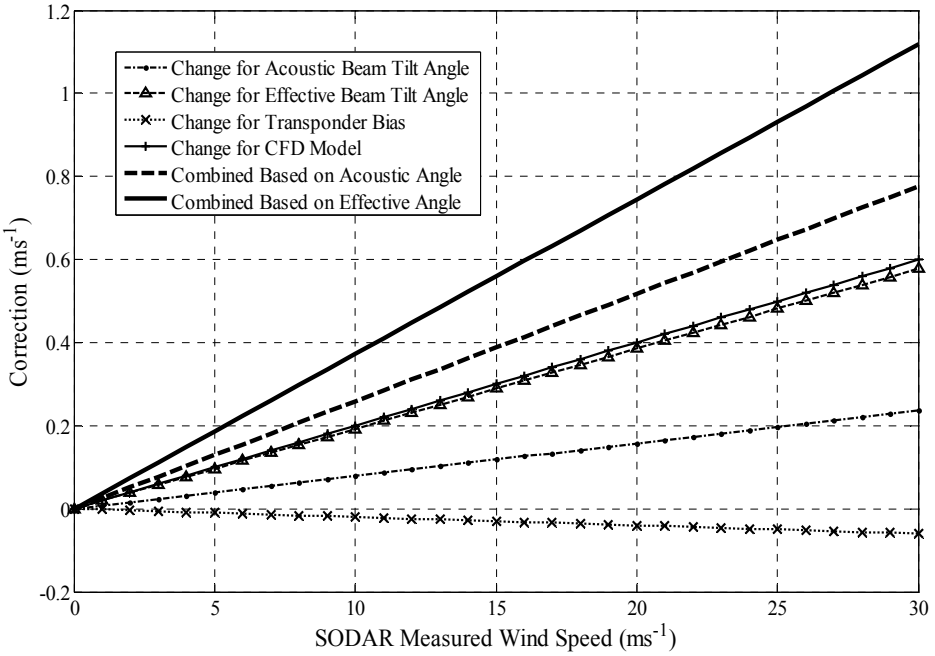

speed at the turbine based on both the acoustic beam tilt angle and the effective beam tilt angle.

The difference between the two tilt angle corrections is approximately 1% of the SODAR measured speed and therefore investigation into which of these corrections gives the best agreement with the measurements of other wind sensors is required. In

Chapter 1 results from SODAR cup comparisons measurements presented in WISE demonstrated that regression slopes of up to 10% can occur in simple terrain conditions. Whilst the analysis here is speculative and requires full testing corrections of 4% are within the range of the differences commonly found in SODAR cup comparisons. It is likely that this combined method would improve the measurement comparison.

5.2.3 Summary of Hypothetical Example

The example shown here demonstrates how to combine the various aspects of this research to find a correction for the wind speed measured by a SODAR and the wind at a turbine. The method requires some CFD modelling and the full operation of the transponder system but with these in place it is relatively simple to achieve and could be carried out in less than two weeks providing the weather conditions allowed the tilt platform and transponder measurements to be carried out, that reliable directivity information for the transducers used in the SODAR is obtainable, and that 'plug and play' data processing and modelling programmes are available from the start. Figure 5.2.8 shows a flow diagram of the approach. The correction slopes found with this approach are within the range of differences found in real SODAR comparison studies. Full testing is required but it is likely that this methodology will enhance the agreement between SODAR and mast anemometry comparisons.

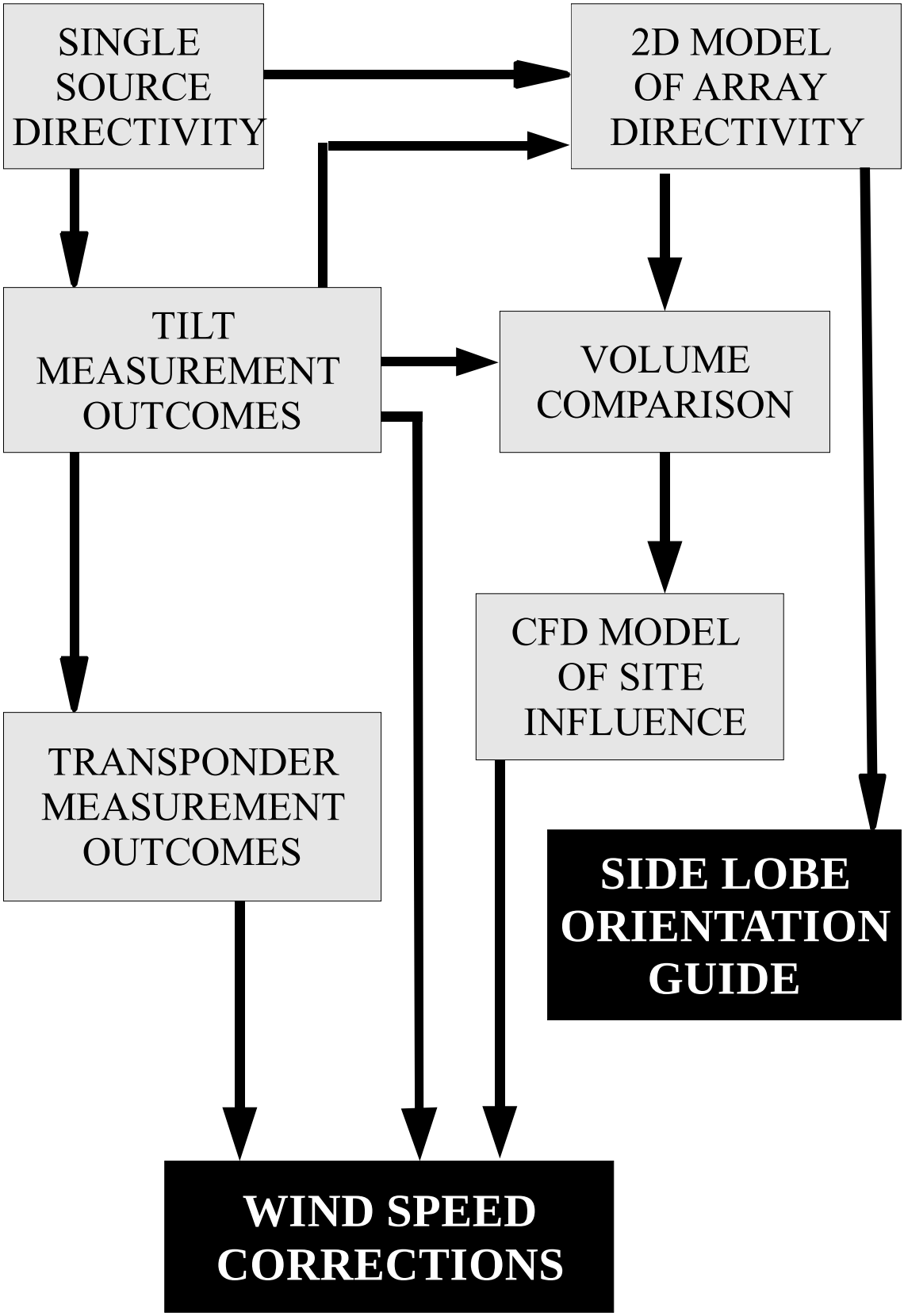

Figure 5.2.8 – Flow diagram of integration of SODAR comparison research.

5.3 Implications for Wind Energy Measurements with SODARs

The wind energy industry requires measurements with a high certainty level due to the large investments that are required to build wind turbines. Bradley (2008) identifies that a 1% error in wind speed estimation results in a 3% error in turbine power output due to the cubic relationship between incident velocity and power output. Therefore the requirement is for errors no larger than 1%.

In IEC 61400-12 cup anemometry is stated as the standard measurement method for deriving turbine power curves. Cup anemometry is calibrated in a wind tunnel to within the required accuracy levels. A single cup measurement does not represent the profile that covers the span of a turbine blade and is susceptible to overestimating wind speeds when encountering strong turbulence. SODARs and remote sensing options in general offer the ability to measure at several points across the turbine blade span meaning that a better estimation of the wind incident on the turbine is possible than that offered but a single cup at hub height. However the accuracy of SODAR measurements has yet to be confirmed to be within the required accuracy limits.

The majority of previous work carried out on confirming the accuracy of SODARs has involved the use of a comparison to another instrument such as a cup anemometer with a regression slope between the measurements of the two instruments being the indicator used. Crescenti (1997) collates several comparison studies with the regression slopes being shown to be between 0.88 and 1 from a range of studies in different circumstances. In Bradley (2005) several SODARs were tested at the same sight with the regression slopes found to be . This data is shown in Table 1.3.1. In both studies the SODARs have been shown to underestimate the reference instruments speed up to 12%. The speculative example of the application of the methods discussed in this thesis showed slopes of up to 4% so it is likely that if the approach in this thesis could be applied successfully then the regression slopes shown in SODAR comparisons should be reduced to less than 8%.

5.3.1 How Does the Proposed SODAR Comparison Method Fit into the UpWind Project?

In Chapter 1 it was stated that the work in this thesis is carried out as part of the remote sensing work package of the UpWind project. The objectives of the work package are to examine how remote sensing techniques, focussed on LIDAR and SODAR, can be used as replacements for mast mounted measurements. The methods described in this thesis are part characterisation and part calibration method if SODARs.

Within the same work package work has been carried out on a traceable calibration technique for LIDARs. A method is detailed in Hill (2010b) for a ZephIR Heterodyne LIDAR. The method described is a relatively simple process that makes use of a moving belt to calibrate the instrument for wind speed, wind direction and sensitivity. With the addition of a 45º mirror and a large moving belt target such as a running machine a calibration of measurement focus height can also be achieved. This process is simple and results in a higher certainty than the methods described in this thesis for SODARs.

The majority of LIDAR-mast anemometry comparisons studies show better regression slopes than those found in the SODAR-mast anemometry studies. This is mainly due to the measurement volume in a LIDAR measurement being much smaller than in a SODAR measurement, smaller separation distances between the LIDAR and mast as there are no fixed echo problems and more strenuous data filtering.Locating a SODAR next to a turbine is currently not possible and it is unlikely that this will be possible in the near future. The ratio between the measurement volume of a SODAR and the volume passing a turbine in this thesis has been shown to be around 5%. This will be considerably lower for a LIDAR and mast mounted anemometer measurement. So while LIDAR and a mast mounted anemometer show good agreement they have considerably smaller measurements volumes than a SODAR and therefore the statistical significance of how they represent the wind passing a turbine is reduced.

The high levels of data filtering applied by a LIDAR reduces the significance further.

It is clear that considerable work is being applied to remote sensing methods to make it a viable method for measuring wind speeds for the purposes of power performance measurements and site evaluations. The work undertaken in this thesis contributes to making SODARs a part of this.

5.4 Specific Further Work to Realise Comparison Methods for SODARs

In Chapter 2 a calculation of the effective measurement volume was described and it was stated that this could be used as a basis for finding a statistical relationship between the measurements made by the SODAR and the likely wind at another location. For this to be achieved a reliable CFD model or other means of finding this relationship is needed. Currently work on the use of CFD for these kind of problems is being carried out in other projects so the application of those needs to be made.

The transponder system presented in Chapter 3 requires several improvements before it is a fully realised comparison tool. Firstly the issue of spectral width needs to be solved. This may be achieved through convolving the signal with a set of filter coefficients to achieve a desired spectral width or through the use of a more complex turbulence model such as the one presented in Kendrick (2010).

A method to remove the influence of the atmospheric echo is needed. This could be achieved through the use of a more complete frame housing for the transponder that features extensive use of acoustical absorbent material. Further investigation into tent frames may yield a more appropriate option than the square gazebo frame currently used.

It was noted that the transponder may be able to find the magnitude of fixed echoes influencing the SODAR measurement. An experiment to quantify these effects is required. This could be achieved by placing the SODAR on a rotating platform and making measurements at different angles over a period of steady wind. This should

highlight the relative influence of fixed echoes for each orientation of the SODAR.

Measurements of a SODARs directivity using a tilting platform have shown promising results. Further measurements could be made in a range of conditions and using different SODARs to further validate the methods. For this a more practical tilting mechanism is needed since creating a concrete base may not be possible at all sites. This could be made from strong metal tubing and should be designed to handle the high loading exerted when a fully baffled SODAR is titled to a large angle.

The integration of the different methods of this thesis needs to be tested as a full technique on several SODARs at different locations with reference to mast mounted anemometry or other sensors. This requires the developments detailed already in this chapter to be achieved. The computer programming used in the different parts of this thesis needs to be compiled into a user friendly version so that the technique can be applied by any user.

5.5 Summary

In this Chapter the results found in the previous three chapters are integrated into an approach for explaining the differences between SODAR measured wind speeds at one location and wind speeds occurring at the location of a turbine. The integration relies heavily on the assumption that CFD modelling can be used to explain the differences that occur due to the separation of the measurement locations. This is thought to be a reasonable assumption in simple terrain but further advancements in modelling methods are required if this is to be a reasonable assumption in complex terrain. The example shown finds a difference of close to 4% with half of this being the contribution from the beam tilt angle difference.

The consequence of this for wind energy measurements is that the slopes found in SODAR-mast anemometry comparison studies should be reduced to be less than 8% for the majority of cases. This needs to be confirmed through full testing of this

integration method in order to confirm the findings of this work. Before this can be done the improvements to the various aspects of the method need to be carried out.

6. Conclusions

6. Conclusions

The aim of this work has been to investigate acoustic based methods to reduce the uncertainty in SODAR measurements specifically aimed at the requirements of the wind industry. The methods investigated included theoretical analysis, use of a transponder system to provide simulated wind and measurements of array beam width and tilt angle. The results are then combined to form an integrated approach. The conclusions of this work are given here in terms of the initial research questions.

i. Can the quality of SODAR measurements be improved and uncertainty reduced through theoretical analysis of the acoustic behaviour of SODARs?

The theoretical analysis presented in this thesis has largely focussed on the acoustic behaviour of the SODAR beam. Details of the theory behind SODAR measurements have been presented several times before and in Bradley (2005) and Bradley (2008) the various types of SODAR processing have been analysed and discussed at length so there is little to add to that work although aspects can be used in the approach proposed here. Similarly the behaviour of sound sources is well researched and published. Full derivations of sound source behaviour equations are given in Kinsler (2000). The aim of the theoretical analysis presented in this thesis is to create 'tools' for understanding how SODAR measurements compare to other measurement types and how related the SODAR wind estimations are to wind turbines placed a distance away.

It has been shown that the FWHM can easily be obtained from the beam pattern, this is not new. From this the effective volume can be calculated taking into account the weighting within the volume presented by the beam shape and the assumption that a SODAR must apply an amplitude window in order to extract information for a single range gate. The result is that the effective volume measured by a SODAR is approximately 15% of a cone section volume based on the FWHM. Previously this cone section has been used to describe the measurement volume and it

is clear from the analysis presented here that this is not the case. Knowledge of the volume measured by the SODAR sets up the basis for calculating the probability that the wind speeds measured by a SODAR in one place are representative of the wind speeds in another. This does require some modelling using CFD to give the relationship of a particular scenario.

Using the a model of the acoustic radiation from a SODAR array it is easy to identify the directions where the strongest side lobes exist. This knowledge can then be applied to a map of the measurement site in order to identify the best orientation for the SODAR. Performing this analysis should result in the weakest influence of fixed echoes for a given site and therefore the quality of the SODAR measurement is improved.

Two Doppler shift equations have been found in previous literature for calculating the wind speed estimates in SODARs. They result in estimations that are between 2 and 3% different and therefore further investigation is needed to identify the most correct one although it is highly likely that the version from Ostashev (1997) is more correct.

In summary the quality of SODAR measurements can be improved through theoretical analysis of the acoustic behaviour of the SODAR in question. The whole uncertainty can not be predicted but knowledge of the measurement volume can be used with a CFD model to find a statistical relationship between the wind speed measured by a SODAR and the wind at a related location.

ii. Can a transponder system be created that goes further than a simple diagnostic test to find information about a SODAR's operation and offer the possibility of direct comparison between the measurements of different SODARs with the ability to test in the field?

The transponder system detailed in Chapter 3 can act as a simple diagnostic test in the same way that the APT presented in Baxter (1994 a and b) acts but it is designed to test more than this. It is set up to operate over the whole height range of the SODAR and to offer the possibility of testing a range of wind speeds, various wind profile shapes and background noise levels. Testing the transponder system with a METEK DSDPA.90-24 SODAR in semi-anechoic conditions has shown that the Doppler equation used by a SODAR can be found through analysis of the differences in wind speed over a range of speeds, that a background noise level can be found that causes degradation in the accuracy of the SODARs wind speed estimation, and that a lag effect can be identified for profiles featuring a sharp wind change. Further testing in semi-anechoic conditions has highlighted two flaws in the transponder system. The first is that the spectral width of the return echo is insufficient to be accepted as a real echo by all SODARs and tests with the METEK and an AQ500 SODAR have shown this with the former reporting an error code but allowing the measurement and the latter rejecting the echo. The second is that the measurement method needs to be based on ten minute averages rather than two minute averages. This allows for SODARs that overlap ten minute averages to give the appearance of shorter averages. This was also highlighted in testing with the AQ500 SODAR.

Some adaptation of the transponder system was made so that it could be operated in field conditions. The aim of this adaptation was to remove the influence of the real atmospheric echo and prevent any outdoor conditions from making the transponder system trigger incorrectly. Testing with the METEK SODAR suggested that both of these aims had been achieved but this was later found to be a false result due to faulty amplification in the SODAR. Testing carried out with an ASC4000 SODAR in an autonomous set-up highlighted that the atmospheric echo continued to influence the

measurement.

A transponder system can be used to test a SODAR beyond a simple diagnostic test. The design detailed in this thesis has been used to find out some information about one SODAR type but further work is required to make the system fully functional with all SODARs and in a field environment. If this is achieved then a comparison of how different SODARs interpret the echoes from the transponder can be made.

iii. What is the best method or methods for finding a SODAR's beam shape and tilt angle?

Several methods of measuring a SODAR's beam shape and tilt angle have been explored in Chapter 4 with varying results.

Measurements of a single source from a speaker array have been shown as a useful method for obtaining the effective size of the source. This information is used to improve models of the whole array and for calculating a SODAR's theoretical tilt angle based on the source separation in the array, temperature and frequency.

Far-field measurements of the central part of the beam shape and the tilt angle give estimates of the FWHM and of the acoustic tilt angle. The tilt angle estimates found are within the measurement error of the theoretical angle reported by the SODAR. Better quality estimates could be achieved using computer controlled changes to the tilting platform. This is a good approach as the accuracy demonstrated is as good as measurements made in anechoic conditions and it can be performed in the field with a 10m tower, a sound level meter and a tilting platform.

Using the same tilt platform the technique presented in Bradley (2010) was trialled to find the effective tilt angle. The results found were not as close to the theoretical tilt angle as previously found. This was due to a number of factors including a shorter measurement period and the possible presence of fixed echoes. The technique could easily be carried out for a longer period and therefore it is considered

a good approach for finding the effective tilt angle.

These three methods are the best methods for obtaining the required information about the SODARs directivity. It would be useful to conduct an experiment to see if the differences between the measured and theoretical tilt angles result in better agreement between SODAR measurements and measurements from other wind sensors.

iv. Can these aspects be combined into a unified approach for to improve SODAR measurement certainty and therefore increase the usefulness of SODAR measurements for the wind industry.

The hypothetical example given in the previous Chapter demonstrates that the separate aspects of investigation explored in this thesis can be combined into a complete method for improving the quality of SODAR measurements and the representation of the wind speed at a related location based on these measurements. Some of the methods need to be fully realised into reliable techniques and a CFD model needs to be incorporated. The models and transponder software also need to be converted into user friendly formats that require only simple inputs to achieve the required goal. With these advancements it is likely that the measurements within the integrated method could be carried out over a two week period to achieve a set of correction slopes that could be applied to a SODARs measurements. These correction slope are expected to be between a 0% and 5% change to the wind measured by a SODAR which should bring the typical agreements found in SODAR-mast anemometry comparison studies to less than 8% difference based on the majority of previous comparison studies. If cup speed up effects and the bias caused by the difference in averaging methods applied by SODARs compared to cups is taken into account this difference is a lot closer to the wind energy requirement.

This methodology can reduce the uncertainty in a SODAR measurement making it more attractive as an alternative to cup anemometer measurements. The

SODAR has the advantages over a cup anemometer of not requiring a tall and expensive mast, being able to measure over the whole of a turbines blade span allowing for an effective wind speed to be used in the calculation of AEP and being a volume measurement which gives a better representation of the wind encountered by a turbine. With the further work set out in Chapter 5 achieved the level of confidence in SODAR measurements will be at a trustworthy level for the wind energy industry.

References

- Antoniou I, Jørgensen HE, Ormel F, Bradley SG, von Hünerbein S, Emeis S and Warmbier G (2003): On The Theory Of SODAR Measurements. *Final Reporting On WP1, EU WISE project NNE5-2001-297, RISØ-R-1410(EN).*

- Antoniou I, Pedersen SM and Enevoldsen PB (2009): Wind Shear and Uncertainties in Power Curve Measurement and Wind Resources. *Wind Engineering, 33(5) 449-468*

- Asimakopoulos DN, Helmis CG and Petrakis M (1996): Mini-acoustic sounding- A powerful tool for ABL applications: Recent advances and applications of acoustic mini-sodars. *Boundary Layer Meteorology. 81(1) 49-61*

- Asimakopoulos DN, Helmis CG and Stephanou GJ (1987): Atmospheric Acoustic Minisounder. *Journal of Atmospheric and Oceanic Technology, 4, 345–347.*

- Azima H, Panzer J and Reynaga D (1999): Distributed-Mode Loudspeakers (DML) in Small Enclosures. *Presented at the 106th Convention of the Audio Engineering Society, Munich*

- Bass HE, Bauer H-J and Evans LB (1972): Atmospheric Absorption of Sound: Analytical Expressions, *Journal of the Acoustical Society of America, 52(3B), 821-825*

- Bass HE, Sutherland LC and Zuckerwar AJ (1995): Atmospheric absorption of sound: Further developments, *Journal of the Acoustical Society of America, 97(1), 680-683*

- Baumann K and Piringer M (2001): Two-years of boundary layer measurements with a sodar - statistics and applications. *Physics and Chemistry of the Earth, Part B: Hydrology, Oceans and Atmosphere 26(3) 205-211*

References

- Baxter (1994b): Performance of Sodar Audits Under the New USEPA Guidance, *presented at the 7th International Symposium on Acoustic Remote Sensing and Associated Techniques of the Atmosphere and Oceans, Boulder, Colorado, October*.

- Baxter R., (1994a): Development of a Universal Acoustic Pulse Transponding System for Performance Auditing SODARs. *Presented at the 7th International Symposium on Acoustic Remote Sensing and Associated Techniques of the Atmosphere and Oceans, Boulder, Colorado, October*.

- Behrens P, Bradley SG and von Hünerbein S (2008): A Scanning Bi-static SODAR, *IOP Conference Series: Earth and Environmental Science, 1 012010*

- Behrens P, Bradley SG and Weins T (2010a): A Multi Sodar Approach to Wind Profiling, *Proceedings of the International Symposium for the Advancement of Boundary Layer Remote Sensing, Paris, June,* P-MEA/06

- Behrens P, O'Sullivan J, Archer R and Bradley S (2010b): Underestimation of sodar and anemometer wind speed measurements in complex terrain, *Proceedings of the International Symposium for the Advancement of Boundary Layer Remote Sensing, Paris, June, P-SUR/03*

- Beran D, Carsey F and Willmarth B (1973): Acoustic Doppler Wind Measuring System (A), *Journal of the Acoustic Society of America,Volume 54, Issue 1, pp. 303-303 July*

- Bingöl F(2009): Complex Terrain and Wind LIDARs, *PhD Thesis, RISØ-DTU National Laboratory for Sustainable Energy, Denmark*

- Boquet M, Sauvage L, Parmentier R, Cariou JP, Bingöl F, Fossekis D, Dupont G and Meissner C (2010): WINDCUBE Wind Speed Correction in Complex Terrain, *UpWind WP6 52nd Month Project Meeting Invited Presentation, Paris*

- Bradley SG (1999): Use of Coded Waveforms for SODAR Systems, *Meteorology and Atmospheric Physics Volume 71, Numbers 1-2, 15-23*

References

- Bradley SG (2008): Atmospheric acoustic remote sensing, *CRC Press, Taylor & Francis Group, Boca Raton, FL.*

- Bradley SG and Underwood K (2010a): Integration of a Scanning Bi-static Option into a Commercial SODAR, *Proceedings of the International Symposium for the Advancement of Boundary Layer Remote Sensing, Paris, June, P-MEA/17*

- Bradley SG, Antoniou I, von Hünerbein S, Kindler D, de Noord M and Jørgensen HE (2005): SODAR Calibration For Wind Energy Applications, *Final Reporting On WP3, EU WISE project NNE5-2001-297, The University of Salford, Greater Manchester, UK ISBN 0-9541649-1-1*

- Bradley SG, Mursch-Radlgruber E, von Hünerbein S(2007): Sodar measurements of wing vortex strenght and position. *Journal of Atmospheric and Oceanic Technology, 24, 141-155*

- Bradley SG, Perrott Y, Behrens P and Oldroyd A (2010b): Myres Hill LIDAR/SODAR/Mast Intercomparison Revisited, *Proceedings of the International Symposium for the Advancement of Boundary Layer Remote Sensing, Paris, June, P-MEA/08*

- Caughey SJ, Crease BA, Asimakopoulos DN and Cole RS (1976) :A comparison of acoustic Doppler vertical velocities with direct measurements in the atmospheric boundary layer, *Nature 262, 274 - 276 (22 July)*

- Clive PJM, Chindurza I , Ravey I, Bass J, Boyle RJ, Jones P, Lang SJ, Bradley S, Hay L, Oldroyd A and Stickland M (2008): The Myres Hill remote sensing intercomparison study: preliminary results, *IOP Conference Series: Earth and Environmental Science, 1 012019*

- Crescenti GH (1997): A Look Back on Two Decades of Doppler Sodar Comparison Studies, *Bulletin of the American Meteorological Society, 78(4), 651-673*

References

- Cronenwett WT, Walker GB and Inman RL (1972): Acoustic Sounding of Meteorological Phenomena in the Planetary Boundary Layer, *Journal of Applied Meteorology, vol. 11, Issue 8, pp.1351-1358*
- Danilov SD, Guryanova AE, Kallistratovaa MA, Petenkoa IV, Singal SP, Pahwab DR and Gera BS (1992): Acoustic calibration of sodars, *Measurement Science and Technology, Volume 3, Number 10*
- Danilov SD, Guryanova AE, Kallistratovaa MA, Petenkoa IV, Singal SP, Pahwab DR and Gera BS (1994): Simple method of calibration of conventional sodar antenna system, *International Journal of Remote Sensing, Volume 15, Issue 2 January 1994 , pages 307 - 312*
- Davey RF(1978):Comparison of Doppler sodar antenna configurations used for horizontal wind measurement, *Journal of the Acoustical Society of America, Volume 60, Issue S1, pp. S68-S68. November*
- De Noord M, Curvers A, Eecen P, Antoniou I, Jørgensen HE, Pederden TF, Bradley S, von Hünerbein S, Kindler D, Mellinghoff H and Emeis S (2005): WISE Wind Energy SODAR Evaluation Final Report, *ECN-C--05-044 NNES-2001-297, March*
- Elisei G, Maini M, Marzorati A, Morselli MG, Fiocco G, Cantarano S and Mastrantonio G (1986): Implementation of Multiaxial Doppler SODAR System with Advanced Data Processing, *Atmospheric Research, 20, 109-118*
- Emeis S and Schäfer K (2006): Remote sensing methods to investigate boundary-layer structures relevant to air pollution in cities, *Boundary-Layer Meteorology Volume 121, Number 2, 377-385*
- Evans LB, Bass HE and Sutherland LC (1972): Atmospheric Absorption of Sound: Theoretical Predictions, *Journal of the Acoustical Society of America,51(5B), 1565-1575*
- Finkelstein PL, Kaimal JC, et al. (1986): Comparison of wind monitoring systems. Part 2: Doppler Sodars, *Journal of Atmospheric and Oceanic Technology 3(4): 594-604*

References

- Foussekis D (2010): Measurements of flow tilt angles and velocity profiles in complex terrain, *UpWind WP6 52nd Month Project Meeting Report, Paris*

- Fujita EM, Bowen JL, Green MC and Moosmüller H (1997): 1997 Southern California Ozone Study-NARSTO Quality Assurance and Data management, *Report prepared by the Desert Research Institute, Reno, NV for the California Air Resources Board, Sacramento, CA*

- Gaynor, JE (1977): Acoustic Doppler measurement of atmospheric boundary layer velocity structure functions and energy dissipation rates, *Journal of Applied Meteorology 16(2): 148-155*

- Georges TM, and Clifford SF(1972): Acoustic sounding in a refracting atmosphere, *Journal of the Acoustical Society of America 52(5): 1397-1405*

- Gera BS and Singal SP (1990): Sodar in Air-Pollution Meteorology, *Atmospheric Environment Part a-General Topics 24(8): 2003-2009*

- Gilman GW, Coxhead HB and Willis FH (1946): Reflection of Sound Signals in the Troposphere, *Journal of the Acoustical Society of America Volume 18, Issue 2, pp. 274-283*

- Gómez P, Elizalde O, Navarro I, Alzueta G and Rodriguez G (2010a): Power Curve with LIDAR in Complex Terrain, *Proceedings of the International Symposium for the Advancement of Boundary Layer Remote Sensing, Paris, June,P-SER/13*

- Gómez (2010b): Measurements in complex terrain: Approach to Power Curve measurement, *UpWind WP6 52nd Month Project Meeting Report, Paris*

- Gómez (2010c): Fog Filtering, *UpWind WP6 52nd Month Project Meeting Report, Paris*

- Hayashi T, Liu W and Sassa K (2003): A Preliminary Investigation of Low-Cost SODAR Anemometry, *Wind Engineering, Volume 27, Number 4, August*

References

- Helmis CG, Asimakopoulos DN and Cole RS (1985): A low-level atmospheric vertical velocity comparison between a high-resolution acoustic sounder and a turbulence probe, *IEEE Transactions of Geoscience and Remote Sensing, GE23, 164-170*

- Helmis CG, Asimakopoulos DN, et al. (1997): Thessaloniki '91 field measurement campaign. 1. Wind field and atmospheric boundary layer structure over Greater Thessaloniki Area, under light background flow, *Atmospheric Environment, 31(8): 1101-1114.*

- Hill C and Harris M (2010a): CloudRemoval Algorithm, *UpWind Progress Report, June 2010*

- Hill C and Harris M (2010b): Lidar Calibration Report*, UpWind Progress Report, June 2010*

- IEC 61400-12 Power Performance Measurement Techniques (1998)

- Ito Y(1997): Errors in Wind Measurements Estimated by Five-Beam Phased Array Doppler Sodar, *Journal of Atmospheric and Oceanic Technology*, *14, 792–801*.

- Kallistratova MA (1968): Study of optical turbulence in the atmospheric boundary layer by acoustic remote sensing, *Proceedings of SPIE, Vol. 1968, 607*

- Kallistratova MA and Coulter RL (2004): Application of SODARs in the Study and Monitoring of the Environment, *Meteorology and Atmospheric Physics, 85, 21-37*

- Kendrick P and von Hünerbein S. (2010): Atmospheric sound scattering model to test signal coding methods for SODARs'. *Presented at the 2010 International Symposium on Atmospheric Remote Sensing, Paris*

- Kinsler LE, Frey AR, Coppens AB and Sanders JV. (2000): Fundamentals of Acoustics. *John Wiley & Sons, Inc, New York*

References

- Kurzeja RJ (1994): Comparison of a Doppler Sodar with Bivanes and Cup Anemometers, *Journal of Atmospheric and Oceanicic Technology*, 11, 192–199.

- Little, C. G. (1969):Acoustic Sounding of Lower Atmosphere, *Proceedings of IEEE, 57, 571-578.*

- Mann J, Søren O, Jørgensen BH and Helmuth PF (2000): WAsP Engineering 2000, *RISØ-R-1356(EN)*

- Mastrantonio G, and Fiocco G(1982): Accuracy of wind velocity determinations with Doppler sodars, *Journal of Applied Meteorology 21(6)*

- Maynard JD, Williams EG and Lee Y (1985): Nearfield Acoustic Holography: I. Theory of Genralized Holography and the Development of NAH, *Journal of the Acoustical Society of America, 78 (4)*

- McAllister, L. (1968): Acoustic Sounding of Lower Troposphere, *Journal of Atmospheric and Terrestrial Physics 30(7): 1439-1440*

- Moulsley TJ, Asimakopoulos DN, et al. (1978). Design of Arrays for Acoustic Sounder Antennas, *Journal of Physics E-Scientific Instruments 11(7): 657-662*

- Mursch-Radlgruber (1993a): Mobile High-Frequency Mini-SODAR and its Potential For Boundary-Layer Studies. *Applied Physics B-Photophysics and Laser Chemistry, 57(1): 57-63.*

- Mursch-Radlgruber (1993b) NOAA`s portable high frequency Mini Sodar Design and first results, extended version of 24.. *International Journal of Remote Sensing, 25 (2) 325-332*

- Neff WD and Coulter RL (1986). Acoustic remote sensing. *Probing the Atmospheric Boundary Layer. D. H. Lenschow: 201-239*

- Oppenheim AV, Schafer RW and Buck JR. (1999): 'Discrete-time signal processing'. *Prentice-Hall International, London.*

References

- Ormel FT, Herman SA and Eecen PJ(2003): Comparative Measurements of SODAR Systems, *ECN-C--02-045*

- Ostashev VE, (1997): Acoustics in moving homogeneous media. *E & FN Spon, London, pp 161-162*

- Piper B and S. von Hünerbein, (2008): Development of a Transponder Based Technique for the Acoustic Calibration of SODARs, *IOP Conference Series: Earth and Environmental Science, 1 012044*

- Piper B and von Hünerbein S (2010): Results from Testing a System Calibration Transponder with Two Different SODARs, *Proceedings of the International Symposium for the Advancement of Boundary Layer Remote Sensing, Paris, June, P-MEA/09*

- Piringer M (2001): Exploring the urban boundary layer by sodar and tethersonde, *Physics and Chemistry of the Earth, Part B: Hydrology, Oceans and Atmosphere 26(3), 213-217*

- Srinivasa Rao I, Anandan VK and Shravan Kumar M (2009): Multifrequency Decoding of a Phased Array Doppler Sodar, *Jouranl of Amospheric and Oceanic Technology, 26(4), 759–768*

- Reid (2003): Hilltop Wind Profiles Using SODAR, *Boundary-Layer Meteorology 108, 305-314*

- Salomons EM, (2001): Computational Atmospheric Acoustics. *Kluwer Academic Publishers, Dordrecht,* pp 109-110

- Scott G, Elliott D and Scwartz M (2010): Comparison of Second Wind Triton Data with Meteorological Tower Measurements, *National Renewable Energy Laboratory, Golden, Colorado, NREL/TP-550-47429, Feb*

- Short DA and Wheeler MM (2003): MiniSODAR Evaluation, *NASA CR-2003-211192, Kennedy Space Center, Florida*

References

- Stangroom P (2004): CFD Modelling of Wind Flow Over Terrain, *PhD Thesis,University of Nottingham, UK*

- Tomkins O and Raferty P (2007): Validation of SODAR Measurements on a Complex, *Forested Site, Presented at EWEC 2007, Milan, Italy*

- Underwood KH and Warmbier G (2010): Autonomous SoDAR Configurations, *Proceedings of the International Symposium for the Advancement of Boundary Layer Remote Sensing, Paris, June, O-FSE/04*

- Vogt S and Thomas P (1994): Test of a Phased Array Sodar by Intercomparison with Tower Data, *Journal of Atmospheric and Oceanic Technology*, 11, 94–102.

- Von Hünerbein S, Bradley S and Kendrick P (2010): A flexible new SODAR Design for chirped signals and conformable beam forming, *Proceedings of the International Symposium for the Advancement of Boundary Layer Remote Sensing, Paris, June,P-MEA/05*

- Wagner R (2008): Remote Sensing used for Power Curves. *IOP Conference Series: Earth and Environmental Science, 1 012059*

- Wagner R, Antoniou I, Pedersen SM, Courtnet MS and Jørgensen HE (2009): The influence of the wind speed profile on wind turbine performance measurement, *Wind Energy Volume 12, Issue 4, pages 348–362, May*

- Wagner R, Courtney M, Gottschall J and Lindelöw PJP (2010a): Improvement of power curve measurement with lidar wind speed profiles, *Presented at EWEC 2010, Warsaw, Poland*

- Wagner R (2010b): Power curve measurement uncertainty: Ueq/ Uhub, *UpWind WP6 52nd Month Project Meeting Report, Paris*

- Walls (2010): Understanding and Quantifying the Uncertainty in Tower Extrapolation and AEP Estimations using SODAR, *Presented at EWEC 2010, Warsaw, Poland*

References

- Warmbier G, Albers F and Hanswillemenke K (2007): Wind energy related measurements with a commercial SODAR system, *Meteorologische Zeitschrift, Volume 16, Number 4, August 2007 , pp. 425-428*

- Werkhoven CJ and Bradley SG (1997): The Design of Acoustic Radar Baffles, *Journal of Atmospheric and Oceanic Technology, 14, 360-367*

- Williams EG (1982): Numerical Evaluation of the Rayleigh Integral for Planar Radiators Using the FFT, *Journal of the Acoustical Society of America, 72 (6), 2020-2030*

- Williams EG (1991): Measurement and Projection of Acoustic Fields, *Proceedings of Instrumentation and Measurement Technology Conference, 1991. IMTC-91. Conference Record., 8th IEEE, 275 - 278*